Contrail Mitigation

by means of 4D Aircraft Trajectory Optimisation

T. Hendriks (BSc)

Technische Universiteit Delft

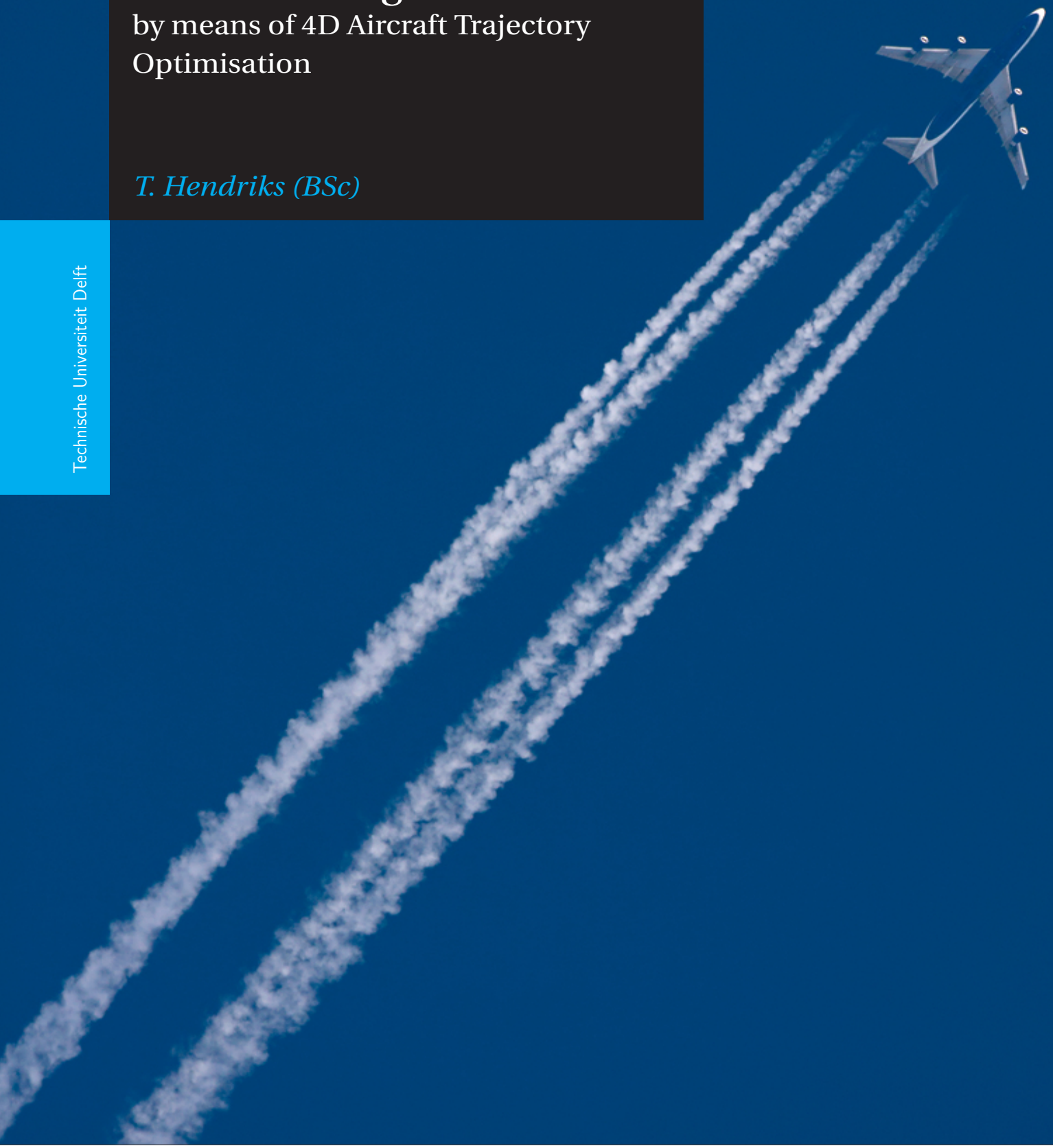

TU Delft Delft University of Technology

Challenge the future

CONTRAIL MITIGATION

BY MEANS OF 4D AIRCRAFT TRAJECTORY OPTIMISATION

by

T. Hendriks (BSc)

in partial fulfillment of the requirements for the degree of

Master of Science
in Aerospace Engineering

at the Delft University of Technology,
to be defended publicly on Thursday April 30^{th}, 2015 at 14:00 PM.

Supervisor (Primary):	Dr. ir. H.G. Visser		
Supervisor (Secondary):	Dr. ir. S. Hartjes		
Thesis committee:	Dr. ir. H.G. Visser,	TU Delft	_____
	Dr. ir. S. Hartjes,	TU Delft	_____
	Ir. J.A. Melkert,	TU Delft	_____

An electronic version of this thesis is available at http://repository.tudelft.nl/.

TU Delft Delft University of Technology

Abstract

Aviation has a significant impact on the global atmosphere. Next to particle and gas emissions, the increase of cloud cover might increasingly contribute to aviation induced climate change. Water contained in the exhaust of jet engines locally raises the relative humidity levels sufficiently for contrail formation to occur. These contrails can persist and evolve into anthropogenic clouding, often indiscernible from natural clouding, in case the ambient atmosphere is saturated. With the projected continued growth of air traffic, increasing propulsive efficiencies and possible introduction of fuels with higher hydrogen to carbon ratios, the importance of contrail mitigation is likely to increase. In this study, contrail mitigation by means of flexible free flight was studied, as this is likely the most efficient (short term) mitigation strategy. Contrail avoidance strategies by means of flexible free flight have been in use with airforces around the globe for some decades. For commercial aviation however, the implementation of any such strategies, requires a thorough assessment of cost-effectiveness.

The purpose of this study is to get a better understanding of the wider context of the problem, next to this a viable proposal is made for a short term contrail mitigation strategy. In this research, the formation of contrails and the costs and benefits associated with contrail mitigation is studied. A tool has been developed so that time and fuel burn optimal trajectories can be determined, while mitigating the formation of persistent contrail formation. Flexible free flight in four dimensions forms the basic means by which the optimisation tool can help evading regions prone to persistent contrail formation. The tool has been designed to rely on up-to-date meteorologic Numerical Weather Predictions (NWP), made available by meteorologic institutes. Test cases have been performed under realistic atmospheric conditions, using the Temperature, Pressure, Specific Humidity and Wind vector output from Numerical Weather Predictions, generated by the Canadian National Meteorologic Institute. With the, there from obtained results, an indication for the technical feasibility of this contrail mitigation strategy for commercial aviation has been created.

This study has shown it is technically feasible for commercial aviation to evade contrail regions, thereby greatly reducing the effective anthropogenic cloud cover. The obtained results, clearly indicate persistent contrail formation can be avoided, at the cost of increased fuel consumption. The contrail reductions are more than sufficient to offset the additional CO_2 emission, induced by the increases in fuel burn, leading to large scale reductions in the flights effective Radiative Forcing. The case dependency of contrail mitigation costs are susceptible to ambient atmospheric conditions. Indicating the great potential of using up-to-date atmospheric data over parametrized and more generic models often used in climate studies.

The implementation of realistic, high resolution atmospheric data, significantly impacts the optimal trajectory in a number of ways. Deviations indicate that the realistic non-uniform temperature distribution can significantly affect the path constraints and hence the optimal trajectory. The inclusion of realistic wind data enhances the accurate representation of commercial aviation. For contrail mitigation, trajectory adjustments in the vertical plane are seemingly preferred over adjustments in the horizontal plane. This is due to the large horizontal extent and limited vertical thickness of contrail regions. A number of characteristic contrail evading manoeuvres are seen in the vertical flight trajectory.

The sensitivity case analysed herein indicates, 90% of the induced contrails can be mitigated against an increased fuel consumption of less than 1.5%. The marginal costs of contrail mitigation are shown to be non-uniform. The more contrails are avoided, the higher the fuel burn penalty becomes. It might therefore be more cost effective for commercial aviation to implement a partial 'contrail-reduction' plan rather than a 'zero-tolerance on contrail' strategy.

The great merit of implementing flexible free flight contrail mitigation in commercial aviation has been shown. This study presents an academic methodology potentially forming the basis for a commercial tool, to be used for scheduling of environmental optimal trajectories throughout the aviation sector. This would enable airliners to optimise their fleet movements while accounting for both economic and ecological impact factors.

Acknowledgements

Met dit schrijven tracht ik mijn Master's graad te behalen aan de faculteit Lucht- en Ruimtevaart van de Technische Universiteit Delft. Ik wil me graag richten naar allen die mij geholpen hebben, bij het tot stand komen van deze thesis, dan wel gedurende de lange aanloop die daaraan vooraf gegaan is. Allereerst wil ik graag Dries Visser en Sander Hartjes bedanken, bij wie ik afgelopen 1,5 jaar op elk moment aan heb kunnen kloppen voor advies. Bedankt voor de tijd en moeite die jullie gestoken hebben in het begeleiden van mij gedurende mijn afstuderen. Daarnaast wil ik de ATO afdeling en de faculteit Lucht- en Ruimtevaart bedanken voor het faciliteren van een prachtige studie.

Verder wil ik bedanken: mijn verdieping-genoten en mede afstudeerders. Bedankt voor het brainstormen, meedenken, checken, de koffie en het samen eten, en natuurlijk voor de gezelligheid. In het bijzonder Zhong, Victor en Collin.

Mijn huisgenoten met wie ik zo gezellig in de GR heb gezeten, bedankt. In het bijzonder: Tjeerd, aan wie ik moet toekennen dat het direct afspoelen van de vaat wel degelijk voordelen kent. Koen, dankzij wie ik de ware betekenis en schrijfwijze van batsjas ken. Thijs, met wie je op elk moment van de nacht nog een filmpje aan kan zwengelen.

Daarnaast wil ik alle BBQ'ers, Koffieleuters, Studiegenoten, DUTers, Proteëers, T.A.'s, Brabo's, Borrelaars, Paalzitters en Reizigers bedanken voor de mooie gesprekken en de belevenissen. In het speciaal wil ik nog aantal vrienden bedanken: Mark, want Brabantse nachten zijn lang. Luc, met wie ik voor de rest van mijn leven een gedeelde jeugd zal hebben. Lucas, wiens vastberadenheid altijd inspiratie biedt. Niet eerder heb ik iemand gelanceerd met de kracht als waarmee ik jou lanceerde bij het Valkhof. Hugo, die zich door geen enkele hoeveelheid regen zal laten weerhouden te BBQ'en. Willem, die als puntje bij paaltje komt op de eerste rij zit te genieten van het zonnetje. Gerwin, voor wie geen shoarma berg te hoog en geen lasagna schotel te diep is. Julius, met wie ik een schijnbaar oneindige race naar de eindstreep heb gehad. Hierbij gefeliciteerd met je overwinning.

Ik wil mijn familie bedanken, omdat ze altijd voor mij klaar staan. De Uppies omdat ze me met huis en haard opgenomen hebben in de familie. Opa Harrie en Oma Gerda, voor de verhalen en mooie reizen die ik met jullie heb mogen maken. Oma Riet, omdat ik altijd aan heb kunnen waaien voor een kopje thee of worstenbroodje. Mijn nichtjes Elisa en Madelief en neefje Harrie, die een onuitputtelijke hoeveelheid blijdschap uitstralen. Mijn zwagers Gijs en Ben, voor het delen van hun huis en (Nieuw) Zeeuwse thuisland. Janneke, één van de meest sociale en attente personen ter wereld. Eva, bij wie ik altijd geruststellend advies heb kunnen halen. Pap, van wie ik heb geleerd kritisch na te denken. Mam, wiens eerlijkheid ongeëvenaard is. Bedankt voor jullie geduld en vertrouwen.

Als laatste wil ik natuurlijk Emmy bedanken, met wie ik alles kan delen, omdat je altijd in mij gelooft en omdat het een voorrecht is 's ochtends naast jou wakker te worden.

Bij dezen wil ik mijn scriptie opdragen aan Adrianus Theunisse. Voor de fietstochten en de belevenissen, de verhalen en de inzichten, het schúpe en het ritselen, je onbevangenheid en aanstekelijke enthousiasme en voor het openen van mijn ogen naar een wereld waarin alles mogelijk is.

Delft, University of Technology — T. Hendriks
April 2015

Dedicated to:

Adrianus Theunisse
For teaching me to Perceive.

Contents

Nomenclature

Acronym /Symbol	Meaning	Units
δ	Pressure over mean sea level Pressure	*[-]*
$\dot{Con}$	Contrail-Time change	*[s/s]*
$\dot{m_f}$	Fuel burn	*[kg/s]*
η	Overall Efficiency	*[-]*
γ	Flight path angle	*[rad]*
Γ	Normalized throttle setting	*[-]*
λ	Longitude	*[rad]*
μ	Bank angle	*[rad]*
ϕ	Latitude	*[rad]*
ψ	Heading angle	*[rad]*
ρ	Density	*[kg/m^3]*
θ	Temperature over mean sea level Temperature	*[-]*
ε	Ratio of molecular masses of water and air	*[-]*
AFWA	Air Force Weather Agency	
AMS	Amsterdam Schiphol Airport	
ang	Angle	*[rad]*
ATO	Airline Transport and Operations	
BFS	Belfast International Airport	
$c.\gamma$	Isentropic expansion factor	*[-]*
c_p	Isobaric specific heat	*[$J/(kgK)$]*
CAS	Calibrated Air Speed	*[m/s]*
Con	Contrail-Time	*[s]*
$Contrail$	Atmospheric contrail data	*[%]*
D	Drag	*[N]*
DEA	Differential equations	
DLR	Deutsches zentrum für Luft- und Raumfahrt e.V.	
DOC	Direct Operating Cost	
$dTdz$	Temperaure derivative over altitude	*[K/m]*
ECMWF	European Centre for Medium-Range Weather Forecasts	
EI	Emission Index	*[-]*
F	Force	*[N]*
FL	Flight Level	
G	Mixing Line gradient	*[Pa/K]*
g_0	Gravity Constant Earth	*[m/s^2]*
GPM	Gauss Pseudospectral Method	
GPOPS	General Pseudospectral OPtimal control Software	
HND	Tokio, Haneda Airport	
IPCC	Intergovernmental Panel on Climate Change	
ISA	International Standard Atmosphere	
ISSR(s)	Ice Super Saturated Region(s)	
KIAD	Washington Dulles Airport	

(Continued)

Acronym /Symbol	Meaning	Units
Lagrange	Lagrange cost (Time dependent)	
M	Mach	*[-]*
Mayer	Mayer cost (Final)	
NASA	North American Space Agency	
NLP	Non Linear Program	
NWP	Numerical Weather Prediction	
Obj	Objective	
p	Pressure	*[Pa]*
PCP	Persistent Contrail Probability	*[%]*
p_{sat}^{L}	Liquid saturation pressure	*[Pa]*
PEK	Beijing Capital International Airport	
Q	Specific heat	*[MJ/kg]*
R_{gas}	Specific gas constant (dry air)	*[J/kg · K]*
R_e	Radius Earth	*[m]*
RCP	Representation Concentration Pathway(s)	
RF	Radiative Forcing	*[W/m²]*
RH	Relative Humidity w.r.t. Water	*[-]*
RHI	Relative Humidity w.r.t. Ice	*[-]*
Rhi	Relative Humidity w.r.t. ice	*[-]*
RPK	Revenue Passenger per Km	
SFC	Thrust Specific Fuel Consumption	*[g/(kNs)]*
$sRHw$	Specific Relative Humidity w.r.t. Water	*[kg/kg]*
sw	Switch function	
t	Time	*[s]*
$t_{Contrail}$	Contrail-Time	*[s]*
T	Temperature	*[K]*
T_{LC}	Threshold temperature for varying relative humidity conditions	*[K]*
T_{LM}	Threshold temperature for a relative humidity of 100%	*[K]*
TAS	True Air Speed	*[m/s]*
u	Control vector	
UTC	Coordinated Universal Time	
V	Velocity	*[m/s]*
v_{snd}	Speed of sound	*[m/s]*
W	Weight	*[N]*
WGS84	World Geodetic System 1984	
x	State vector	
z	Altitude	*[m]*

Subscript

Subscript	Meaning
0	Initiation/zero/sea level
CAS	Calibrated Air Speed
CO_2	w.r.t. Carbon Dioxide
contr	Contrail Critical
Contrail-Fuel	Applicable for optimisation w.r.t. Contrail Fuel
Contrail-Time	Applicable for optimisation w.r.t. Contrail Time
CostIndex	Applicable for optimisation w.r.t. the specified Cost Index
drift	Wind induced drift, deviation of aircraft heading
f	Final
Fuel	Applicable for optimisation w.r.t. Fuel
ground	With respect to ground
H2O	Water
i	Ice
l	Liquid water
mach	Mach
min	Minimum
mo	Maximum operating
TAS	True Air Speed
Thrust	Thrust
Time	Applicable for optimisation w.r.t. Time
w	Wind
w_{abs}	Wind absolute
wU	Wind in East direction
wV	Wind in North direction

List of Figures

List of Tables

Introduction

In this section first the background and rationale for this research problem is set out, after which the research question and objectives will be introduced. This section will conclude with an outline of the report structure.

1.1 Background and Rationale

Aviation is known to have a significant contribution with regards to anthropogenic air pollution and climate forcing. The impact is caused by emissions, aerosols and from the changes in cloudiness in the upper troposphere[12]. Within the ATO group extensive research has led to the development of a multi-phase/multi-criteria trajectory optimisation framework supporting the synthesis of green mission profiles, establishing optimised aircraft routing with respect to noise and emissions[61]. The purpose of this project is to evaluate the cost and benefits associated to 4D flight trajectory optimisation with the intention of mitigating contrail formation. Condensation trails, or contrails, occur behind aircraft flying in sufficiently cold air, they appear due to ice crystallisation of the condensation of water vapour, emitted from the exhaust. Contrails evaporate if the ambient air is dry, but they persist and can even evolve into cirrus clouds, in case the ambient air has a sufficiently high humidity level. Evolution of contrails into cirrus clouding occurs due to the deposition of ambient water vapour onto the already present ice particles, whereby the size of the ice particles grows. This evolutionary phase is an important, but poorly understood phenomenon[48].

Contrails have been studied since 1919 [46], the foundation for current day contrail research was however established in 1953, in the theories as described by Schmidt and Appleman [8]. With stealth being an important characteristic for any combat aircraft[63], the United States military forces have been interested in contrails ever since aircraft capable of flying at high altitudes have entered their inventory. Contrails form an irrefutable proof of the presence of aircraft and thereby impair the survivability of an aircraft. The presence of contrails enhances visual contact, by showing the number and spacing of the engines it can reveal aircraft type[6]. The importance of contrail research to aviation in this project is however more so related to its apparent climate impact. According to NASA[37]: *"Even small changes in the abundance or location of clouds could change the climate more than the anticipated changes caused by greenhouse gases..."* In fact, contrail cirrus is responsible for the largest single radiative forcing component associated with aviation[12]. The biggest properties for contrail induced climate change are due to changes in regional and global cloud cover, optical properties, radiative forcing and possible effects on the atmospheric composition and the hydrological cycle[48, 27]. Aircraft induced line shaped contrail cirrus may evolve into cirrus clouds, which are more extensive in scale and are no longer distinguishable from naturally occurring cirrus[27]. Radiation forcing related to this overarching contrail induced cirrus clouding is about nine to ten times larger than that from the initial line-shaped contrails alone[12, 35]. Especially in regions with a high air-traffic density, the increase of cloud cover in situation favouring contrail formation is significant[48].

Research has indicated the propulsive efficiency to have a large effect on the threshold conditions at which contrail will form. Higher efficiencies will result in contrail formation at higher ambient temperatures and over a wider range of flight altitudes[47]. In the likely case the historic trend of improving propulsive effi-

ciencies for aero engines will continue [30], contrail formation in the future will start under less restrictive conditions and with it the importance of contrail mitigation will increase[27]. This, in combination with other factors such as, alterations in atmospheric temperature and humidity, the possible increased usage of aircraft fuels with higher hydrogen content and the obvious effects of increases in absolute air traffic[27], are bound to affect the importance of contrail mitigation. The irrefutable effect of contrails are yet to be determined, this will however not be the main focus of this study. This study will accept the current academic stance on the impact of contrails, as presented by the IPCC[27], and will focus on finding a viable strategy, by means of which the impact of contrails, can be mitigated.

Previous literature investigating contrail mitigation has indicated the great potential by means of alterations to the flight trajectory. Mannstein et al.[21] for instance indicates that "a substantial fraction of contrails and contrail induced cirrus can be avoided by relatively small changes in flight level"[21].

Several studies have already been performed into the implementation of flexible free flight for contrail mitigation. Noppel[39], has in his dissertation for instance used a generally parametrized optimisation routine to investigate the large scale affects of contrail mitigation strategies being implemented by general and commercial aviation. In his dissertation, Noppel applies his tool to a year long data record of transatlantic flights between New York and London to investigate the large scale effects of his contrail mitigation strategy[39]. The results are meant to give an indication of the large scale effects of contrail mitigation being generally implemented. The results are not truly accurate and his research is not applicable to optimisation of individual flights.

In Sridhar et al.[38], a trajectory contrail mitigation study was performed in the presence of wind, optimising for minimum fuel consumption. The optimal aircraft heading is calculated in a 2-dimensional plane and the study does not represent truly flexible free flight[38].

In Kaiser[33] a short-haul flight profile optimisation was presented maximising specific range while minimizing contrail production. In this study changes to the en-route flight altitude were allowed even though a flight altitude ceiling was implemented.

All of these studies indicate large amounts of contrail can be prevented at the cost of a few percentage points additional flight time and fuel burn. In section 3.4, a more elaborate representation of the key differences between these studies and the study presented herein will be discussed.

The focus of this study will be the modelling of contrail formation and its implementation in an optimisation framework. Conducting an optimising of individual flights by means of altering the four dimensional flight trajectory, thereby opting for both horizontal and vertical manoeuvring, in order to evade areas prone to contrail formation.

1.2 Research Question, Aims and Objectives

In this section the outline of the problem will be presented. What is the main question and objective of this research study and what are the goals?

Research Question:
Is it possible to develop an appropriate tool which can be used to optimise aircraft trajectories, weighing the mitigation of contrail formation versus economic and environmental factors, using realistic atmospheric data, within the dynamic optimisation framework presented in [14].

Research Objective:
The objective of this research is to develop a methodology optimising the socio-economic costs of an aircraft trajectory while mitigating the effects of contrail formation and to implement it in an existing dynamic optimisation framework.

The main goals:

1. Develop and validate a methodology to optimise a flight trajectory with regards to the formation of contrails and other relevant socio-economic parameters such as fuel cost and flight time.
2. Implement the methodology in the existing dynamic optimisation framework GPOPS[14] and verify its correct implementation.
3. Perform relevant case studies optimising flight trajectories whereby contrail formation is mitigated.
4. Gain a thorough understanding of the cost and benefits involved with various types of flight trajectory alterations in order to mitigate contrail formation.
5. Assess whether it is both economically and technically feasible to mitigate contrail formation by alterations in the flight trajectory.

The sub goals:

- Evaluate existing theories on the physics of contrail formation and select the most suitable theory with respect to feasibility, accuracy, availability of input data and processing time.
- Develop a contrail formation model from the selected theory.
- Implement and integrate the contrail model in the trajectory optimisation framework.
- Verify the contrail optimisation with known contrail data or existing prediction tools.
- Analyse and implement the trade-off criteria by which the optimisation will weigh contrail formation against other socio-economic and environmental factors.
- Evaluate the optimisation model with predetermined experimental benchmark cases.

1.3 Report Structure

In chapter 2 the theory behind contrail formation, persistence and evolution, as well as the methodology used to model contrails will be discussed. In chapter 3 the rationale for contrail mitigation and the current understanding of how contrails affect us will be presented. Chapter 4 elaborates upon a number of modules within the optimisation structure and how they have been integrated within the GPOPS optimisation framework. An overview of the optimisation structure, the GPOPS optimisation framework, the aircraft model and the path constraints, the contrail model, the atmospheric module, the cost functional and the parameter tradeoff will all be discussed. Next to the function of the modules the way in which they have been implemented and integrated into the framework will also be presented. In chapter 5 the correct implementation and integration of the various modules will be verified. Chapter 6 gives a clear picture of the set up of the experimentation and test cases, and will give some additional information on the meteorologic input data used. In chapter 7 the results for the various test cases will be presented. Some Time and Fuel burn dependent test cases will be presented, with and without wind affecting the model. The results of several Cost Index flight optimisations will be combined into a sensitivity study, in which the interaction between costs and contrail mitigation will be analysed. In chapter 8 the results will be discussed and briefly compared to the results as presented in scientific literature. Finally, both the conclusions of this study as well as the recommendations for future research will be presented in section 9.

Contrails

In this chapter the theory and characteristics of contrail formation will be discussed. The terminology will be explained as well as the conditions under which contrails can form. Methods to map the evolution of contrails throughout their life cycle will be explained.

2.1 An Introduction to Contrails

This section is meant to briefly introduce the reader with definitions and key concepts of contrails. This has been done in order to visualise the concepts and can benefit the reader throughout the rest of this thesis.

Condensation trails, or contrails, sometimes occur behind aircraft. Whether these contrails occur and how long they remain visible in the air depends on both ambient atmospheric conditions and engine related combustion characteristics[6, 48]. When discussing contrails two terms may be used to distinguish between contrails, images of these two distinct types of contrail can be seen in figure 2.1.

- Threshold or Non-Persistent contrails: short lived contrails, occurring when the ambient air is dry and not sufficiently cold. Threshold contrails evaporate quickly and are not considered to be environmentally harming[39]. In this case contrails disappear after seconds to minutes, which can range to distances of one to several kilometres behind the aircraft[46].
- Persistent contrails: occur in case the ambient humidity is above its saturation levels over ice surfaces i.e, the relative humidity over ice has to be larger than 100% (RHI $\geq$ 100%). In these ice-supersaturated air masses, the ice particles within the contrails grow by deposition of water vapour molecules from the ambient air. Contrails may last as long as the surrounding air remains at least ice-saturated[46]. Contrary to threshold contrails, persistent contrails do affect the environment.

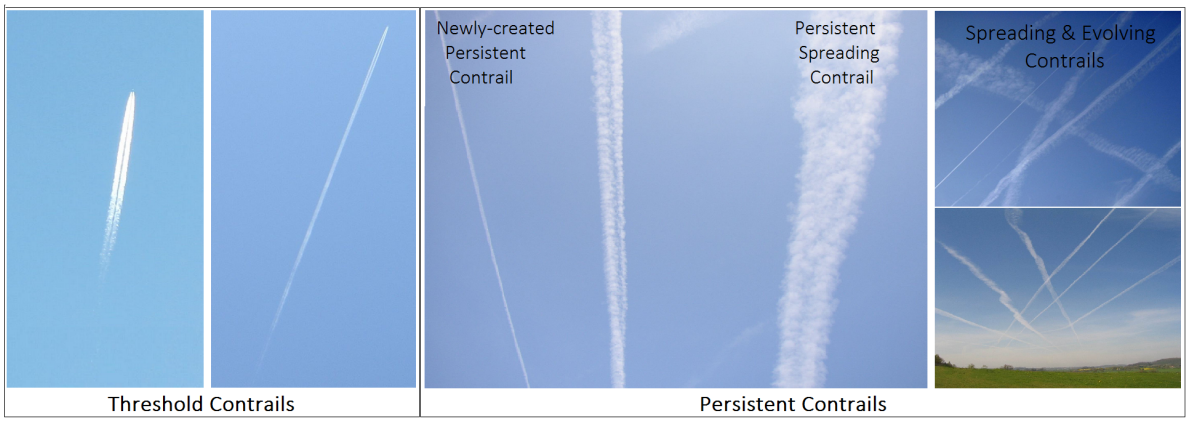

Figure 2.1: Comparison of different types of Contrail. The photo's are obtained from[34]

Some other contrail related definitions, used in this thesis are:

- Line-shaped contrail: Persistent contrail, not yet evolved enough, to have lost its distinctive line shape.
- Spreading & Evolving contrail: Persistent contrail, spreading out under the influence of wind and shear effects. In ice-supersaturated conditions the ice crystals will form a catalyst for additional ice crystallisation. May be anywhere in the transition between a Line-shaped contrail and Contrail-cirrus clouding.
- (Natural) cirrus clouding: Naturally occurring type of high altitude clouding.
- Contrail-cirrus clouding: Anthropogenic cirrus clouding originating from a spreading and evolving contrail, no longer discernible from naturally occurring cirrus clouding.
- Secondary-cirrus clouding: Cirrus clouding, anthropogenically formed due to locally increased soot and aerosol concentrations, emitted by aircraft. These additional nuclei are catalysts from which ice crystallisation and so clouding can spread.

In short, contrails can persist for varying periods of time. They can spread and evolve into cirrus clouding, and at the same time coexist with natural occurring cirrus. With aircraft flying at different altitudes, this interaction can occur at a multitude of different altitude layers. The combination of all of this can lead to panoramas, as visualised in figure 2.2, in which newly created line-shaped contrails, evolving contrails, contrail-cirrus and natural-cirrus can all be seen at the same time.

Figure 2.2: Cirrus clouded sky over Rotterdam, natural clouding can no longer be discerned from evolved anthropogenic contrail-cirrus[41].

2.2 Contrail Model

In this section the theory behind contrail formation will be discussed. The theory will be illustrated with the use of the applied contrail model, established by Schumann.

2.2.1 *Thermodynamics of Contrail Formation (developed by Schumann)*

Contrail formation is dependent on ambient pressure (P), ambient humidity (RH), ambient temperature (T), the combustion properties of hydrogen containing fuels with air and the ratio of water vapour to heat discharged by the aircraft's engines[6, 48].

In 1996 Schumann[48] did a re-examination of the contrail formation theory as developed by Schmidt and Appleman[8], who until then were seen as the most significant authorities in the field of contrails. In his work, Schumann included the partial conversion of combustion heat into kinetic energy of the air movements in the wake of aircraft, causing higher critical temperatures required for the formation of contrails. In this section Schumanns[48] version, of this so called Schmidt-Appleman criterion, will be discussed.

A geometrical visualisation of the thermodynamic process of contrail formation can be seen in figure 2.3. The saturation pressure lines indicate whether liquid or frozen water will evaporate or not. In case conditions fall below the water saturation pressure, air will not be saturated and liquid water will evaporate, if conditions falls above the water saturation pressure line, the air will have become saturated.

The blue line represents the critical mixing line. It runs from the engine exhaust conditions (A) and runs tangential to the water saturation pressure line (green line). Temperature conditions of air leaving the engine exhaust normally far exceed ambient conditions and point (A) therefore falls outside the scope of the graph. The slope of this critical mixing line is equated to parameter G. Point T_{LM} (red marker) represents the critical temperature for ambient conditions with a relative humidity of 100%, in case the temperature falls below this point contrails can occur. Point T_{LM} is located at the intersection of the critical mixing line and the water saturation pressure line.

Point T_{amb} (red marker) represents the ambient atmospheric conditions and has a certain RH. To evaluate whether contrails occur under ambient conditions, the critical temperature needs to be derived for RH_{amb}. Point T_{LC} has the same relative humidity as the ambient atmosphere and is therefore located at the intersection of the critical mixing line and the relative humidity pressure line at ambient conditions (not shown). Contrails will occur in case the ambient temperature T_{amb} falls below the critical temperature T_{LC}.

The actual mixing line for ambient condition T_{amb} runs directly from the exhaust conditions (A) (thin dashed blue line). This mixing line can be seen to cross the water saturation pressure line, indicating that at some point moisture will turn from its gaseous state into liquid water and ice, hence contrails will form.

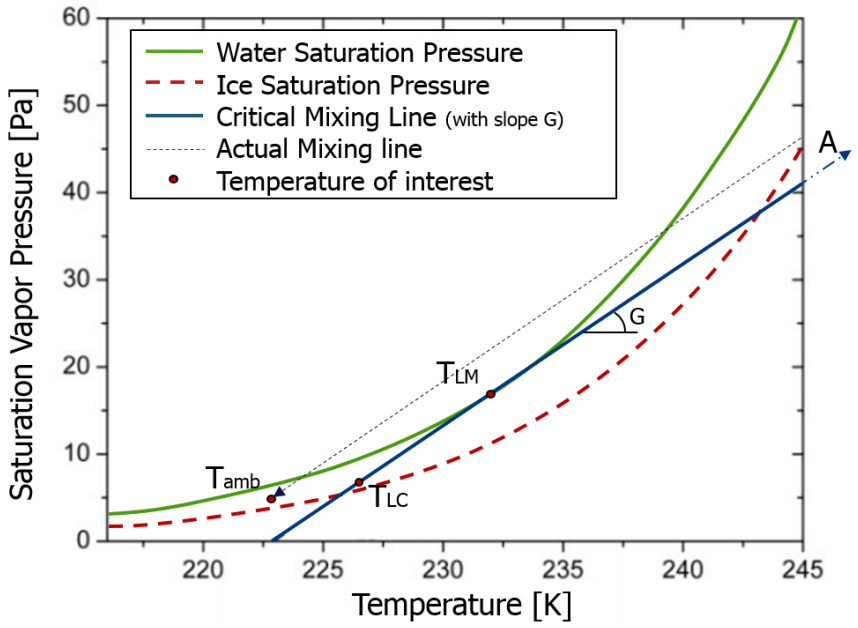

Figure 2.3: Geometrical analysis of contrail formation, water pressure v.s. temperature.

The threshold temperature (T_{LC}), from which contrail formation occurs, depends on the ratio G (PaK^{-1})

and the relative humidity level of the ambient air (RH). The ratio G describes changes in water vapour pressure and temperature during mixing and can be determined using equation 2.1.

$$G = \frac{EI_{H_2O} \cdot c_p p}{\varepsilon Q(1-\eta)} \tag{2.1}$$

In equation 2.1, c_p $(J(kgK)^{-1})$ represents the specific heat at constant pressure and ε the ratio of molecular masses of water and air and p the ambient pressure (Pa). The combustion related parameters in equation 2.1, represent the additional amount of heat and moisture added to the exhaust air due to combustion. These are: the emission index of water vapour EI_{H_2O} (gr/kg), the propulsion efficiency related to the jet engine and aircraft configuration η and the specific combustion heat Q $(MJkg^{-1})$ [1]. The combustion related parameters indicate the effects of specific fuels and aircraft characteristics on contrail formation[46].

The local slope of the saturation curve with respect to water can be equated to this ratio G, and by doing so the parameter G can be used to determine the gradient of the critical mixing line. In case the slope of a mixing line is higher than that of the critical mixing line, contrails will occur, in the case the slope is lower, contrails will not form. An attempt to geometrically visualise this distinction, has been made in figure 2.3.

$$\frac{dp^L_{sat}(T_{LM})}{dT} = G \tag{2.2}$$

In equation 2.2, p^L_{sat} is the saturation pressure with respect to liquid water and T_{LM} is defined as the critical temperature for a relative humidity of 100%. The critical temperature T_{LM} (K) is derived by Newton iteration, for which equation 2.3 provides a good first approximation. The temperature $T_0 = 273.15$ represents absolute zero Kelvin and transforms the output to the Kelvin scale.

$$T_{LM} = T_0 - 46.46 + 9.43ln(G - 0.053) + 0.720[ln(G - 0.053)]^2 \tag{2.3}$$

The critical temperature under varying relative humidity conditions with respect to water can be obtained through equation 2.4. The parameter $e_{LM}(T_{LM})$ stands for the water pressure for the to-be-derived temperature T_{LM}. The estimation of the relative humidity with respect to water and ice will be described in the next section in equation 2.7.

$$T_{LC} = \frac{T_{LM} - [e_{LM}(T_{LM}) - RH \cdot e_{LM}(T_{LM})]}{G} \tag{2.4}$$

Despite of Schuman's adaptations to the original methodology this criterion is called the Schmidt-Applemann criterion and can see equation 2.5.

$$T_{amb} \leq T_{LC} \tag{2.5}$$

In short, this theory predicts the critical temperature T_{LC} from which contrails can form. Contrails can form in the cases were the ambient atmospheric temperature is colder than the critical temperature.

The probability for contrail formation increases for mixing conditions with higher values of G, resulting from alterations in the engine exhaust conditions such as, engines with higher propulsive efficiencies (η)[39] or fuels with a higher hydrogen to carbon ratio[49]. Higher values for G give the critical mixing line a steeper slope and make it more likely the mixing line will cross the water vapour pressure saturation line. This could be visualised in the geometrical analysis, by a steeper critical mixing line, running from a new engine exhaust

[1] The following constants were used for the contrail analysis:
$c_p = 1004J(kgK)^{-1}$
$\varepsilon = 0.622$
$EI_{H_2O} = 1223gr/kg$, for typical fuels with 13.8% hydrogen fraction
$\eta = 0.35$ taken as constant
$Q = 43.2MJkg^{-1}$, typical for Kerosene

conditions (A', not shown) which would enter the graph frame at a higher saturation vapour pressure. These steeper critical mixing lines will therefore allow for higher critical temperatures and hence contrail formation will occur under less stringent conditions.

For kerosene fuelled aircraft, G typically falls within the range $(0.6 - 4PaK^{-1})$. Larger values of G occur for fuels with larger water mass contents (EI_{H_2O})[49], making contrail formation specifically interesting in the case more aircraft start to fly on hydrogen fuels, or other fuels with lower carbon content.

Anticipating the phasing out of older engines, the propulsive efficiency was fixed at 0.35 throughout this study, this is in line with current engines in use. Disconnecting the assessment of the propulsive efficiency from the engine model, made it possible to pre-process the contrail data. Removing the contrail analysis from the simulation and optimisation loop decreased the computation power required.

Besides Schuman's model, Schrader[45] has also presented a method to predict contrail formation. This method is similar to Schumann's approach, but it differs in the way the critical slope is derived, which is the point of the critical mixing line tangent to the water saturation vapour pressure curve. For this research it was decided to use the method as specified by Schumann[46], which has seen widespread application throughout the scientific community.

2.2.2 *Relative Humidity and Contrail Persistence*

The equations in the previous section describe the initial formation, but do not indicate the contrail's persistency. Contrails evaporate quickly in the case the ambient air is dry, however they persist and evolve into extended cirrus clouds and grow in the case the ambient air is sufficiently humid, allowing the particles size to grow by deposition of water vapour on the contrail ice particles[48]. For contrails to persist and grow for longer times (up to hours), a supersaturated atmosphere is required with respect to ice (ISSR). An ice supersaturated atmosphere is one were the ice saturated pressure has been reached and surpassed, indicating ice particles will not sublimate once formed. Persistent contrails will transform into threshold contrails, and start to decay, in case the atmospheric ice saturation falls below RHI=100%. Figure 2.4 shows a water phase diagram, similar to the one as seen in the previous section. The critical mixing line (blue) defines the critical formation temperatures at which contrails can occur and is tangent to the water-saturation pressure line (green). The formation of persistent contrails occur, if the conditions of the ambient atmosphere falls within the "persistent" area (orange), as in this case the mixing line would cross the water saturation pressure line. Persistent contrails therefore occur when ambient conditions fall above the ice and below the water saturation pressure line.

A threshold contrail will occur if the ambient atmosphere will fall within the "non-persistent" area (cyan) as seen in figure 2.4. This is the case when ambient conditions fall below the ice saturation pressure line and temperatures are still below the critical temperature, for which non-persistent or threshold contrails will occur. When threshold contrails occur, ice particles formed during the mixing of the exhaust and ambient air will sublimate until the contrail has dissolved[39]. As mentioned, this study will focus on the persistent type contrail formation.

In order to analyse the persistence of contrail formation the following procedure is used. The saturation pressure over liquid water p_{sat}^{L} is derived for local conditions using equation 2.6, expressed in (Pa) with the ambient temperature T_{amb} in (K) [54].

$$p_{sat}^{L} = 100 \cdot e^{-6096.9385/T_{amb}+16.635794-0.02711193 \cdot T_{amb}+1.673952 \cdot 10^{-5} \cdot T_{amb}^{2}+2.433502 \cdot ln(T_{amb})} \tag{2.6}$$

The relative humidity over liquid water RH can be approximated by equation 2.7. The parameter $sRHw$ represents the specific humidity with respect to water $(kg \cdot kg^{-1})$[17]. Finally, in order to check the contrail for persistence, the relative humidity with respect to ice RHI needs to be derived. The RH and ambient temperature T_{amb} (C^o) measurements can be used to compute RHI this can be achieved using equation 2.8. The numerator on the right hand side of the equation 2.8 is the saturation vapour pressure over water, the

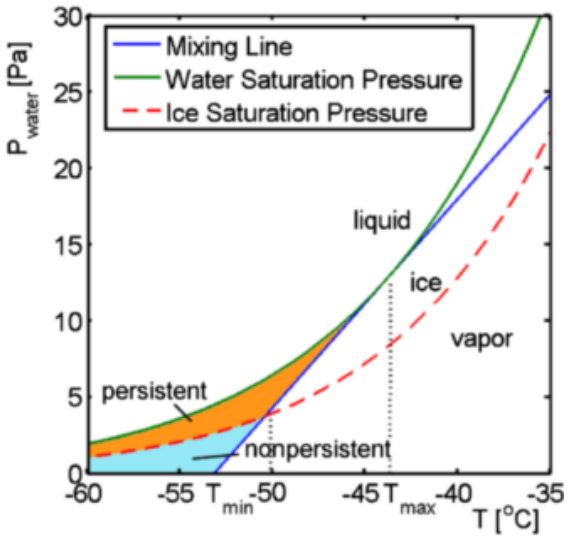

Figure 2.4: Critical contrail formation temperatures [39], indicating the saturation pressure lines (water=green, ice is dashed red) and critical mixing line (blue).

denominator is the saturation pressure over ice[7, 17].

$$RH = 100 \cdot sRHw \cdot p/((EI_{H_2O} + (1 - EI_{H_2O}) \cdot sRHw) \cdot p^L_{sat}(T_{amb})) \tag{2.7}$$

$$RHI = RH \cdot \frac{6.0612e^{18.102 \cdot T_{amb}/(249.52+T_{amb})}}{6.1162e^{22.577 \cdot T_{amb}/(273.78+T_{amb})}} \tag{2.8}$$

With the RHI known, the atmospheric conditions can be analysed for contrail persistent formation. In case the before mentioned Schmidt-Appleman criterion, presented in equation 2.5, is satisfied, contrails will occur. The persistency of the contrail is analysed using the criterion specified in equation 2.9.

$$RHI \leq 100\% \tag{2.9}$$

2.3 The Characteristics of Contrail Formation

In this section a brief introduction into ice crystallisation and ice super saturated regions will be made. After which the impact of these on contrail formation will be discussed.

2.3.1 *Ice Crystallisation and Ice Super Saturated Regions*

In recent years it has become clear that cloud free air in the upper troposphere is often in a thermodynamic state of supersaturation with respect to ice. These are the regions were persistent contrail formation can occur and they have been termed “ice supersaturated regions” (ISSR’s)[52].

A study by Jensen et al.[23] makes use of measurements to correlate environmental conditions with contrail formation and persistence and validate the current theories. The results are consistent with the theory assuming that liquid saturation must be reached in the plume for contrail formation. Contrails may persist for as long as the ambient air in which the contrail forms remains ice saturated, also in a weakly saturated air. Whenever contrails occur at temperatures over -44 degrees Celsius, they will be forming in (substantially) supersaturated air with respect to ice and should be able to persist and grow. In case the

ambient air is not saturated with respect to ice, contrails dissipate rapidly at the moment aircraft vortices become unstable and break up.

Humidity data was gathered from instruments installed on commercial airliners as part of the MOZAIC research study[52] in the period of 1995 to 1997. The results indicate a mean ice supersaturation of around 15% and 2% in the troposphere and stratospheric measurements, respectively. Ice supersaturated regions are 3 to 4 K colder and contain more than 50% more vapour than other regions in the upper troposphere. MOZAIC measurements have indicated that modern airliners are flying through ice supersaturated air about 15% of the flight time. Though these measurements are mainly obtained between Europe and North America, the exponential relation of the humidity distribution will most likely be valid globally[52].

According to Gierens et al.[52], spontaneous ice crystallisation, the natural form of cirrus cloud formation, requires a supersaturation with respect to ice of on average 30%. Which is close to conditions necessary for the homogeneous freezing of droplets, for which a supersaturation of 45% to 65% is required[50]. The formation of heterogeneous nucleation, the ice crystallisation around an existing nucleus(e.g. emitted particles), requires a RHI of 110% or more[58]. A summary of these numbers can be seen in table 2.1. Anthropogenic perturbations in the composition of the atmosphere, caused by for instance aviation, can lower the RHI levels from which ice crystallisation occurs. For the particles with longer life spans, this effect plays a major role in the appearance of secondary-cirrus, where cirrus clouding otherwise would not have formed, in regions with high air traffic densities[39]. Next to this aircraft engines emit vast amounts of water into the air. This temporarily raises the RHI, a steep relative humidity peak occurs seconds after the air has been emitted, enough to initiate ice crystallisation, this will be shown in the next section in figure 2.5. Once the wake vortex collapses and ice crystals spread out, they form catalysts for further crystallisation[29]. This thereby explains the frequent occurrence of cloudless regions were aircraft generate persistent contrails when they fly through it.

The vertical structure of the ambient relative humidity layers in the atmosphere could be very important for contrail persistence. Several measured cases indicated contrails forming in narrow vertical or small patches of high humidity. In case contrails form over a level of very dry air, ice will sublimate as soon as the crystals grow large enough to begin sedimentation[23, 48]. The study indicates several cases in which large areas of ice supersaturated regions existed in ambient air, with either diffuse or no cirrus present. The lack of cirrus in these regions indicates a lack of nuclei present around which ice crystallisation can start. These areas and upper tropospheric clouds are prone to contrail formation and may be very sensitive to the introduction of heterogeneous nuclei[52, 23].

Table 2.1: Relative humidity requirements for initial Ice crystallisation

Ice crystalisation condition	RHI [%]	
Homogeneous nucleation	≥ 145 or 165%	[50]
Natural nucleation (Cirrus)	$\geq 130\%$	[52]
Heterogeneous nucleation (Contrails)	$\geq 110\%$	[58]

2.3.2 *Contrail Formation*

The parameters, which determine whether or not the wake of an aircraft becomes saturated and contrails form, fall into two classes. Three of the parameters: Pressure (P); Temperature (T) and Relative Humidity (RH), are environmental parameters. The other one is an aircraft related parameter namely, the combustion properties of hydrogen containing fuels with air, and the ratio of water vapour to heat injected[6, 48].

The Schmidt-Appleman criterion as implemented by Schumann and presented in section 2.2, forecasts contrail formation thermodynamically. Contrail formation is caused by the increase in relative humidity (RH) from the engine exhaust with the cool ambient air. This mixing of heat and water vapour, from the hot and moist air leaving the engines, in combination with the non-linear increase in saturation humidity and temperature, results in contrails. In the case the ambient atmosphere is cold enough, humidity may reach liquid saturation in the exhaust plume trailing the aircraft. If this is the case liquid water droplets

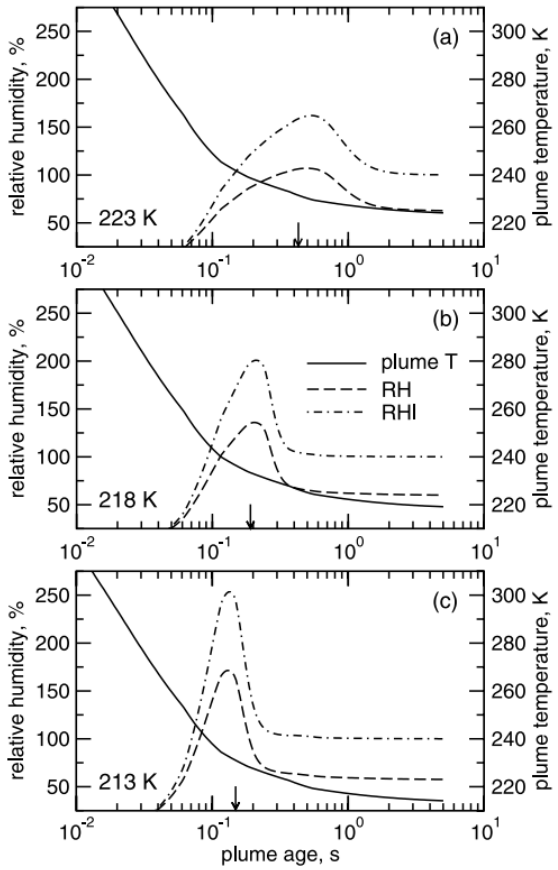

Figure 2.5: Evolution of plume temperature (solid),relative humidity over water (RH, dashed) and ice (RHI, dot dashed) as a function of plume age for ambient atmospheric temperatures of (a) 223 K, near the contrail threshold temperature, (b) 218 K, close to the mean temperature at mid-latitude upper tropospheric flight levels, and (c) 213 K, a temperature found commonly at high latitude flight routes. The arrows on the plume age axis indicate the start of ice formation in contrails[29].

will form, due to condensation of water vapour on soot and volatile particles in the exhaust plume, and ice crystallisation will occur[48].

In Figure 2.5 the evolution of the plume temperature and relative humidity over liquid (RH) and ice (RHI), as a function of time, is shown for 3 varying ambient atmospheric temperatures. It projects the before mentioned processes of contrail formation in the exhaust plume. A small arrow on the vertical axis, marks the initiation of ice crystallisation. The start of ice crystallisation coincides with the peaking of RHI, occurring when the plume age is between $t = 10^{-1}$ and $10^{0}s$. The high levels of RH can only be seen in this short initial phase, when the air has shortly before left the engine and is cooling down rapidly. After this short period during which the emitted air is mixed, the RHI levels settle down to more stable levels. In the threshold case (a), RH only slightly overshoots water saturation when ice particles start to form. In colder conditions, the plume cools faster due to colder ambient air being mixed with the exhausts, resulting in a steeper rise of the RH and RHI curves, with higher maxima and an earlier start of contrail formation[29].

In figure 2.6, the altitude prone to contrail formation is depicted. In this figure the international standard atmospheric temperature(ISA) is set out against the altitude (line). Next to this, the lines with varying RH's can be seen (dashed). These RH lines depict their respective critical temperature from which contrail formation can occur in the jet exhaust trail. As the atmospheric humidity, with respect to liquid, must always be

between 0 and 100 percent, the graph can be divided into three sections. In the case the ambient temperature line falls below or left of the 0 percent line, contrails should always form, regardless of air humidity levels. In the case the ambient temperature fall to the right of the 100 percent line, contrails should never form. In the case the point falls between the 0 and the 100 percent lines, contrail formation can occur depending on the local relative humidity[6, 48].

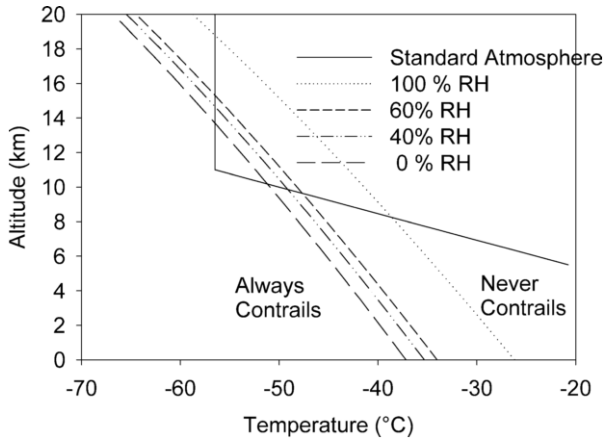

Figure 2.6: Relative humidity required for Jet aircraft contrail formation as a function of standard (pressure) altitude vs temperature of the environment. $\eta = 0.3$, $EI_{H_2O} = 1.223$ and $Q = 43.2MJkg^{-1}$ [48].

2.4 Atmospheric Data

In order to start actual testing on trajectory optimisation and to analyse the regions prone to contrail formation, inputs regarding the local atmospheric temperature, pressure and humidity are required. For such an optimisation scheme to be tested, meteorological data used as input has to be available for varying altitudes. Next to this, a high geographic resolution with a large coverage is desired to accommodate the trajectory optimisation over the entire cruise phase. This requires a sufficiently large grid, where the relevant atmospheric conditions are known, and where the grid cells are spread out equally over the covered area. Whereas the optimisation routine itself optimises in a four dimensional space, the atmospheric data serving as input for the routine consists of data in a three-dimensional space. Time dependent alterations to the atmospheric data have not been taken into account, due to computation power constraints.

In climate models, where the same or similar parameters are considered, parametrizations or generic atmospheric models are often used[64]. Climate models, however, focus on effects over a long period, whereas the purpose of this research is to assess the atmospheric influences on individual flights, thereby focussing on a smaller time period. A way to identify parametrization deficiencies is to analyse climate models in a short-range (less then 5 days) weather-forecast framework[64], which will result in significant deviations between the two models. The research performed herein focusses on the optimisation of individual flights, in doing so a parametrized atmospheric model will not suffice, as it would result in parametrized final solutions rather then individual solutions attuned to the local atmospheric conditions. To illustrate the deficiency for short-range forecasting, resulting from the highly variable nature of the atmosphere, consider figure 2.7. It represents the relative humidity at varying pressure altitudes as measured over a period of 6 days, using data obtained from radiosondes launched with a 3h interval (ARM) and the numerical weather prediction (ERA-40), as produced by the European Centre for Medium-Range Weather Forecasts (ECMWF). Radiosondes are small rockets or weather balloons, outfitted with instruments which will measure a multitude of atmospheric parameters on location. The advantage of this data is that it is highly accurate. The disadvantage, however,

is that it is only available on a limited number of locations. Numerical Weather Predictions (NWP) are used to translate the data (e.g. obtained by radiosondes and observation satellites), into a coherent picture of the global atmosphere. These figures indicate the large degree of variance to which the atmospheric relative humidity is subjected throughout the day, thereby indicating why "live atmospheric measurements" are preferred for the purpose of this contrail mitigation study.

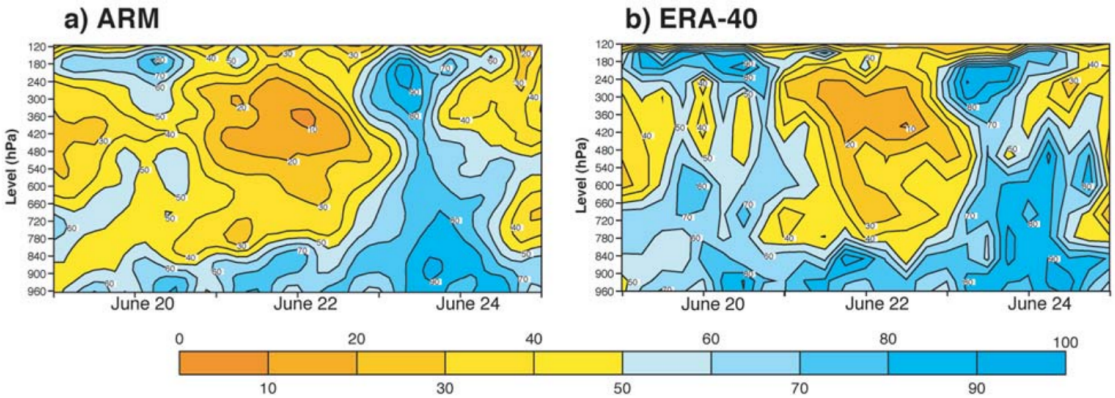

Figure 2.7: Plots of the vertical atmospheric relative humidity profile (%) for the period 19-25 June 1997, as obtained from (a) ARM observations, (b) ECMWF ERA-40 reanalysis[64].

The Canadian Meteorological Institute has made data available on its website[40]. This data covers the most recent Numerical Weather Predictions (NWP), published daily at 12:00 and 24:00. The data consists of a current atmospheric analysis as well as hourly forecasts. The database can be accessed free of charge and is available to the general public. The advantage of the database, as provided, is its large coverage (global, no black spots), its high geospatial resolution and the fact that it is available for a multitude of pressure altitudes. All data is present at a 0.24x0.24 degree resolution (roughly 25x25 km) and at the following pressure levels: 50, 100, 150, 175, 200, 225, 250, 275, 300, 350, 400, 450, 500, 550 and 600 mb. Most of the data used for this research corresponds to the atmospheric data as observed of 12 february 2014 at 12:00 UTC. From this data a 750x1500x15 matrix is obtained, spanning the global atmosphere for each variable over the before mentioned pressure altitudes. Time dependent evolution of the atmospheric data has not been considered, in order to minimize memory usage. Taking the time dependent evolution of atmosphere into account could compromise overall optimisation performance and extend run times. Neither has the vertical wind vector been included in the atmospheric data, serving as input for the optimisation routine. It is discarded, because the data is only available at four altitude levels, whereas the other data is available for a multitude of altitudes. Next to this it was expected that inclusion of the vertical wind vector would not significantly enhance the optimisation routines accuracy.

As advised by the meteorologic service: "Specific humidity (SPFH) is the model's native moisture variable. It should be used in all NWP applications. Dew point depression is a diagnostic parameter and is not meant for use in high-precision applications[40]."

The following variables have been used as input for this research:

- Temperature $[K]$
- Geopotential Altitude $[m]$
- U wind Component $[m/s]$
- V wind Component $[m/s]$
- Specific Humidity $[kg/kg]$

Input data verification

The methodology described in this study requires atmospheric input. A solution is as good as its input, so let us therefore consider the accuracy of the atmospheric data. No information could be obtained on the accuracy of the observed atmospheric parameters. However, in order to get an impression, let us briefly consider the accuracy of the results of the numerical weather predictions set against radiosonde observations. Figure 2.8 shows the progression of the root mean square errors of the CMC GDPS model, the model used by the Canadian Weather Service for atmospheric predictions. In this case the figure shows the root mean square error of the temperature at an altitude of 850 hPa (generally representative for the free atmosphere above the Earth's turbulent boundary layers). The errors increase nearly linearly with forecast time, behaviour representative for most model forecast parameters[40]. From this it seems reasonable to assume that the atmospheric input can serve as a realistic representation of en-route atmospheric conditions.

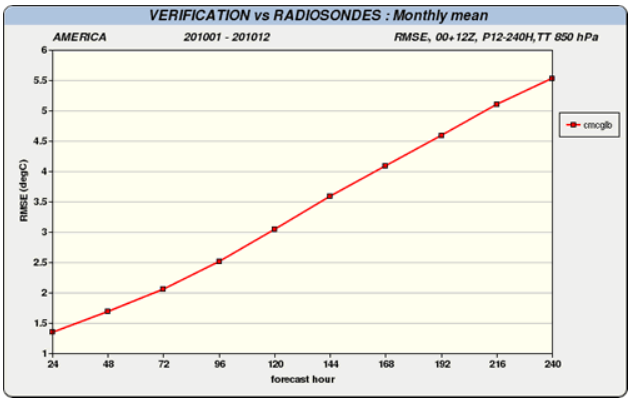

Figure 2.8: Progression of the Root Mean Square Errors of the CMC GDPS models temperature predictions at 850hPa, from 24 to 240 hours lead-time predictions, mean taken over the year 2010 and verified against the North American radiosonde observation network[40].

2.4.1 *Ice Super Saturated Regions in NWP*

In Numerical Weather Predictions data, the reported relative humidity will be the grid-mean. With the large resolution of the meteorological data, namely 0.25x0.25 degrees in longitude and latitude or roughly at about 25x25km in size, local humidity levels can deviate from this mean. Even when the grid mean is not 100% in all likelihood pockets of ice-supersaturated air will be present within the grid. To accommodate for the discrepancy between predicted and actual local conditions, the modelled critical RHI is often selected to be somewhat below saturation[17, 16]. In order to best satisfy the persistent contrail occurrence at all attitudes the critical RHI, as used during this research, is set at 80%, as discussed by Xu and Krueger[65].

2.4.2 *Processing the Atmospheric Data*

The atmospheric data is processed prior to the optimisation in order to decrease the computation power required. In figure 2.9, a schematic representation of this process is presented.

The blue box represents the original meteorologic data loaded into the function. The desired scope is used to specify the region for which the contrail and atmospheric data is prepared. Next to this the combustion parameters are loaded, depending on the aircraft configuration and type of fuel used.

In the first process box the critical temperature is assessed as described by the contrail methodology in section 2.2.1. Next to this the relative humidity with respect to ice is derived in order to be able to assess the persistence criterion, as presented in section 2.2.2. As the TLC and the RHI are known, the Schmidt-Appleman criterion is applied, as presented in equation 2.5. In case the criterion is satisfied, the contrail

parameter will be set equal to the local RHI. If the criterion is not satisfied, the Contrail parameter will be set equal to zero. The persistency criterion will not be applied in the preprocessing of the atmospheric data, it will, however, be applied during the optimisation itself, the reason for this will be explained later.

The contrail parameter in combination with the atmospheric parameters are know stored in the Processed Atmospheric Data matrix. This is a MATLAB based matrix enabling easy access during the optimisation.

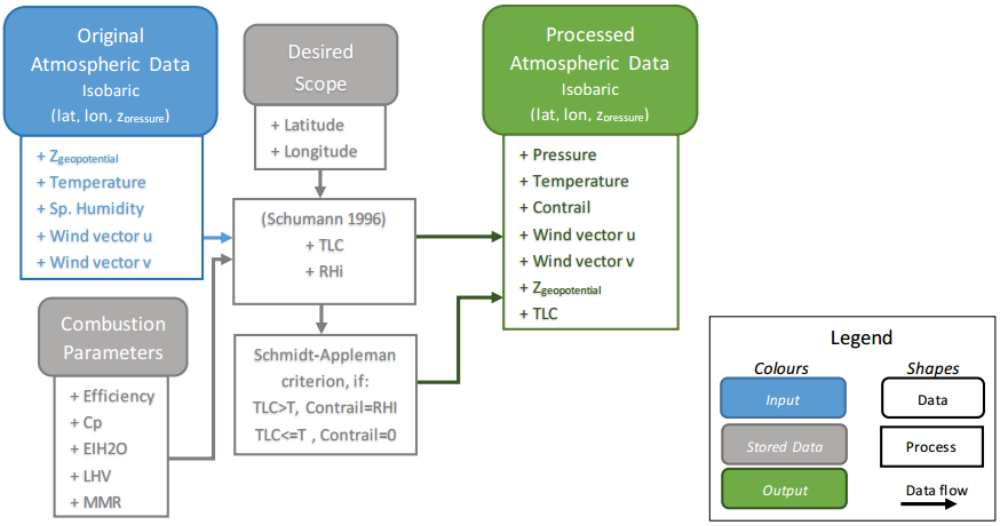

Figure 2.9: Schematic representation of the processing of the atmospheric data.

2.5 The Evolution of Contrails

2.5.1 *Contrail Dynamics*

Concerning the development of contrails, the process can be separated into 2 phases: the initial phase up to the weakening of the wake vortex, having made it lose its grip on the contrail; after which mesoscale atmospheric parameters affect the evolution of the contrail; this phase is the mesoscale phase[48].

The initial phase, during which the formation of contrails occur. In this phase contrail formation is affected by exhaust gases, ambient temperature, humidity and by the jet and vortex dynamics present in the wake of an aircraft. The structure of contrails depends on the air flow trailing an aircraft, varying due to the size, weight, velocity, number and position of engines and further geometrical characteristics of the aircraft. The early wake dynamics and jet turbulence can strongly influence the properties of the persistent contrails later on. The thermodynamic processes responsible for contrails cause the formation to start on the outer boundaries of the hot exhaust jet mixing with the ambient air. Due to the adiabatic compression caused by the downward motion of the vortex, the total ice crystal number can be reduced significantly. Even though fuel consumption may vary significantly for small and large transport aircraft (up to a factor of five), the persistent contrails produced may still be equally sized[59, 60, 32, 20].

The mesoscale phase, during this phase of a contrails 'life', the contrail evolution depends on the ambient humidity, wind shear, turbulence and stratification and possibly radiative cooling. This later phase is yet to be studied extensively, up to this moment only a few exploratory studies have been directed at this later stage of persistent contrail dynamics[48].

2.5.2 *Modelling the Evolution of Persistent Contrails*

The DLR has developed the so called *"Contrail Cirrus Prediction Tool"* (CoCiP), a model in which next to the initial contrail formation phase also the latter evolutionary phase is simulated, predicting the contrail cirrus for air traffic based on weather forecasts[3, 49]. For the research presented herein, the scope lays at the cost-benefit analysis of the optimised persistent contrail mitigated trajectories, the decision has thereby been made to discard the evolution of persistent contrails for the time being. The CoCiP tool may for future reference, however, give a good indication of how the evolutionary phase could be implemented in the tool presented herein.

The model is developed in order to forecast contrail cirrus cover and to analyse its climate impact. In order to be able to use CoCiP for aircraft optimisation regarding contrail mitigation, the model has been developed to compute contrail properties for both individual flights and combined regional air traffic, without compromising on the computation times. In order to satisfy this latter requirement, models with parametrized physics are required, providing proper results throughout the contrail life-cycle. In figures 2.10 and 2.11 an outline of the CoCiP framework is given as well as a list of the modules used.

The model assumes contrails form when the Schmidt-Appleman and the ambient air humidity criteria are satisfied. In order to analyse the contrails life cycle, the model makes use of a Lagrangian Gaussian plume model, with bulk contrail ice properties. The initial plume properties are aircraft dependent. The evolution of a contrail is computed considering wind, temperature, humidity, and ice water content from numerical weather prediction (NWP) output. The plume trajectory is set to follow the horizontal and vertical wind to which it is subjected. The contrail plume spreading resulting from shear and turbulence is simulated. Ice water content is included assuming the conditions inside the contrail are equal to the ambient ice supersaturation. Next to this, the processes causing the loss of some ice particle are simulated as, turbulent mixing, aggregation and sedimentation. The most critical input parameter is the NWP humidity field. The developer states that CoCiP can be used in order to forecast and minimize the climate impact of contrails, as can be seen in the DLR-project "Climate-compatible Air Transport System" (CATS)[3]. Radiative cloud forcing is estimated from the contrail properties using the radiative fluxes without contrails from NWP output.

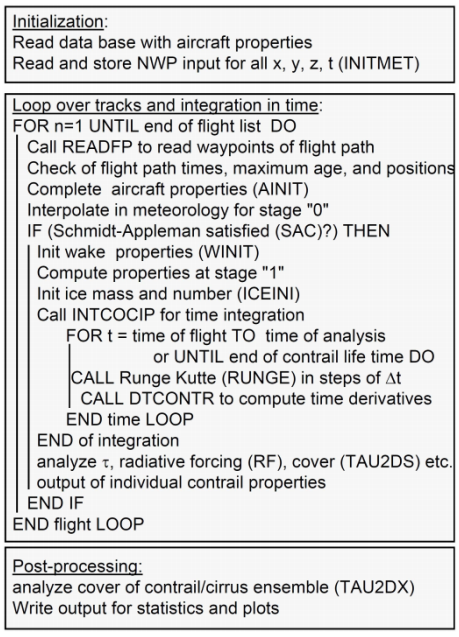

Figure 2.10: A general outline of the CoCiP framework [49].

Name	Purpose
INITMET	meteorological fields
READFP	reads flight plans
AINIT	aircraft properties
SAC	Schmidt-Appleman criterion
WINIT	wake vortex
ICEINI	ice mass and number initialization
INTCOCIP	integration over several time steps
RUNGE	Runge-Kutta
DTCONTR	time derivatives and contrail properties
RADI	radiative forcing analysis
TAU2DS	cloud mask for one contrail
TAU2DX	cloud mask for cirrus

Figure 2.11: A list of the modules in sequence of call [49].

Rationale for Contrail Mitigation

Looking at the skies, quite often aircraft can be seen flying over with large white condensation lines trailing them. Even from a great distance separate trails are often discernible directly behind the aircraft, each of them originating from one of the engines. It will not take long for the lines to get caught into the wing vortices increasing their diameters. Sometimes these condensation trails disappear, but quite often they remain, filling the sky with artificial line-shaped clouds.

If conditions permit some of these line-shaped contrails might even evolve into or induce artificial cirrus clouding indiscernible from their naturally occurring counterparts[48, 35]. To illustrate the effect of aviation on this phenomenon, two photo's are shown side by side in figure 3.1. These pictures are taken on the same location on days with similar atmospheric conditions. The photo on the left shows a clear sky after the grounding of air traffic in 2010 and the photo on the right shows a contrail filled sky resulting from regular air traffic.

Figure 3.1: The sky over Würzburg, Germany, after the grounding of air traffic, due to the eruption of the Eyjafjallajökull (left, 18 April 2010) and on a day with regular air traffic (right, 29 April 2010) [62].

To get a good impression of the extent and scale of the problem, please consider figure 3.2, showing aviation induced clouding in varying stages of transition, over the Channel region in North West Europe. In this section first the impact of this additional clouding will be discussed after which the changes in impact and probability of contrail formation will be discussed.

3.1 Impact of Contrails

Aircraft are known to emit pollutants directly into the upper troposphere and lower stratosphere, thereby affecting the atmospheric composition[27]. These emissions, including CO_2 and equivalent emissions, alter the concentration of atmospheric greenhouse gases; trigger formation of contrails; and quite possibly increase so called secondary-cirrus clouding, all of which results in climate change[27].

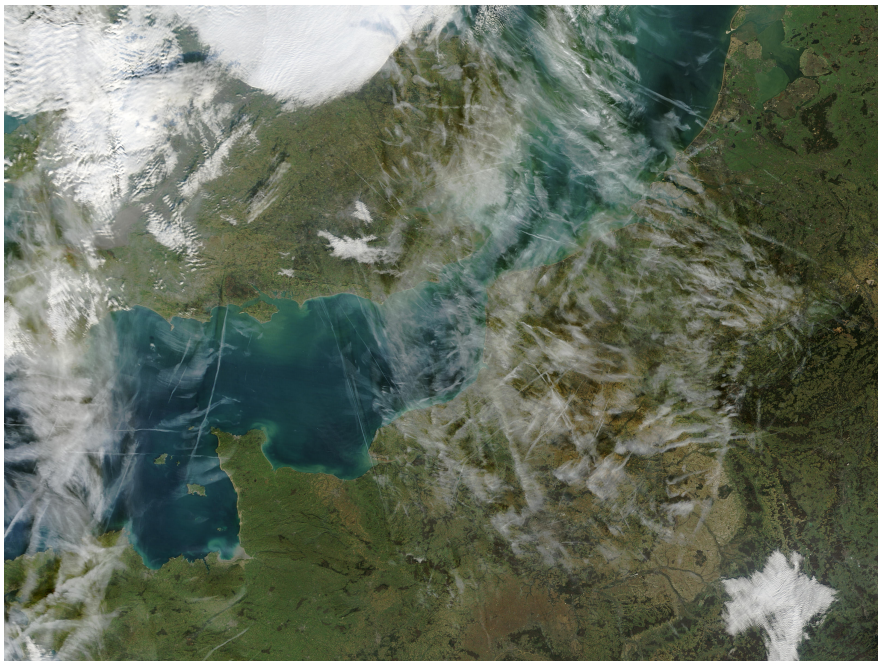

Figure 3.2: Line shaped and evolving contrails in combination with natural clouding over the Channel, Europe [2].

The sun is the single biggest contributor of energy reaching the Earth's atmosphere, but a large part of the energy reaching Earth is reflected outwards into space. In an energy neutral environment, the amount of incoming energy matches the amount of reflected energy, whereby the temperature will remain stable. External factors, such as CO_2, NO_x, soot and also additional clouding, will disturb this balance and result in climate change[27]. The time periods over which the impact of these emissions become noticeable varies per particle. The well known Global Warming Potential for instance is measured in degrees Kelvin change over an extended time period[27]. Some parameters, such as additional contrail, however have an impact within a far shorter timespan.

Global Warming Potential (GWP) is an index that seeks to define the overall climate impact of specific actions. In this index, the impact is related to that of emissions of an equivalent mass of CO_2. Radiative forcing is integrated over a time horizon to account for the duration of the perturbation (IPCC standard horizons have been 20, 100 and 500 years). The time horizon therefore accounts for both the cumulative climate impact as well as the decay of the perturbation. The GWP metric can be a convenient measure for policy-makers to compare relative climate impact of different emissions, but its basic definition can make its application questionable, in particular with regards to aircraft emissions. Impacts such as from contrails can not be directly related to emissions of a particular greenhouse gas. Indirect RF from O_3 produced by NO_x emissions is not linearly proportional to the amount of NO_x emitted, but is instead dependant on the location and season. In essence the radiative impact of gases and aerosols with a short lifespan will depend on the location and even the time of their emissions. Finally, the GWP does not account for an evolving atmosphere, in which the RF from an emission is larger today than in the future. In short, the GWP index is meant to compare emissions of long-lived gases for the present atmosphere; it does not suffice in the determination of the climate impacts of aviation[27].

Instead radiative forcing (RF), assessed for a changing atmosphere, is a better index to estimate the anthropogenic climate change impact from gases and aerosols with varying lifespans. Radiative forcing measures the additional amount of energy added to the Earth-atmosphere system $[Wm^{-2}]$. RF is, however, an instantaneous measure, as it considers the climate forcing at a particular point in time. Positive values of radiative forcing imply a net warming, while negative values imply cooling[27].

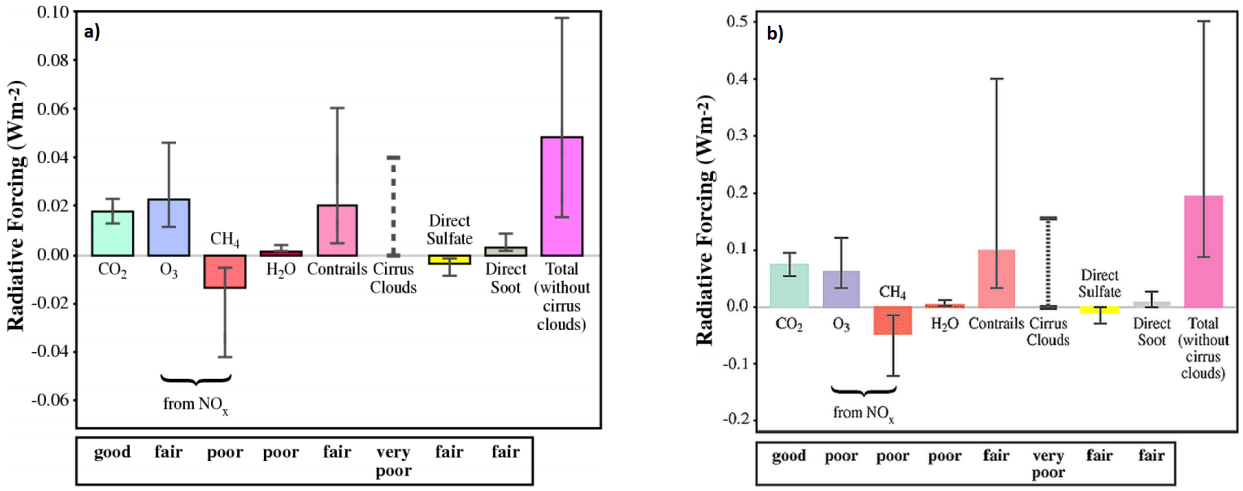

Figure 3.3: Best estimates for aviation induced radiative forcing in 1992 (a) and 2050 (b). The best estimates are accompanied by high-low 67% probability intervals (whiskers). For the cirrus clouds no best estimate is shown, the dashed line indicates a range of possible estimates. Please do consider the change in scale of the radiative forcing axis for the 2 diagrams respectively[27].

In figure 3.3(a)[1], the best estimations for aviation induced radiative forcing are presented for the year 1992[27]. The biggest contributors to aviation induced RF are CO_2, O_3 and contrails, whereas CH_4 and Sulfate most likely have a negative effect. High altitude emissions of NO_x act as a catalyst for the production of both O_3 and CH_4. Large uncertainties still exist concerning the exact magnitude to which each element contributes, as indicated by the 67% probability interval (whiskers). For "cirrus clouds", meaning the indirect effects of aviation on "natural" clouds (e.g. secondary cirrus), no best estimate can be given at all, due to the low academic understanding of this phenomenon (Note the classification stating its impacts are "very poorly" understood). In figure 3.3(b) the same respective diagram is shown for the year 2050. Note however the difference in scale of the y-axis (factor five). From this diagram, it is clear that the impact of contrails is expected to increase in both relative and absolute terms.

This report will focus on Contrails, but for a fair comparison the corresponding effects of contrail mitigation will be compared with the effects of CO_2 emissions using the RF benchmark scale as a reference.

As explained before (section 2), the very presence of contrails in ice supersaturated regions can act as a catalyst and induce the spread of cirrus-clouding, thereby multiplying the total effects of the initial line-shaped contrails. Radiation forcing related to this overarching contrail induced cirrus clouding is about nine to ten times larger than that from the initial line-shaped contrails alone[12, 35]. Especially in regions with a high air-traffic density, the increase of cloud cover in situation favouring contrail formation is significant[48].

These characteristics are most likely satisfied at moderate latitude regions in winter or early spring in the months of February and March[9]. Figure 3.4 (a-d) shows the Northern Hemisphere as seen from an orthogonal projection, with the North Pole (90deg lat) positioned in the centre of the picture. In it the areas prone to Persistent Contrail Production (PCP) are displayed for 4 altitudes favoured for long haul flights. The data supports the research which has indicated contrails typically form at pressures below 300hPa[29], higher limiting pressures at alleviated latitudes and lower near the equator. The meteorology data has been selected arbitrarily and dates to July 7th, 2014. Next to this four great circle lines are drawn (dotted white) connecting Amsterdam [AMS], Peking [PEK], Tokio [HND] and Washington [KIAD] (pink triangles). As can be seen from the figures, flights flying along these routes are likely to produce persistent contrails. If we take these locations as representative for the three main economic regions, air traffic along these routes would account for up to 20% of total air traffic (as represented by RPK)[19]. Large scale contrail occurrence

[1] $Note: CO_2 = carbondioxide, O_3 = ozone, CH_4 = methane, H_2O = watervapour, NO_x = nitrogenoxides$

is therefore expected to have a significant effect on the local environment.

Dependent Radiative Forcing
Contrail radiative forcing is dependent on the time of day due to daily variations in solar radiation on specific locations on the globe. During the night, when solar radiation is absent, outgoing long wave radiation is hindered by contrails. Due to this the overall radiative forcing is increased during the night[39]. Night time flights during the winter are responsible for most of the contrail radiative forcing[36]. However, persistent contrails occurring during the day can spread under the influence of wind and evolve into cirrus clouding lasting during the night when they as well cause a stronger radiative forcing[35].

Positive Feedback effects on the Climate System
Increasing the local temperature at ground level in the before mentioned moderate latitude regions could have an additional aggravating affect, as the release of carbon and methane from thawing permafrost constitutes an additional positive feedback in the heating of the global climate[56]. Positive feedback implies that an initial change will result in another initial change in the same direction, thereby amplifying the effect.

This is one example in which global and local warming has a positive feedback on the climate system thereby aggravating its effects. Amongst other things, climate change is already causing permafrost warming and thawing in high-latitude and high-elevation regions as well as the retreat of glacier and reduction of ice volume, the disappearance of thermokarst lakes, the reduction in Arctic sea ice cover, the increase in lake water temperatures and prolonged ice-free seasons. Most of which can cause a similar positive feedbacks[13].

3.2 Changing Parameters affecting future Contrail Probability

In the previous section the impact of contrails has been discussed. However, with the changes in the global atmosphere becoming apparent the factors contributing to the effects are likely to change over time. In table 3.1 a number of parameters likely to impact the effective contrail occurrence are shown. The sign of change indicates in which direction the parameter is most likely to change in the future, increasing (+) or decreasing (-). Global Contrail & Induced-Cirrus Coverage indicates the change in occurrence in case of a change in the considered parameter. In the next column of the table, the corresponding effect on global radiative forcing can be seen[27].

Looking at the table two sets of parameters can be seen, the first five parameters are related to environmental changes, whereas the remaining parameters are related to general trends in aviation. The effective impact the environmental parameters have on contrail occurrence and RF is not uniform. Most of the aviation induced alterations however, seem to positively affect contrail formation. The number of aircraft is likely to increase and even though the overall efficiency of propulsion is bound to increase it will not offset the total amount of fuel consumption. In fact increases in overall propulsive efficiency will positively contribute to the occurrence of contrails in itself. In figure 3.5 the historic trend of propulsive efficiency can be seen. Correspondingly the solid circles also denote the critical altitude at which contrails form in ice-supersaturated regions under ISA-conditions. The current trends in propulsive technology is bound to increase the occurrence of contrails under varying conditions and thereby increase its respective RF effects. The effects of the last three, fuel related, parameters are still uncertain. Lowering the emissions of soot and fuel sulphur content could potentially decrease contrail occurrence. Whereas the increase of hydrogen content will in turn increase contrail occurrence, with yet undetermined effects on RF.

The air traffic along the routes connecting the regions, as represented by the routes in figures 3.4(a-d) (e.g. North America, Europe and East-Asia), will steadily account for about 20% of total air traffic (expressed in % total RPK), whereas in absolute numbers the total traffic connecting these regions will increase ranging from 140% to 180% by 2030[19]. From this figure it becomes clear that the likelihood of these long-haul

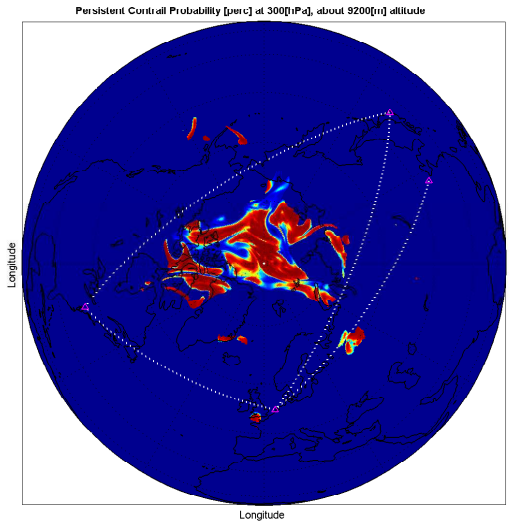

(a) Pressure altitude 300hPa ($\pm 9200m$)

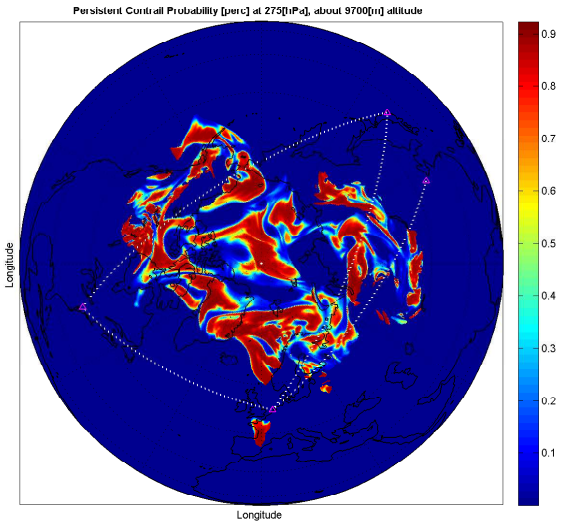

(b) Pressure altitude 275hPa ($\pm 9700m$)

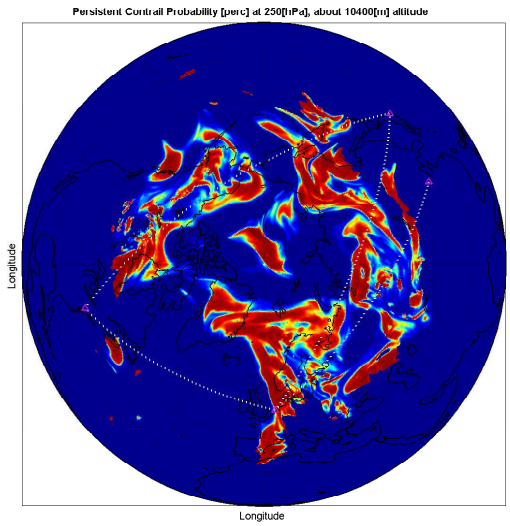

(c) Pressure altitude 250hPa ($\pm 10400m$)

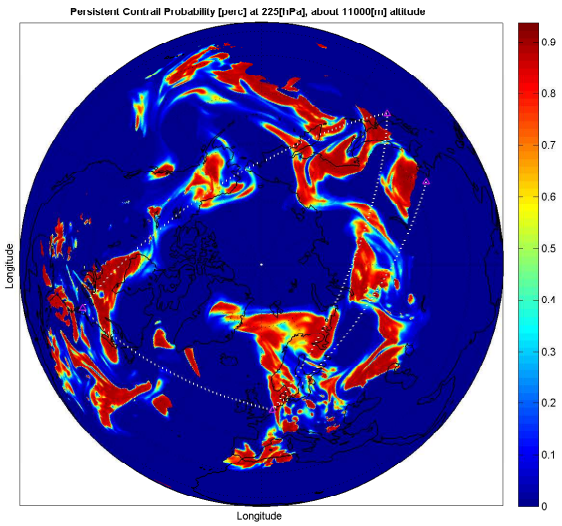

(d) Pressure altitude 225hPa ($\pm 11000m$)

Figure 3.4: Persistent Contrail Areas in an orthogonal projection of the northern Hemisphere as seen from the North Pole. In combination with the great circle route connecting: AMS-PEK, AMS-KIAD, KIAD-HND, HND-AMS. Produced using Meteorologic data from 07 July 2014 at 00:00UTC.

flights flying through areas prone to contrail production is rather large.

The effects of changing conditions on radiative forcing per emission type can be seen in table 3.2 as published by the IPCC[28]. In conclusion let us state that aviation induced RF is bound to increase the coming decades, with contrails most likely being responsible for an increasing share in the net surplus.

Table 3.1: Parameters affecting future changes in aviation induced cloudiness. The symbols represent the parameters sign of change and impact. Question marks indicate uncertainties. The symbol x indicates a lack of a known or important impact. (Reference Table 3-10[27])

Parameter	**Sign of Change**	**Global Contrail & Induced-Cirrus Coverage**	**Global Contrail Radiative Forcing**
Upper troposphere temperature	+?	-	-
Lower stratosphere temperature	-	x	x
Humidity of lower stratosphere	+	x	x
Humidity of upper troposphere	+?	+	+
Tropopause altitude	+	+	+
Number of aircraft	+	+	+
Global aviation fuel consumption	+	+	+
Overall efficiency of propulsion	+	+	+
Cruise altitude at mid-latitudes	+	-	-
Cruise altitude in the tropics	+	+	+
Traffic in tropical regions	+	+	+
Soot emissions	-?	-?	-?
Fuel sulfur content	-?	-?	-?
Fuels with higher hydrogen content	+?	+	?

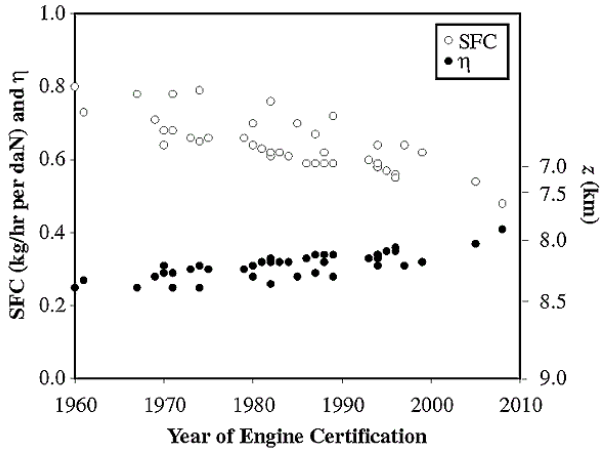

Figure 3.5: Trend in overall propulsive efficiency η (solid circles) from 1960 to 2010, computed from aircraft specific fuel consumption (SFC) data (open circles). The solid circles also denote the critical altitude z (right axis) above which contrails form (for 100% relative humidity under ISA atmosphere conditions) [27].

Table 3.2: Total aviation induced radiative forcing for the years 1990, 2000, 2015, 2025 and 2050 as projected by the IPCC, (Table 6-2)[28].

Radiative Forcing $[W/m^2]$	**1990**	**2000**	**2015**	**2025**	**2050**
O_3	0.024	0.029	0.04	0.046	0.06
Contrails	0.021	0.034	0.06	0.071	0.1
CO_2	0.016	0.025	0.038	0.048	0.074
Soot(BC) aerosol	0.003	0.004	0.006	0.007	0.009
H_2O	0.002	0.002	0.003	0.003	0.004
Sulfate aerosol	-0.003	-0.004	-0.006	-0.007	-0.009
CH_4	-0.015	-0.018	-0.027	-0.032	-0.045
Indirect clouds	n.a.	n.a.	n.a.	n.a.	n.a.
Total	*0.048*	*0.071*	*0.114*	*0.137*	*0.193*
% *Contrails*	44%	48%	53%	52%	52%
% CO_2	33%	35%	33%	35%	38%

3.3 Military Rationale for Contrail Avoidance

With stealth being an important characteristic for any combat aircraft[63], the United States military forces have been interested in contrails ever since aircraft capable of flying at high altitudes have entered their inventory. As contrails form an irrefutable proof of the (recent) presence of aircraft it impairs the survivability of an aircraft, for both combat as well as non-combat aircraft. Contrails thereby can be seen as a form of military intelligence in a number of ways, they generally aid the defender and hinder the attacker[51]. During an aerial invasion, contrails are therefore of vital importance.

The incorporation of stealth technology has helped modern aircraft to significantly reduce their radar cross section. Next to this, aircraft can penetrate airspace through black spots in the enemies radar system or use electronic countermeasures. However, all these efforts are rendered in vain when aircraft are trailed by contrails, revealing their position and direction of flight[6]. The presence of contrails enhances visual contact thereby assisting in the interception by means of vectoring defending forces to their target. An example of which can be seen in the case as illustrated in figure 3.6, in which two Soviet MiG-29 aircraft are intercepted by two USAF F-15 aircraft over Alaska, USA. Next to this contrails can help defenders with the identification of aircraft by showing the number and spacing of the engines[6]. Contrails spreading out into cirrus clouding can hinder the rendezvous of aircraft and air-to-air refuelling operations. Contrails can furthermore reveal tactics by clearly marking the ingress and egress routes.

Accurate contrail forecasts and according route optimisation can assist mission planners and reduce the risks for pilots, enhancing the overall mission effectiveness[51].

Figure 3.6: Two Soviet MiG-29 aircraft en route to an air show in British Columbia, Canada, are intercepted by two USAF F-15 aircraft of the 21st Tactical Fighter Wing[10].

3.4 Previous Contrail Mitigation literature

3.4.1 *The theory of Contrail Mitigation by means of Flexible free flight*

Regions with ice supersaturation have occurred with a horizontal reach of the order 150 km and a vertical extend of normally only about 500m[31]. In Mannstein et al.[21], operational radiosonde data is used to assess the effect of a change in-flight altitude on contrail formation. It indicates that "a substantial fraction of contrails and contrail induced cirrus can be avoided by relatively small changes in flight level, due to the shallowness of ice-super-saturation layers"[21]. As can be seen in figure 3.7, the probability of remaining in a super saturated region alters significantly when the flight altitude is changed. It opts for flexible free flight as a solution, in the case ice-super-saturation is signalled and if a positive radiative forcing during the lifetime of the contrail is to be expected. "In this case a flight level change of less than 2000ft up or down is generally sufficient to avoid 50% of contrails. An even more efficient strategy to avoid contrails would be possible, based on a precise prediction of position and extent of Ice Super Saturated Regions (ISSRs)." It continues stating a change of only 1000ft would be sufficient to reach 50% contrail reduction if the nearest "dry" layer is known[21]. Mannstein et al. hereby indicates exactly the main purpose of our current study, to analyse how the flight trajectory can best be optimised in order to mitigate contrail formation. This technique is already applied by military aviation in order to suppress their visibility[51, 6].

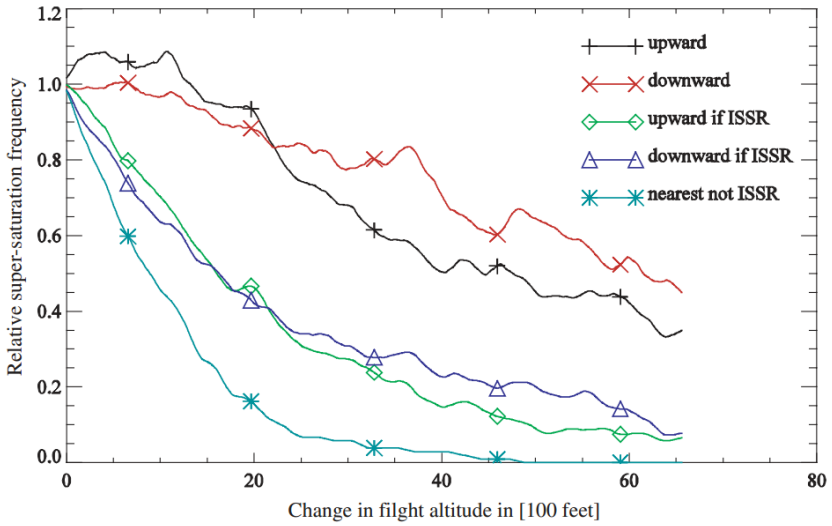

Figure 3.7: The probability of remaining in super saturated air after an altitude change from FL290 [21].

3.4.2 *Flexible free flight Contrail Mitigation in literature*

In this section previous contrail mitigation studies will be presented such as, Noppel 2007[39], Sridhar 2011[38] and Kaiser 2012[33]. The comparisons and differences between these studies, and with the study performed herein will be discussed.

In Sridhar et al.[38], a trajectory contrail mitigation study was performed in the presence of wind, optimising for minimum fuel consumption. The optimal trajectories are established by means of solving a non-linear optimal control problem with path constraints. Persistent contrail formation is modelled through the presence of ice-supersaturation, in this paper no mention is being made of the Schmidt-Appleman criterion and whether it has being satisfied in these regions. The optimal aircraft heading is calculated in a 2-dimensional plane. Soft penalties are imposed to model for the regions prone to persistent contrail formation. The imposed penalties are derived from a radial penalty function, which is related to the distance between

the aircraft and the centre of regions where persistent contrails can potentially form. The cost coefficient of the penalties is adjustable. The aircraft fuel consumption model consists of a Specific Fuel Consumption (SFC) over altitude parametrization, multiplied with the elapsed time and thrust. The optimal trajectories are computed by repeatedly solving the horizontal plane problem. The tradeoff between persistent contrails formation and additional fuel consumption is investigated, with and without this altitude optimisation.

In order to assess the contrail avoidance optimisation routine, the air traffic connecting 12 city-pairs in the United States, dating back to May 24, 2007, was selected. The additional travel times required for completely avoiding persistent contrail formation at various flight altitudes ranged from approximately 0% to 4.3%. In case the altitude is optimised, fuel burn, required for contrail avoidance, can be reduced drastically. The average results with and without altitude optimisation can be seen in figure 3.8. It concludes that when altitude is optimised a two percent increase in total fuel consumption can lead to a reduction in contrail-time of more than 83%, after which the gains level out. In its conclusion, Sridhar et al.[38] relate mitigation of contrail-time to its required fuel burn penalties; no attempt has been made to translate these costs into RF or climate temperature impact.

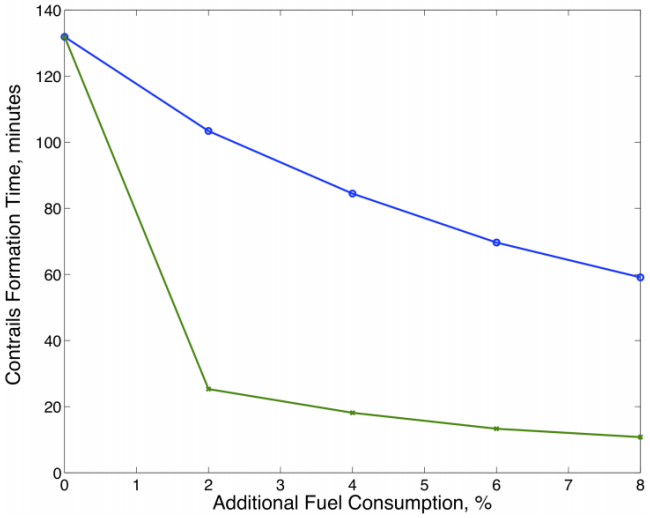

Figure 3.8: Tradeoff curves between fuel consumption and contrail avoidance, with (green) and without (blue) altitude optimisation[38].

In Kaiser[33], a flight profile optimisation was presented maximising specific range while minimizing contrail production. In this study changes to the en-route flight altitude were allowed even though a flight altitude ceiling was implemented. For his optimisation Kaiser makes use of the so called Enhanced Trajectory Prediction Model (ETPM). The ETPM provides a discrete solution of the trajectory differential equation using a final element method (FEM) and the so called Enhanced Jet Performance Model (EJPM), continuously providing all necessary (environmental) parameters at each grid intersection using analytic equations and algorithms. The FEM analysis in the ETPM maked use of dynamic grid sizing in order to get more information on important areas of the trajectory (e.g. turns and climb/descent segments). The meteorologic data used by Kaiser consists of radiosonde data from five locations, located more or less along the ground track. In short the ETPM application will obtain "an ecological optimised 4D en-route flight path between Amsterdam and Salzburg [AMS-LOWS], under consideration of minimum CO_2 emissions, contrail build up and lifelike wind and atmospheric conditions."

For the short continental flight [AMS-LOWS], a contrail formation was avoided at the expense of an increased fuel burn of 2.5%, in the case of fixing the en-route altitude and 1.5%, in case en-route altitude optimisation is applied. From this Kaiser[33] estimates a reduction in RF of 92.4% and 92.5%, respectively.

In his dissertation, Noppel[39] investigates the feasibility of contrail and cirrus cloud avoidance technology in general. In his study, Noppel explores the potential and feasibility of adjustment of air traffic, engine and aircraft technology, fuels and potential contrail avoidance devices. In its conclusion Noppel[39] warns: "The numbers are first estimates and not the results of accurate assessments, having the purpose to support the identification of priorities for further research activities." Furthermore continuing: "Changing aircraft cruise altitude during flight (free flight) exhibits an effective and viable method for contrail avoidance. It is accompanied by a fuel burn penalty of below 1% and can be applied to current aircraft technology[39]." Our study is interested in finding a feasible free flight contrail mitigation strategy and will therefore only discuss the most relevant conclusions related to its free flight contrail mitigation depending on ambient conditions[39]. In this case, this means a case in which aircraft cruise altitude is altered during the flight, depending on ambient conditions.

For the optimisation a commercially available simplex optimisation algorithm was used. Initially the flight path is parametrised, dividing it into equally long sections. Starting from the great circle route, the horizontal and vertical offset from way points are specified, yielding a realistic flight path. Weather data, containing the records for the year 2005, including temperature and humidity in a 6 hour interval and on a global grid, was used in order to assess a contrail probability. Wind effects have not been taken into consideration during this study. The grid is evaluated for persistent contrails and a parametrized monthly averaged contrail probability is derived for each grid cell. The ESDU aircraft performance program predicts the aircraft performance. In the case the appropriate aerodynamic and engine data are available, it can predict point and path performance, take-off and landing performance and mission performance. The ESDU derives the fuel flow rates for each waypoint, after which time integration yields the overall block fuel consumption.

A year long record of transatlantic flights between London and New York was used to analyse possible contrail reduction per month. The results of this study can be seen in figure 3.9. A mean of 78% contrail-length reduction was achieved against an 0.8% increase in fuel burn.

Independent from this, Noppel also investigated the effect of a contrail mitigation strategy on the (aviation) induced temperature change. It is concluded that contrail avoidance forms a strategy, with a short term effect decelerating the global temperature increase. For this research a fuel burn penalty of 10% was chosen. Despite the rather large fuel burn penalty, the difference in aviation induced CO_2 emissions between the contrail mitigation and no-mitigation strategy has an insignificant impact on global temperature[39].

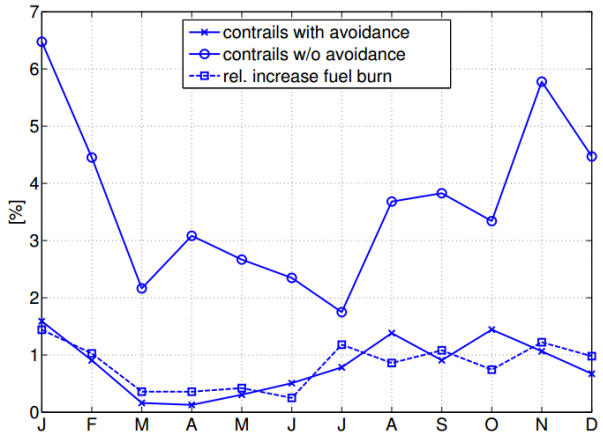

Figure 3.9: The annual variation in contrail formation along the flight path with and without contrail avoidance and the relative increase in fuel burn[39].

Optimisation for Contrail Mitigation

In section 2 and 3 the benefits of free flight contrail mitigation have been presented. In this section the trajectory optimisation framework, in which this will be realised, will be discussed. This section will elaborate on the required architecture, most relevant to the contrail optimisation problem.

4.1 Optimisation Structure

The tool presented here is used for the optimisation of individual flights. The flights assessed in this research are departing from Amsterdam and have Washington as destination. For one short-haul flight case the destination was altered from Washington to Belfast. The objective parameters considered by the optimisation routine are:

- Fuel Cost: total fuel weight consumed in flight (N).
- Flight Time: total time in flight(s).
- Contrail-Time: cumulative flight time during which persistent contrails are produced (s).

What sets this research apart from previously conducted research is the fact that the optimisation scheme presented here opts for the inclusion of realistic high resolution atmospheric data throughout the flight, namely: Temperature, Pressure, Contrail persistence and the Wind vector field. At the same time the optimisation routine is allowed to refine the optimal trajectory in four dimensions.

During optimisation, ideally all objective parameters would be minimised. Some parameters will however, adversely affect other objective parameters, a trade-off therefore needs to be made in order to come to an optimal solution. The MATLAB based GPOPS framework will be used in order to solve this multi-objective optimisation problem. According to the authors, GPOPS has specifically been designed to serve as an optimisation framework widely applicable to a multitude of problem types. Its suitability for contrail mitigation optimisation problems results from its successful previous use in research on noise abatement during terminal arrivals[61]. This framework will be discussed briefly in the next section.

Figure 4.1 gives a schematic outline of the optimisation structure, implemented within the GPOPS optimisation framework, represented by the light blue dashed box. In this schematic, the grey boxes represent the input required to run the routine, the blue boxes represent processes within the optimisation routine and the green boxes represent the final optimal solution.

In a green box on the left side, the problem statement can be seen; this is where the optimisation problem is defined. In order to find an optimal solution, first the problem needs to be clearly defined: the state, control and constraint bounds needs to be specified, as well as an initial guess for the solution. The specific requirements of the problem statement required by GPOPS will be discussed in section 4.2.

In the *DAE function*, the Differential-Algebraic Equations affecting the aircraft model are defined. In this function state and control variables as well as their derivatives are determined. For additional data required to derive the alterations to the aircraft model several functions are called upon, namely: the *Live Atmosphere*,

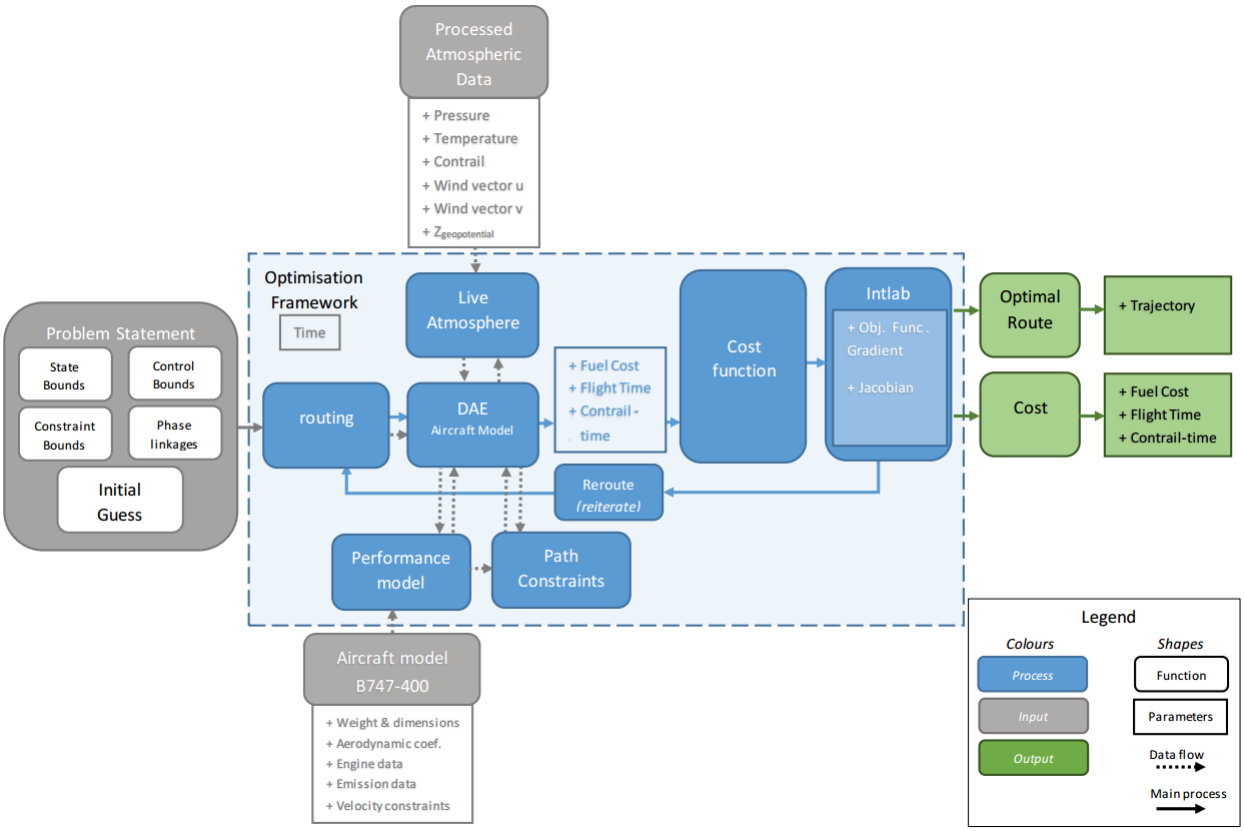

Figure 4.1: A schematic representation of the optimisation program.

the *Performance model* and the *Path Constraints* function. In section 4.3 the details of this function will be discussed.

The *Live Atmospheric* function is called upon by a number of functions. After receiving the coordinates and pressure altitude of the aircraft's location it is able to provide a multitude of local atmospheric properties for that location. To do so the Live Atmospheric function draws upon the atmospheric data file, loaded during the initiation of the tool. The atmospheric data file can consist of meteorologic information for a specific date and time, but it can also contain the International Standard Atmosphere. The live atmospheric function is discussed in more detail in section 4.5.

The *Performance Model* function determines the drag, thrust and the fuel flow of the aircraft. In order to derive these parameters the function requires the control variables, the aircraft weight, velocity and altitude as well as the local atmospheric conditions. Next to this, a number of aircraft specific data are required consisting of: the weight & dimensions, the Aerodynamic coefficients and engine data, next to this it also provides the velocity limits to the path constraints. The performance model used in this study is based on the B747-400 aircraft.

In the *Path Constraints* function, the minimum and maximum velocity limits are calculated depending on the atmospheric conditions. In section 4.4 a more detailed description of this function is given.

In the *Cost* function, the objective functions are specified. The objective functions are the equations in which the problems optimisation parameters are specified. A more detailed description concerning the cost function can be found in section 4.6.

Intlab, an acronym for INTerval LABoratory, is a commercial available MATLAB based toolbox[44]. In this routine Intlab is used to determine the gradient of the objective function.

The problem is solved using a gradient-based non-linear programming optimisation method. Only after the solution has converged completely, satisfying all constraints and conditions, can the solution be assumed to be both feasible and optimal. The optimal solution consist of a detailed account of the state and control variables for each time step, in the diagram it is represented by the green boxes on the right.

4.2 GPOPS

GPOPS is the generic-trajectory optimisation framework within which the contrail model is implemented. GPOPS stands for: *Gauss Pseudospectral OPtimal control Software*. It is a pseudo spectral software used for solving multiple-phase optimal control problems. It makes use of the technique of collocation for the trajectory optimisation, relying on gradient-based algorithms[14]. The Gauss pseudospectral method, discretizes a continuous optimal control problem into a finite-dimensional non-linear problem. In order to find the objective function gradients, required for the non-linear optimisation as proposed in this research, the MATLAB based INTLAB Gradient toolbox will be used[44].

Solving optimal control problems, such as aircraft trajectory optimisation, requires the approximation of three types of mathematical objects: the control systems differential equations, the state-control constraints, and the cost function integration[18]. The method solving this problem should ideally fulfil all three approximation tasks equally efficiently. This requirement is what makes a pseudospectral method suitable, as it is efficient in the approximation of all three mathematical objects.

The optimisation routine enables the use of multiple phase problem solving. Phases can be used to prescribe different stages within the flight (e.g. a turn, continuous descent or level flying). Several MATLAB functions are conceived in order to accurately specify the optimal control problem and should be defined for each phase. These functions consist of[14]:

1 The cost functional, which needs to be minimized.

2 The right-hand side of the differential equations and path constraints.

3 Boundary conditions (e.g. events).

4 Linkage constraints (how will the phases be connected to each other).

Problem statement
The optimisation routine GPOPS is capable of solving user defined optimal control problems, but in order to do so the problem statement needs to be defined. The problem statement gives a detailed definition of the set up of the problem. It serves as input for the optimisation routine defining the bounds, the upper and lower limits, for each variable and component[14]. The problem statement consists of the following:

(a) Initial and final time of the phase

(b) The state conditions in time (e.g. at the beginning, during and at the end of the phase)

(c) The control conditions in time

(d) Static parameters

(e) Path constraints

(f) Boundary conditions

(g) Phase duration (e.g. total time length of phase)

(h) Linkage constraints (e.g. conditions concerning the phase connections)

The problem is solved using the direct trajectory optimisation technique of collocation with non-linear programming (NLP). In this method, the trajectory dynamics are discretized in order to transform the optimal control problem into an NLP problem. The trajectory is divided into a specified number of time intervals, connected by node points. The system differential equations are discretized and transformed using implicit integration[22].

4.3 Aircraft Model and Reference System

The aircraft model used, consists of a point-mass model with a variable mass[15], modelled in the World Geodetic System of 1984 (WGS84). The WGS84 system is used in geodesy and navigation and defines a reference frame for the earth. The Earth surface is represented by an ellipsoid, rotated around the Earth's spin axis. This system is the reference system upon which all geospatial intelligence is based[5].

When assessing aircraft performance, modelling of the fast aircraft dynamic behaviour is discarded, as it will have a low impact on overall performance prediction and will disadvantageously effect processing times[15].

A state vector describes where, in the coordinate system, an object is located, how it is positioned and how it is moving. The state vector x of the problem described here consists of 6 state variables defined in equation 4.1. The variables ϕ and λ in equation 4.1, represent the aircraft Latitude and Longitude positions in the WGS84 coordinate system. The variables z and V represent the altitude (m) and true airspeed of the aircraft (m/s), respectively. The state variable ψ is the heading in radians, represented by the true compass heading and W represents the aircraft weight (N).

$$x = \begin{pmatrix} \phi \\ \lambda \\ z \\ V \\ \psi \\ W \end{pmatrix} \tag{4.1}$$

A control vector is used to alter the state vector and manipulate the objects trajectory. The control vector u consists of 3 controls, as seen in equation 4.2, in which: Γ is the normalized throttle setting, γ is the flight path angle of the aircraft $(radians)$ and μ represents the aircraft's bank angle $(radians)$, with a right turn positive.

$$u = \begin{pmatrix} \Gamma \\ \gamma \\ \mu \end{pmatrix} \tag{4.2}$$

Time derivatives are used to express how changes in the control vector affect the state vector. The time derivatives of the states are defined as[15]:

$$\dot{\phi} = \frac{V cos\gamma \cdot sin\psi + V_{wV}}{R_e + z} \tag{4.3}$$

$$\dot{\lambda} = \frac{V cos\gamma \cdot cos\psi + V_{wU}}{(R_e + z)cos\phi} \tag{4.4}$$

$$\dot{z} = V sin\gamma \tag{4.5}$$

The variables V_{wV} and V_{wU} in equation 4.3 and 4.4, represent the North and East wind vectors (m/s), (attained from the *"Live Atmosphere"* function) and $R_e = 6,378,137$ the radius of earth in (m)[53]. The

time derivative for V is attained using Newton's second law of motion along the axis of the speed vector, with F_{Thrust}, D and W representing the Thrust, Drag and Weight of the aircraft respectively, all expressed in N[15].

$$\dot{V} = g_0[\frac{F_{Thrust} - D}{W} - sin\gamma] \tag{4.6}$$

The expression for the time derivative of ψ is derived from the force equilibrium of a horizontal steady turn, resulting in:

$$\dot{\psi} = \frac{g_0}{V} tan(\psi) \tag{4.7}$$

$$\dot{W} = -\dot{m_f} g_0 \tag{4.8}$$

The weight change caused by the fuel burn $\dot{m_f}$ is calculated separately in a fuel consumption model, based on the actual engine characteristics[55].

4.4 Path Constraints

The path constraints to which the solutions have to comply, as well as the velocity constraints and the method by which they are derived will be discussed in this section.

Velocity Constraints

The path constraints regarding the minimum and maximum velocity are calculated using the atmospheric derivatives from the *Live Atmosphere* function as input. In equation 4.9, the maximum velocity is derived from the Mach number. Equation 4.11 shows the conversion used to derive the True Air Speed (TAS) from the Calibrated Air Speeds (CAS)[55]. The operating limits are defined by the maximum Mach number (Mmo), the maximum operating velocity (Vmo) and the minimum speed, or stall ($Vmin$).[1] The latter two are specified in terms of calibrated airspeed and will be transformed into TAS using equation 4.11. The variable v_{snd} represents the local speed of sound. The resulting velocity boundaries in the (V,h) space for a B-747 flying through ISA atmosphere can be seen in figure 4.2.

The crossover altitude is the altitude at which the maximum operating velocity (red) and maximum Mach number (green) constraints return the same TAS limit. The velocity limit obtained at this altitude represents, by definition, the maximum TAS allowed for an aircraft. The crossover altitude has been verified at about 8350 [m], using the Hochwarth crossover calculator[25].

$$Vmach = Mmo \cdot v_{snd} \tag{4.9}$$

$$v_{snd} = \sqrt{c.\gamma \cdot R_{gas} \cdot T} \tag{4.10}$$

$$V_{TAS} = \sqrt{2 \cdot \frac{\gamma}{\gamma - 1} \frac{p}{\rho} ((1 + \frac{p_0}{p}((1 + \frac{\gamma - 1}{2\gamma} \frac{\rho_0}{p_0} V_{CAS}^2)^{\frac{\gamma}{\gamma - 1}} - 1))^{\frac{\gamma - 1}{\gamma}} - 1)} \tag{4.11}$$

[1] The operating limits for the B-747 are: $Mmo = 0.9$, $Vmo = 365(knts)$ and $Vmin = 192(knts)$ ($Flapsupminimum$). The Service Ceiling is 13.716km[57].

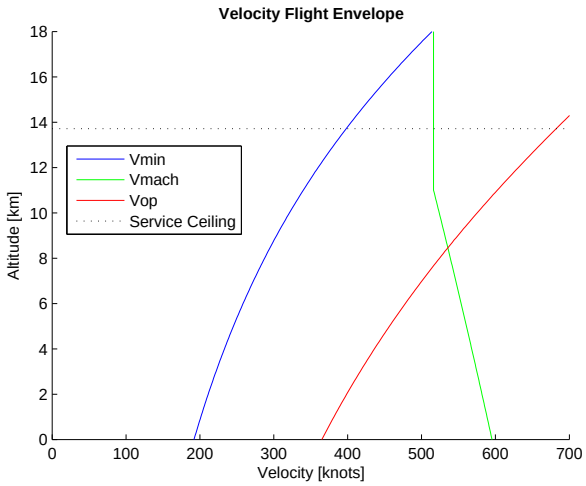

Figure 4.2: The velocity boundaries for a B-747 flying through ISA atmospheric conditions (Maximum Mach number $Mmo = 0.9$, the maximum operating speed, $Vmo = 365$ and the minimum stall speed $Vmin = 192(knts)$).

Ground speed conversion

In order to get a better understanding of the results and the way in which the wind affects them, the ground speed V_{ground} is calculated using equations 4.15, requiring the True Air Speed, Heading and the wind vectors attained from the *Live Atmosphere* function. Again V_{wV} and V_{wU} represent the North and East wind vectors in (m/s), from which the absolute wind velocity Vw_{abs} and the angular direction ang_w are established. The drift angle ang_{drift} is calculated and from this the ground speed V_{ground} in (m/s) is calculated as specified by H. Hirabayashi and Y. Fukuda[24], with the addition of the $cos(\gamma)$ term, taking into consideration the effect the flight path angle γ has on the ground speed. A small proportion of the velocity is used to climb in case of a non level flight.

$$Vw_{abs} = \sqrt{V_{wU}^2 + V_{wV}^2} \tag{4.12}$$

$$ang_w = atan(\frac{V_{wV}/Vw_{abs}}{V_{wU}/Vw_{abs}}) \tag{4.13}$$

$$ang_{drift} = asin(\frac{Vw_{abs}}{V_{TAS}} sin(ang_w - \psi)) \tag{4.14}$$

$$V_{ground} = V_{TAS} \cdot cos(ang_{drift}) \cdot cos(\gamma) + Vw_{abs} \cdot cos(ang_w - \psi) \tag{4.15}$$

Other Path Constraints

Next to these velocity related path constraints, minima and maxima have been applied to the TAS acceleration and the rate of climb as well. An overview of the path constraints and limiting aircraft parameters can be seen in table A.2 in Appendix A.

4.5 Live Atmosphere

The *"Live Atmosphere"* function is created to find a multitude of local atmospheric properties. It allows for the meteorological data to be interpreted and allows for optimal trajectories to be found under realistic atmospheric and contrail conditions. Its key objectives are to allow for data interpretation, to accommodate a transition between nodes and intervals that is as smooth as possible and to do so requiring a minimum of computational power and time. This last objective should not be underestimated, as the function is used for each data point and for every iteration, it can easily be called upon 100.000 times during an optimisation run.

Figure 4.3 gives a schematic representation of the function. The position coordinates are matched to the coordinates known from the atmospheric datafile, where after the Pressure, Temperature, "Contrail" and U and V-wind vectors, the closest lower and upper grid points are retrieved. Next, a tri-linear interpolation over the latitude, longitude and the altitude is performed. With the atmospheric parameters known for a specific location, the other atmospheric derivatives are calculated. For each location the following parameters are estimated:

- T (Temperature)
- p (Pressure)
- Vv_{wind} (Wind vector North positive)
- Vu_{wind} (Wind vector East positive)
- $dTdz$ (Temperature derivative over altitude)
- θ (Temperature over mean sea level Temperature)
- $d\theta dz$ (θ derivative over altitude)
- $dpdz$ (Pressure derivative over altitude)
- δ (Pressure over mean sea level Pressure)
- ρ (Density)
- $d\rho dz$ (Density derivative over altitude)
- v_{snd} (Speed of sound)
- $v_{snd}dz$ (Speed of sound derivative over altitude)
- z_{geo} (Geopotential altitude)
- PCP (Persistent Contrail Probability, see section 4.5.1)

The variable PCP (Persistent Contrail Probability) is analysed within the Live Atmosphere function and is used to assess the time change of the contrail-time variable, $t_{Contrail}$. According to figure 4.3, the PCP variable is derived from the contrail factor, using the 'Switch function', this process will be explained hereafter, in section 4.5.1.

As mentioned the objectives of the Live Atmospheric function are to allow data interpretation and to accommodate a smooth transition between grid points, while utilizing a minimum of computational power and time. With the computational power and time aspect already discussed, let us focus on the other two objectives. The transition between grid points needs to be continuous and as smooth as possible, because of the differentiability requirement imposed by the gradient-based optimisation of the GPOPS routine. The atmospheric data however, might not be directly differentiable everywhere, considering the implementation of the discontinuous supersaturation requirement for persistent contrail formation ($RHI \geq 100\%$), as discussed in section 2.5. Differentiation might as well be hampered by the non-gradual definition of the temperature change over altitude around an ISA-defined tropopause. In order to interpret the atmospheric data, the function must however not conflict with other routines. In the case of implementing interpolation functions

requiring derivatives, such as cubic or spline interpolation, it is likely to conflict with the Intlab operating routines. This, in combination with the computational specific performance requirements, have lead to the decision to select a tri-linear interpolation for the function.

The atmospheric data is available for a specific range of pressure altitudes resulting in a non-constant resolution over altitude, as can be seen in figure 4.4.

Due to linear interpolation over the altitude, persistent contrail areas are sometimes virtually "extended" in the vertical direction. With a vertical resolution of the data of about 1km, a "simulated" completely contrail-free trajectory will have to be separated from a contrail region by a 0.5km vertical distance. As a result, contrail-time might accrue when in reality the aircraft is flying outside contrail prone areas and as a result might cause contrail evading manoeuvres to be magnified in these cases. This effect will be reduced, but not completely eradicated, through the implementation of the Switch function presented in section 4.5.1. The same effect also works in the reverse direction, when the aircraft is flying near, but still outside of, the upper and lower contrail area bounds, a reduced contrail cost will be incurred due to the vertical linear interpolation with the nearest data point outside the contrail area (for an example, see figure 7.9(b&d) in results section 7.2.1). One might argue that these effects may cancel each other out. Next to this contrails originating on the boundaries are, due to sedimentation of ice crystals, less likely to persist and evolve into cirrus, relative to contrails originating in the middle of a contrail prone region[23, 48]. Neither of these hypotheses were explored in this research project.

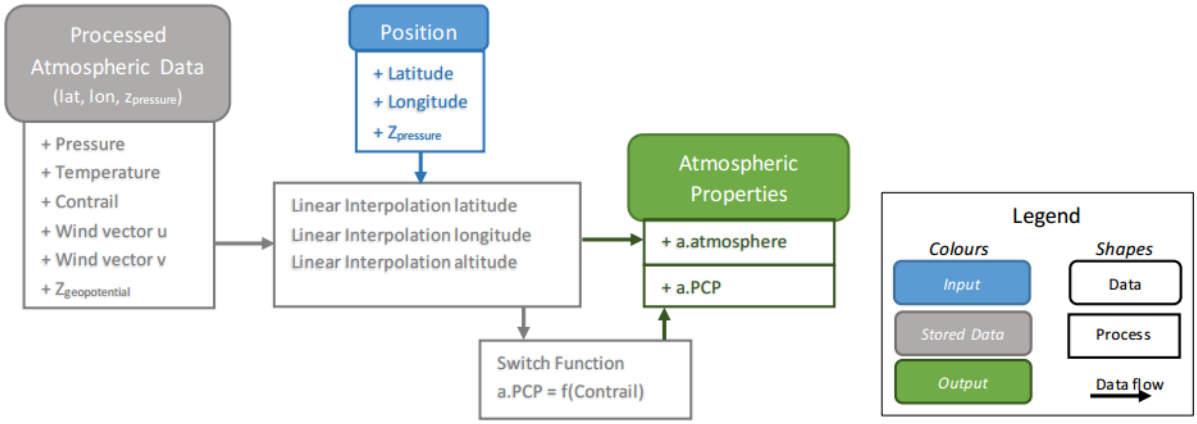

Figure 4.3: Schematic representation of the Live Atmospheric function.

4.5.1 *Switch Function, implementation of the Contrail model*

The general overview of the Live Atmosphere function as well as the parameters it derives has been explained. In this section the calculation of the PCP from the contrail parameter will be discussed.

The methodology used to evaluate the meteorological data for contrail prone areas has been discussed in section 2.2. As discussed in section 2.5, the possibility of persistent contrail occurrence is related to the relative humidity with respect to ice. The RHI requirement, presented in equation 2.9, effectively filters the data in contrail prone regions, to sift out the regions where RHI are below saturation levels. In this study persistent contrails are modelled to occur when the grid cell mean RHI has an 80% saturation level[65].

Due to the implementation of this condition, the magnitude of the contrail data can show discontinuities in, and on the border of, the regions where this condition applies. The data therefore has to be manipulated before it can be implemented in a gradient based optimisation environment. In order to achieve a more smooth integration, a continuous switch function is applied. This has been performed in order to create a

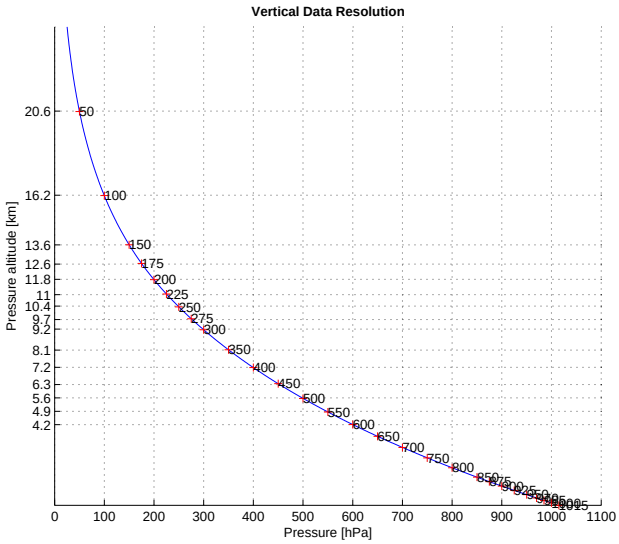

Figure 4.4: Vertical data resolution of the atmospheric input available for altitude.

smooth and differentiable contrail dataset, which can be processed more easily in the optimisation environment.

The switch function, that has been created in this study to smoothly switch between two different magnitudes values, is an arctangent function. Figure 4.5 gives an example of the discontinuous RHI data, after the application of the 80% humidity criterion (in green) and the corresponding response from the switch function (in blue). In summary, the green graph depicts the ideal implementation of the filter and the blue graph shows the continuous response after implementation of the switch function filter, required for the gradient based optimisation.

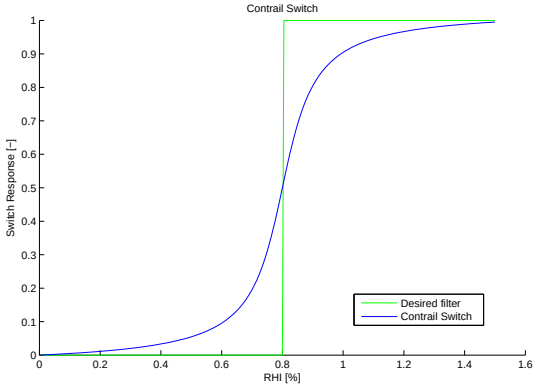

Figure 4.5: Contrail switch function of equation 4.17.

The general form of this arctangent based switch function can be seen in equation 4.16. In this function y represents the switch criterion, the discontinuously responding variable. The parameter A is a correction

factor to define the minimum and maximum magnitudes of the switch function output. The parameter B regulates the initial function value and x defines the range required for the function to switch from its minimum to its maximum magnitude[22]. In this switch function a rather low value of 10 has been chosen for x. A low value for x gives a shallow gradient and thus opts for easier convergence given the possible non-differential nature of the data present. As discussed in section 2.5, the possibility of persistent contrail occurrence is related to the relative humidity with respect to ice and with $y_{target} = 0.8$, i.e. persistent contrails are modelled to occur when the grid cell mean RHI has an 80% saturation level[65]. Note that the parameter *Contrail* basically consists of the RHI levels for the location where the Schmidt-Appleman criterion applies.

With these settings, the optimisation environment was able to handle the discontinuities in the contrail data. Next to this, with the value for $y_{target} = 0.8$ and $x = 10$, the resulting output nicely resembles the continuous character of the atmosphere as can be seen in figure 4.6. Equation 4.17, shows the function with all the before mentioned parameters applied. This is the function deriving the PCP parameter within the Live Atmosphere function. The effect, resulting from the implementation of this switch function can be seen in figure 4.5. In the bottom picture the original/unfiltered meteorologic contrail data can be seen and on top, the same data can be seen after the application of the switch function.

$$sw(y) = A \cdot arctan(\frac{x}{y_{target}} y - x) + B \tag{4.16}$$

$$PCP = \frac{1}{2 \cdot arctan(10)} \cdot arctan(\frac{10}{0.8} \cdot Contrail - 10) + 0.5 \tag{4.17}$$

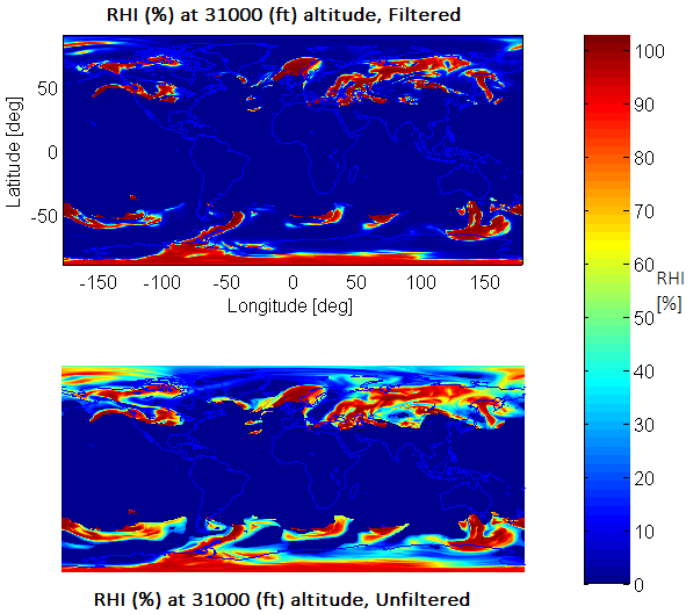

Figure 4.6: Original contrail data, bottom figure (RHI, in areas where the Schmidt-Appleman criterion applies) and the data after application of the switch function in the upper picture. The areas with a relative humidity below the 80% limit are filtered out by the switch function, equation 4.17. Altitude=31.000ft, $x = 10, y_{target} = 0.8, B = 0.5$.

4.5.2 *Contrail-time, PCP and the Contrail parameter*

Throughout this research several contrail related parameters have been used. In order to prevent misconceptions the difference and interconnectedness of these parameters will be discussed briefly.

The *Contrail* parameter is stored in the Processed Atmospheric data. The parameter serves as an input for the optimisation routine and is accessed by the Live Atmospheric function. The *Contrail* parameter is analysed during the pre-processing of the meteorologic data and consists of the RHI for all the locations where the Schmidt-Appleman criterion has been satisfied.

The PCP or Persistent Contrail Probability, is the parameter used to estimate whether persistent contrails will occur. The PCP is derived in the Live Atmospheric function by the application of the Switch function and basically filters out the Contrail grid points with a RHI below 80%. The PCP is derived using the Switch function in order to better satisfy the differentiability criterion of the gradient-based optimisation routine.

The Contrail-time parameter, $t_{Contrail}$, essentially accumulates the time during which the aircraft is flying through areas prone to persistent contrail formation. It is an objective variable and is calculated by integrating the PCP parameter over time, see equation 4.18. In this equation t_0 represents the initial time and t_f the final flight time, respectively. This calculation of the contrail-time is performed in the DAE function.

$$t_{Contrail} = \int_{t_0}^{t_f} PCP \cdot dt \tag{4.18}$$

An attempt to visualise the differences between these contrail related parameters has been made in figure 4.7. This figure shows a hypothetical case of an aircraft flying through three areas in which contrails will form. The Contrail graph (blue) shows the pre-processed data and indicates the local RHI for locations where the Schmidt-Apleman criterion applies.

At flight periods [1.1-2, 3.5-4.5 and 5.7-8.3], the RHI indicated by the Contrail graph nears or exceeds the RHI criterion of 80% (dotted black), indicating persistent contrail formation is likely to occur during these periods. The PCP parameter (green), analysed from the pre-processed contrail data using the switch function and the, there from derived, contrail-time $t_{Contrail}$ (solid red) are also indicated. The $t_{Desired}$ graph (dotted red) indicates what would happen to the contrail-time in case a logical test, such as an if statement, would be applied to the pre-processed contrail data.

According to this graph, the aircraft will fly through persistent contrail prone regions for about 43% of the total flight time, this is indicated by both $t_{Contrail}$ and $t_{Desired}$. The main difference between the two graphs, however, is that the $t_{Contrail}$ shows a gradual response, whereas $t_{Desired}$ shows an intermittent response. For a smooth conversion of the final solution, assessed by the gradient-based optimisation routine, the behaviour of the $t_{Contrail}$ is preferred over the intermittent response seen in $t_{Desired}$.

4.6 Cost Function

Optimisation schemes require cost functions in order to evaluate the objective. In the contrail mitigation literature, as presented in section 3.4, the optimized objectives have always been minimum fuel consumption or maximum range. In this study however, multiple cost functions have been used, varying from minimum flight time or fuel burn, to a function using a cost index (CI) representing the Direct Operating Cost (DOC). This wide selection of objectives has been used to get a thorough understanding of how the implementation of contrail mitigation strategies would realistically impact commercial aviation. The Mayer functions, corresponding to the objective functions, are presented in equations 4.19-4.23. In these equations the respective Mayer objectives for Time, Fuel and their Contrail equivalents can be seen. The parameters t_0 and t_f represent the time of initiation and final time of the flight respectively.

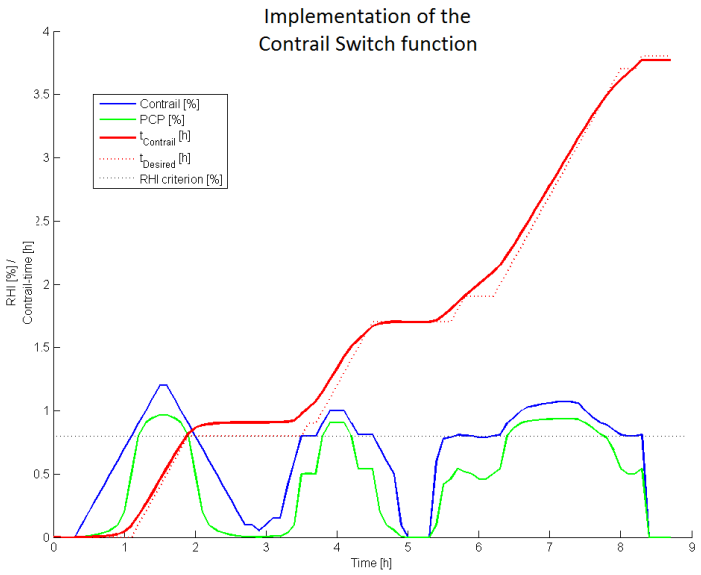

Figure 4.7: Effects of the implementation of the Contrail switch function on $t_{Contrail}$ (red). The pre-processed contrail data (blue), the PCP (green) are both shown. Next to this $t_{Desired}$ (dotted red) indicates the contrail-time, were a normal if statement used on the pre-processed contrail data. The RHI criterion of 80% has also been plotted as a reference (dashed black).

$$Mayer_{Time} = t_f \tag{4.19}$$

$$Mayer_{Fuel} = W(t_0) - W(t_f) \tag{4.20}$$

$$Mayer_{Contrail-Time} = t_f + t_{Contrail}(t_f) \tag{4.21}$$

$$Mayer_{Contrail-Fuel} = (W(t_0) - W(t_f)) + 30 \cdot t_{Contrail}(t_f) \tag{4.22}$$

Airlines rarely schedule their flights purely based on fuel burn or flight time. As the value of time and fuel can vary under varying circumstances, normally both of these parameters are incorporated by means of a Cost Index (CI). In order to gain a better understanding of the additional costs for a more representative case study, the Cost Index approach will be simulated by weighing these two parameters as shown in equation 4.23. The importance of the Fuel and Flight Time parameters, 85% and 15% respectively, have been chosen such that they realistically represent the Direct Operating Cost (DOC) for an airliner. Note that in this case the DOC have not been implemented exactly, a representative method giving a realistic weighing of time and fuel consumption has been chosen.

$$Mayer_{CostIndex} = 0.15 \cdot (t_f \cdot 30) + 0.85 \cdot (W(t_0) - W(t_f)) \tag{4.23}$$

4.6.1 *Parameter Scaling in the Mayer functions*

In two of the previous Mayer functions an additional scaling factor of 30 is present for the final time and contrail time, let us hereby briefly consider this scaling factor.

In the Mayer function for contrail-time, equation 4.21, the contrail-time is weighed equally to the total flight time. As a result the objective value accumulates at twice the rate when it is flying through regions prone to contrail formation. In this case no scaling factor has been applied because these two parameters have the same unit. In a fuel optimisation this is, however not the case. Without a scaling factor the objective would effectively result in a summation of parameters with different units (i.e. N and s). To overcome this a scaling factor is applied in the cases where fuel burn and time (be it flight time or contrail-time) are part of the objective. The overall ratio with which time and fuel consumption contribute to the objective, should be similar to the ratio applied in the case of contrail-time optimisation. In order to achieve this a scaling factor is added to the contrail component in equation 4.22 and 4.23.

The scaling factor is $30N/s^2$, calculated from an obtained fuel burn of about $2700kg/h$ per engine[3]. Through the implementation of this scaling factor, the importance of each of the objective parameters is scaled (i.e. Flight time, Fuel burn and Contrail-time). As such, each of these parameters should have a similar importance and contribute equally to the objective function.

4.6.2 *Penalty function*

The linear altitude interpolation in the atmospheric function and the gradient based routines in GPOPS initially hindered the convergence of results in fuel-cost optimised cases. Due to this conflicting nature of the atmospheric function and GPOPS, a Lagrange cost component was added wherever optimisation with respect to fuel was regarded. In order to counter this, a small cost penalty was given to all flight path angle (γ) deflections, as can be seen in the the Lagrange, equation 4.24. The Lagrange penalty assists the optimisation algorithm in converging, but it should hinder as little as possible in obtaining optimal results. In order to do so, the contribution of the Lagrange part in relation to the Mayer component should be as small as possible. With a weight factor of 10, the optimal balance has been found. With this weight the oscillations disappeared while the size of the Lagrange penalty with respect to the Mayer criterion was 0.1%, small enough not to gravely affect the final results, but sufficiently large to accommodate a smooth problem convergence. As a side effect the Lagrange penalty sometimes may cause the optimisation to favour step climbs over continuous ascend trajectories in order to limit the amplitude of γ deflections over extended periods of time, as illustrated in section 5.2.2.

$$Lagrange_{Fuel} = \int_{t_0}^{t_f} 10 \cdot \gamma^2 dt \tag{4.24}$$

[2] $2700kg/h$ per engine is equal to $0.75kg/s$, with 4 engines and $g_0 = 9.81m/s^2$ this accounts to $29.43N/s$, more or less $30N/s$

[3] A fuel consumption of about $2700kg/h$ per engine is a typical value obtained during the optimisation experiments, see the results section7 and validation section5.2.

4.7 Trade-off Parameters for Environmental Impact

In order to the assess the effects and impact of contrail mitigation procedures, a trade-off needs to be made in order to compare the influencing factors. In this case the Radiative Forcing (RF) climate metric has been chosen as a means to evaluate the results. The methodology presented here is largely the same as used in Kaiser et al.[33], the magnitude of the constants applied have however been independently checked and adjusted where needed. As identified in section 3.1, our understanding of the evolution of contrails into cirrus clouding is still 'very poor'. The trade-off will therefore only consider the impact the initial line-shaped contrail has on radiative forcing.

According to the IPCC[28], the global aviation CO_2 induced radiative forcing component is 0.025 $[W/m^2]$ for the year 2000. Dividing the yearly CO_2 induced RF component by the aviations yearly fuel consumption yields the RF per burned fuel weight, namely: $1.19e^{-11}[W/(m^2 \cdot kN_{Fuel})]$[4]. With this parameter the fuel burn can be expressed into yearly RF equivalents.

The global radiative forcing component for line shaped contrails is assumed to be 0.034 W/m^2 for the year 2000[28]. With the total flight time[5] and the persistent contrail probability[6], a radiative forcing component of $4.85e^{-9}[W/(m^2 \cdot hr_{Contrail})]$ is derived[7]. In order to compare the radiative forcing components, the perturbations on global warming have to be taken into consideration. One unit of radiative forcing of CO_2 (RF_{CO_2}) has the same consequence on global warming as 0.59 units of radiative forcing of the line-shaped persistent contrail ($RF_{contrail}$)[16, 33]. With this the contrail-time will be expressed into RF equivalents, allowing for direct comparison to fuel burn.

[4]The total fuel burn for the year was $2.138e^8$ ton[4], or $2.097e^9[kN]$.
[5]Total flight time for the year 2000: $57e^6$ hours[26]
[6]The persistent contrail probability for the North Atlantic Corridor is 12.3%[43]
[7]Note the deviations with the values given in[33]

Verification

In this chapter the implementation of the contrail model will be verified. The correct implementation of the atmospheric function, as well as the path constraints, into the optimisation routine will be verified using ISA as a reference. Finally, the problem of convergence will be discussed.

5.1 Contrail Model

In this section, a verification of the contrail model will be performed by means of a comparison between the results from the implemented contrail model and the current state of the art.

Figure 5.1(a) displays the same graph as presented in chapter 2.3, figure 2.6. This has been done deliberately in order to explain the conditions required for the occurrence of (persistent) contrails. The relative humidity lines indicate the critical temperatures required for contrails, at varying ambient humidity levels, set against the ISA temperature. As can be seen in this graph, under ISA conditions, contrails are most likely to occur in the 10 to 14 km altitude range.

In figure 5.1(b) the before mentioned theoretic graph is replicated using the meteorologic data, processed using Schuman's contrail methodology as presented in section 2.2. The ambient temperature is set against the altitude for each grid point (blue +). These points basically indicate the temperature range encountered in this atmosphere. The ambient temperatures are on average below the ISA estimations, this is due to the fact that the data points are all positioned on a relatively high latitude of 65.76 degrees. Next to this, the local critical temperatures for each of these grid points is also shown (cyan +). The critical temperatures can be seen to correspond to the relative humidity dependant limit lines as seen in figure 5.1(a). In this graph it can be seen that for a large amount of the local grid points the Schmidt-Appleman criterion, discussed in section 2.2, applies. When the local temperature falls below the critical temperature lines, the ambient temperatures are low enough for contrails to occur trailing behind aircraft, in case they would fly through these grid points.

With the relative humidity acting as a reference for contrail persistence, the relative humidity level with respect to ice is plotted in figure 5.1(c) using the same grid points as seen in the previous graph. With many of the selected data points having a high relative humidity, the contrails prone to be trailing behind aircraft, are bound to persist and evolve for extended periods of time. Rather than relative humidity, the distributed contrail data shown here represent the pre-processed contrail probability data, indicating the relative humidity only in regions where the critical temperatures exceed ambient temperatures. This can be seen by the data uniformity in the "no contrail" region, where the magnitude of the contrail data remains around zero.

Lastly, the filter effects of the switch function mentioned in section 4.5.1, can be seen in figure 5.1(d). The switch function is basically used to filter out regions with a RH below the prescribed 80%, without making the data discontinuous. Through the implementation of this switch function filter, the regions where contrails will persist for extended periods, is indicated.

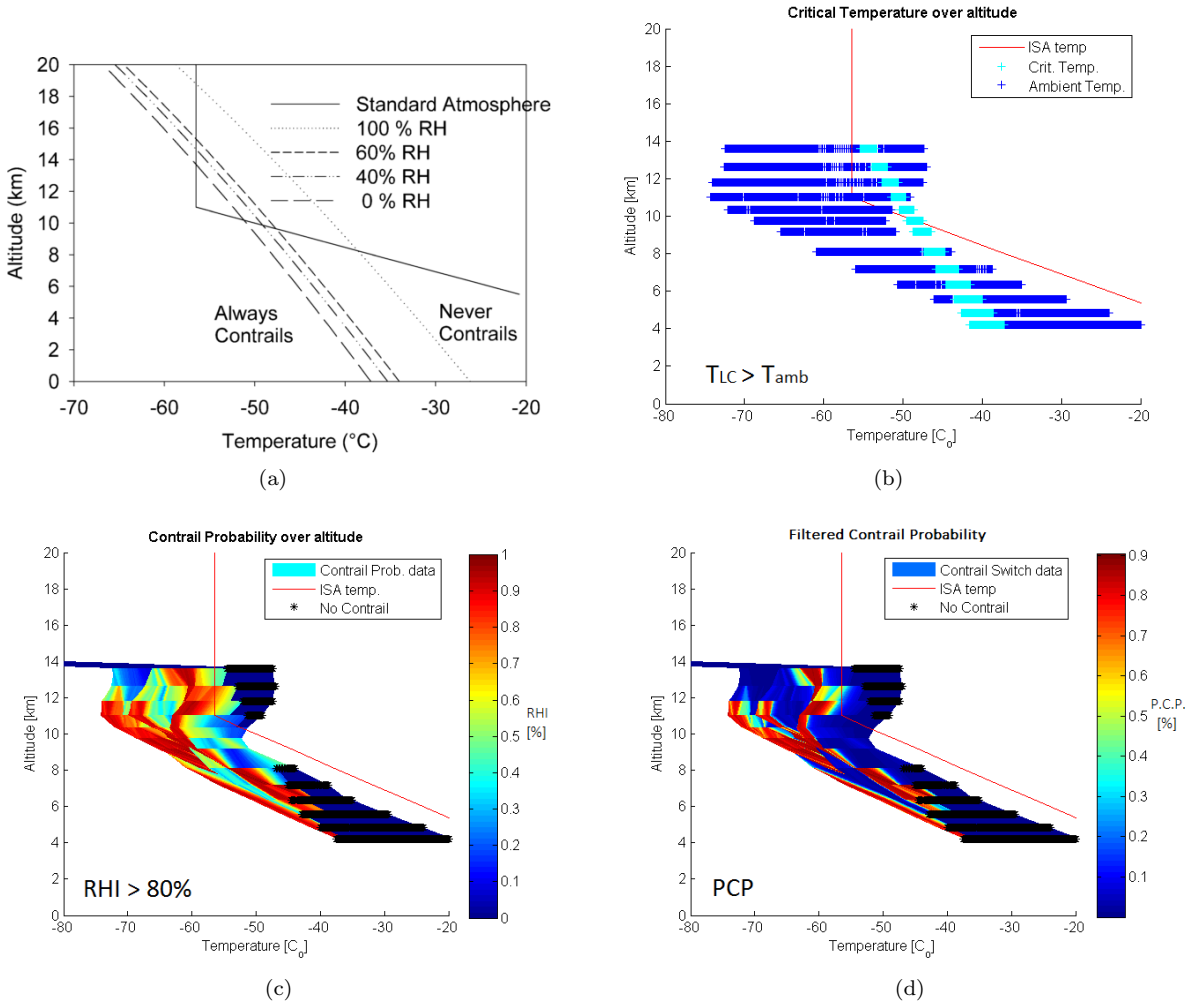

Figure 5.1: Comparison of the implemented contrail model to the contrail theory[48]. The ISA-temperature over altitude is printed as a reference in red. Contrail formation, as a function of standard (pressure) altitude vs ambient temperature. The meteorological data used dates to (12 Feb 2014), from a latitude of 65.76 and longitude ranging between -79.68 and 124.56 degrees. Parameters used for contrail calculations: $\eta = 0.3$, $EI_{H_2O} = 1.223$ and $Q = 43.2 MJkg^{-1}$.

5.2 ISA Atmosphere

In this section a verification will be conducted of the correct implementation of the developed functions, described in section 4, into the GPOPS optimisation routine. For this verification two cases will be considered, namely a minimum flight Time and a minimum Fuel consumption case. These cases will be optimised using a file with the International Standard Atmosphere (ISA) as input.

5.2.1 *Inherent errors associated with the Live Atmosphere function*

Due to interpolation of the available data, the atmospheric function will have an inherent error. Comparing the along trajectory results from the function with the International Standard Atmosphere (ISA)[1], the maximum errors for the input variables can be seen in table 5.1. These errors are marginal, proving the

Table 5.1: Inherent errors of the *Live atmosphere* function.

ISA		
-0.02%	$\leq dp \geq$	$8.40e^{-4}$%
$-1.25e^{-14}$%	$\leq dT \geq$	0%
-0.02%	$\leq \delta \geq$	$8.40e^{-4}$%
-0.02%	$\leq \rho \geq$	$8.40e^{-4}$%

interpolation in the *live atmospheric* function works as intended. Along trajectory deviations of actual "live" atmospheric parameters (temperature and pressure) compared to ISA, are in the range of -3.5% and 4%, as obtained during initial test runs. With these deviations the inherent errors are relatively small, thereby not hampering the functionality of the Matlab based function. Next to this, the relative error for pressure-ratio (δ) and density (ρ) are given. These variables are presented because they show the largest errors amongst all the variables derived in the atmospheric function, as presented in section 4.5. This is due to the fact that they are directly related to the pressure.

5.2.2 *Results of flight optimisation in the ISA*

In figures 5.2-5.4, the Time and Fuel optimal results performed in ISA can be seen, on the left (a) and right (b) respectively. Both the Time and the Fuel cases have been conducted excluding wind effects. In figure 5.2(a and b), the horizontal trajectory and the great circle route can be seen to overlap, indicating the shortest trajectory over the horizontal plane has been found. In figure 5.3(a and b), the geopotential and pressure altitude can both be seen to overlap, as expected in ISA. In figure 5.4(b) a step-climb-like ascend procedure can be seen. This is due to the Lagrange definition in which the flight path angle deflection (γ) is included as a penalty (see section 4.6). The average fuel consumptions per engine can be seen to be 3340 kg/h and 2600 kg/h for the time and fuel optimal results, respectively. For the time optimal result in figure 5.4(a), the optimal flight altitude can be found exactly on the crossover altitude of 7815 [m][25]. The optimal flight altitude, resulting in a flight trajectory matching the crossover altitude, can also be seen in figure 5.5, in which the obtained flight envelope is presented [1].

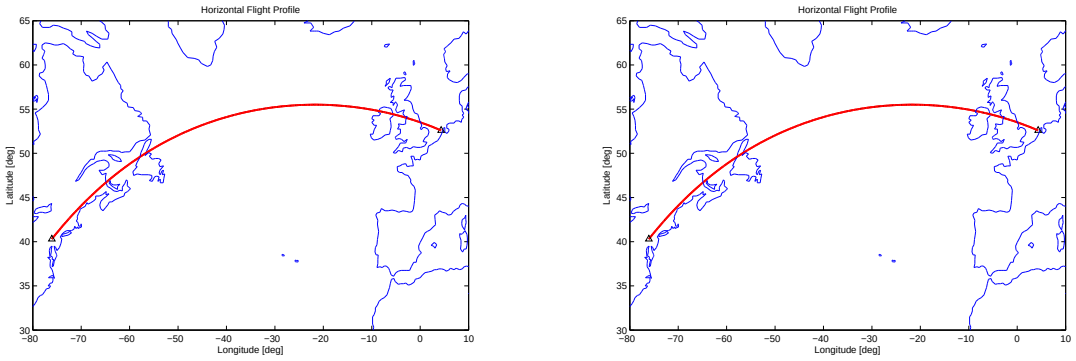

(a) Time Optimal

(b) Fuel Optimal

Figure 5.2: The ground track and the great circle route, under ISA conditions. In this case the ground track and great circle route overlap.

[1] In this case the constraints were set as $Mmo = 0.85$, $Vmo = 356[knts]$; in later optimisations these values were adjusted to $Mmo = 0.9$, $Vmo = 365[knts]$ giving a crossover altitude of 8379[m][25].

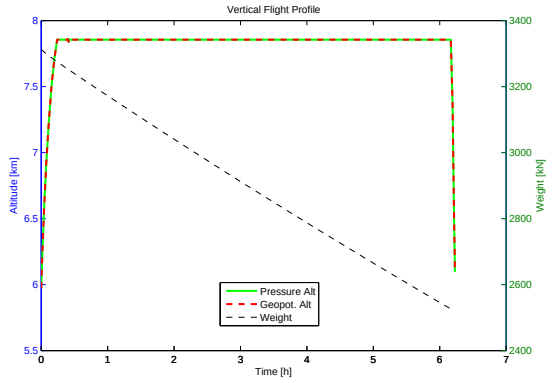

(a) Time Optimal

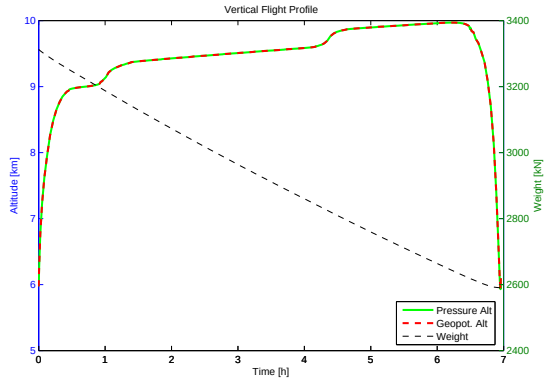

(b) Fuel Optimal

Figure 5.3: The change in weight and altitude. Both Geopotential and Pressure altitude are plotted, but as expected, overlap under the ISA conditions.

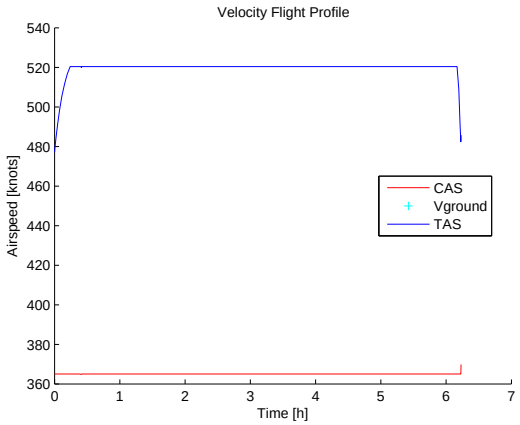

(a) Time Optimal

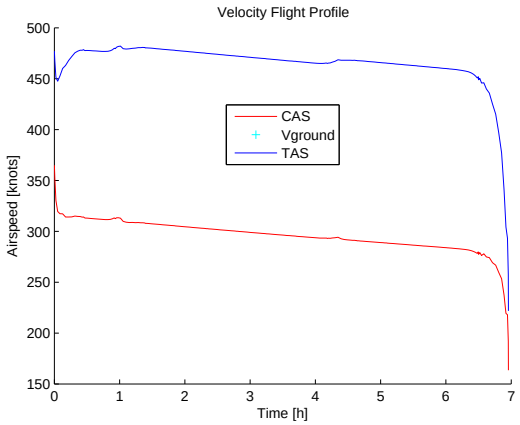

(b) Fuel Optimal

Figure 5.4: The Calibrated and True Air Speed under ISA conditions.

Implementation of velocity constraints in the ISA

In figure 5.5(a and b), the implementation of the velocity constraints can be seen, as discussed in section 4.3. In this figure the results of the Time and Fuel optimisation in ISA are plotted in a flight envelope diagram, together with the internally assessed velocity constraints. As a reference the same velocity constraints are also calculated directly from ISA. As can be seen in this graph the velocity constraint graphs overlap nicely. Next to this, all of the calculated data points, (except for the initial data point) fall within the allowable flight envelope. From this we can conclude a correct implementation and integration of both the atmospheric function and the velocity constraint function in the optimisation routine.

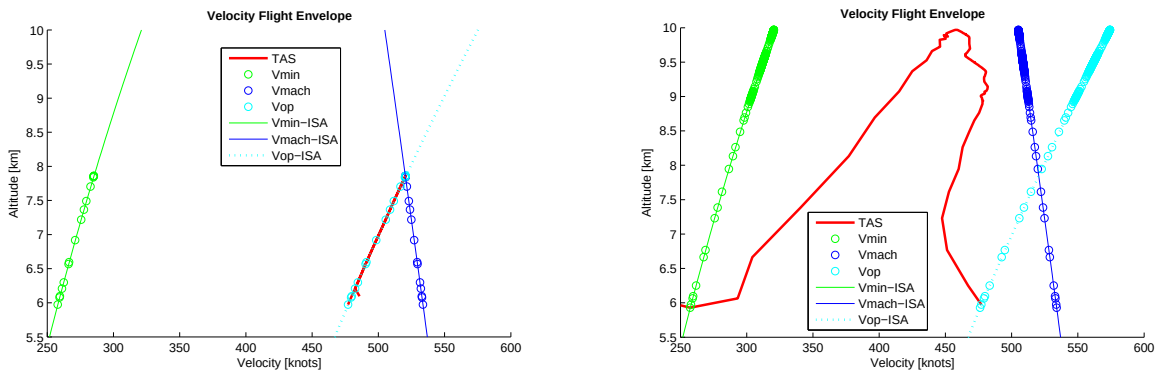

(a) Time optimal

(b) Fuel optimal

Figure 5.5: The flight envelope with pressure altitude on the y-axis and true airspeed on the x-axis. The results for the Time and Fuel optimisation performed under ISA atmospheric conditions can be seen in red. The minimal velocity (Vmin), Mach dependent maximum (Vmach) and maximum operating speed (Vop) can be seen for each data point and next to this all three ISA calculated counterparts (-ISA).

5.3 Convergence Behaviour

During the optimisation runs convergence-to-optimality issues were sometimes encountered. A number of tests were performed over relatively short distance flights in order to determine the origin and extent of this problem.

5.3.1 *Accuracy of obtained Results*

In order to determine the accuracy of the obtained results, a convergence test was performed over a relatively short distance flight from Schiphol to Belfast [AMS-BFS]. For this test multiple optimisation runs were conducted with a varying number of nodes and intervals ranging from 26 to 501. These runs were conducted for both a normal DOC objective (Cost Index: 15% time & 85% fuel burn) and for a 90% contrail reduction objective. During these cases, and all other cases presented in the report, the default feasibility and optimality tolerance of 1e-6 has been applied in the non linear programming (NLP) algorithm implemented in the GPOPS optimisation frame. The feasibility tolerance specifies the accuracy with which the non-linear constraints should be satisfied. The maximum non-linear constraint violation, normalized by the size of the solution, is required to be smaller or equal to the specified tolerance. The optimality tolerance indicates the margins within which the final solution may lay from the estimated actual optimal solution. The optimality tolerance specifies the final accuracy of the dual variables, it shows the target complementarity gap. When terminated successfully, the estimate of the complementarity slackness, normalized by the duel variables, is required to be smaller or equal to the specified tolerance[42]. In Appendix E, the obtained feasibility and optimality criteria, together with the corresponding objective can be seen for all results presented in this study. Please note that even though the optimality condition is compromised for some results, the feasibility constrain has always been well within the specified margins. The results can be seen in figures 5.6-5.8. In these figures the runs are defined as follows:

1 *Cost Index Opt*: The DOC runs where the optimality condition has converged.

2 *Cost Index Non Opt*: The DOC runs where the optimality condition has failed to converge.

3 *min90C Opt*: The DOC runs with a specified 90% reduction in contrail-time where the optimality condition has converged.

4 *min90C Non Opt*: The DOC runs with a specified 90% reduction in contrail-time where the optimality condition has failed to converge.

In figure 5.6, the mean time step can be seen for each run. As expected the mean time step decreases with each increase in nodes and interval grid resolution. The time step is equal for runs with "normal" DOC index and reduced contrail objectives. Looking at the mean distance travelled per time step, this accounts for a convergence limit of a resolution of about 17 km for the normal DOC index case and 10 km for the 90% reduced contrail case, both of which are below the 25 km grid resolution of the atmospheric input data.

In figure 5.7 the resulting objective values can be seen. First of all, the obtained objective values of the contrail reduction runs are about 2% higher, when compared to the reference DOC index objective values. This is expected because contrail areas are evaded, thereby inducing a higher fuel burn and/or flight time, hence a higher cost. Moreover, the objective values can be seen to rise as the number of nodes and interval points decrease, until convergence is no longer obtained.

In figure 5.8, the objective values percentage change with respect to the 501-nodes run, the case with the most optimal result, can be seen. This figure gives us an indication of the accuracy of the obtained results for both converged as well as a small range of non-converged solutions. The normal DOC runs converge down to lower numbers of node points when compared to the reduced contrail runs. The precision of the reduced contrail results, even the non-converged runs, remains higher, however, even though the time step remains the same, as seen in figure 5.6.

This means that with the introduction of an additional variable, contrail-time, somehow the accuracy of the solution obtained by the optimisation routine is increased. However, at the same time the convergence to optimality is negatively affected, making it harder to arrive at the optimal solution.

The convergence problems likely arise from the interaction between the linear interpolation in the live atmospheric function and the gradient based optimisation. The more dense the grid of nodes and intervals used, the smaller the time step size and so, the easier the search to convergence. Increasing the number, however, also increases the number of variables and constraints and thereby the required processing power and time. The optimal nodes & intervals setting, balancing the computation time vs the convergence requirement, has not been established. However, with a mean distance step of roughly half the size of the input resolution, convergence seems to be reached. It is therefore advisable to use this rule of thumb for the overall selection of the nodes and intervals resolution.

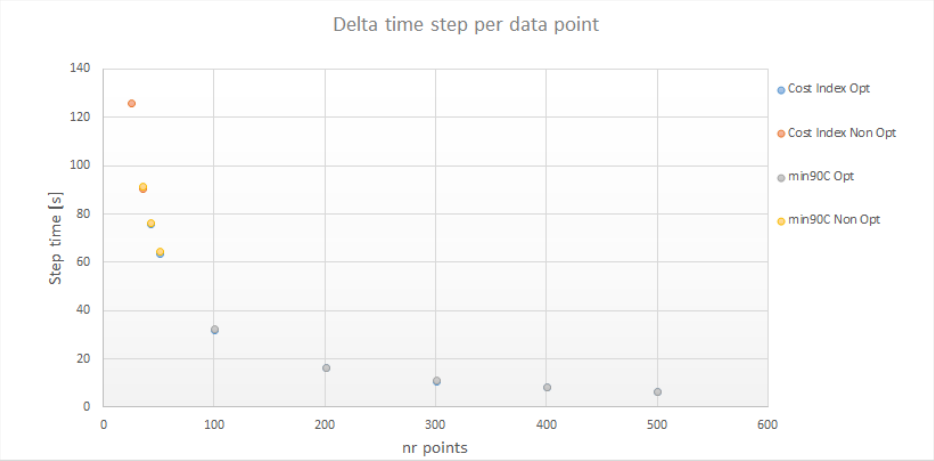

Figure 5.6: Time step size for runs with a varying number of nodes and intervals.

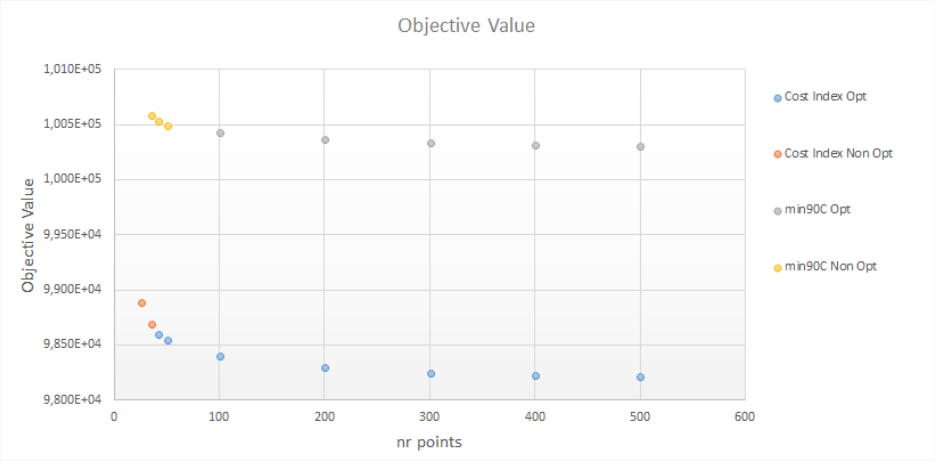

Figure 5.7: Objective value for runs with a varying number of nodes and intervals.

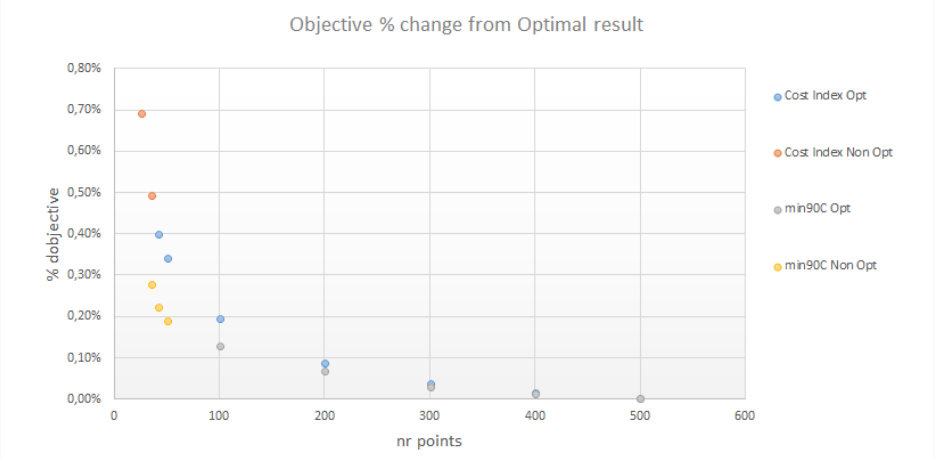

Figure 5.8: Delta objective change from most optimal result [%] for runs with a varying number of nodes and intervals.

5.3.2 *Comparison of a Converged and Non-Converged Optimal Result*

In some cases the optimisation routine has difficulty obtaining a converged optimal solution. In order to determine the accuracy of this non-converged solution, the problem solution is altered (i.e. the length of the flight is shortened), the problem is re-run and the converged optimal results is compared to the non-converged result up to the last coordinate of the shorter trajectory of the converged result. In this section, a part of a long-haul flight will be re-run for an increased number of nodes. The results of the converged optimal re-run will be compared with the initial unconverted flight section. This comparison analysis is performed, as it was not always possible to obtain the converged optimal results for the long haul flights in which wind was present. Obtaining convergence of optimality means that the final solutions normalized complementarity slackness is smaller or equal to the tolerance, in this case specified to be $1e^{-6}$[42]. (Note with convergence, convergence to optimality is meant in this case. In the cases presented in this study the feasibility condition has never been compromised.)

In this case the objective function is set to minimise the DOC. The non-converged optimisation used for comparison is a transatlantic flight between Amsterdam and Washington [AMS-KIAD], originally consisting of 226 nodes and intervals. In order to have the problem converge, the problem is altered and for the new optimisation run the destination is fixed at the 24^{th} node of the non-converged long haul flight. The final boundary conditions specified for the new optimisation problem can be seen in table 5.2. The final velocity

is also specified in order to prevent the optimisation routine from 'saving' fuel by trading kinetic energy into potential energy[2].

With this newly specified problem statement, the problem is optimised again, with a greater number of nodes and the final converged result is compared to the initial non-converged result at the intermediate location of the 24^{th} node. For the converged optimisation run, a total number of 801 nodes and intervals have been selected.

Table 5.2: Final boundary conditions for the converged and non-converged result

Parameter	*Non-Converged* 24^{th} node	*Converged* 801^{st} node
Phi $[rad]$	0.9554	0.9554
Lambda $[rad]$	-0.0735	-0.0735
z $[m]$	9164	9164
V $[m/s]$	249.0	248.9

The resulting comparison can be seen in figures 5.9(a-d). The results of the non-converged optimisation seemingly match the converged section. The difference is most notable in the vertical flight profile, were small adaptations are made to better accommodate for local atmospheric deviations.

In table 5.3, the last data point of the converged section is compared to its non-converged counterpart. In figures 5.9(a-d) this point is marked as the "Comparison limit". The coordinates and altitude were specified to exactly match the 24^{th} node in the non-converged section. The difference between the converged and non-converged accounts to an 0.12% lower fuel burn. The converged time and contrail-time results are about 0.7% higher, when compared to the non-converged result. The difference between the objectives is smaller, however; the objective of the non-converged run is only about 0.02% higher, when compared to the objective of the converged run. Despite the large difference in the number of nodes and intervals used, the results of the non-converged result match the converged results quite well. This is true when comparing both the trajectories as well as the values of the state variables at the final location.

Table 5.3: Converged and non-converged result comparison

Parameter	*Non-Converged*	*Converged*	*Deviation*
$W_{fuelburn}$	94902	94790	-0.12%
$Time$	2656	2673	0.65%
Con	1906	1921	0.78%
$Objective$	92618	92602	-0.02%

[2]A small tolerance margin was specified for the upper and lower bounds of the velocity constraint in order to facilitate a smoother convergence of the optimal solution.

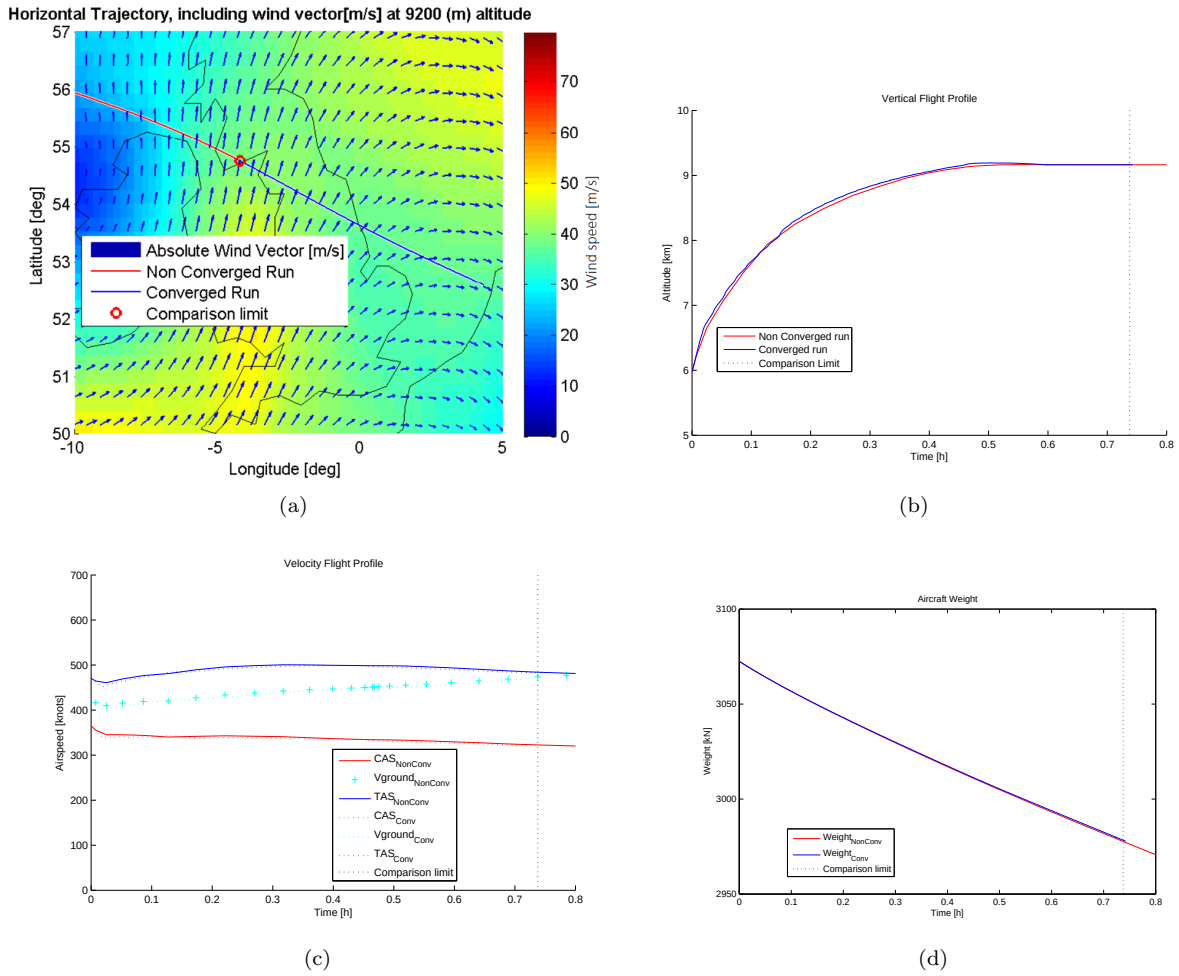

Figure 5.9: The results for the convergence comparison in which a section of a non-converged long haul flight is compared with a converged re-run of the section. Figure (a) shows the horizontal trajectories, which seem to overlap. Figure (b) shows the vertical flight trajectories, Figure (c) shows the Velocity comparison of both runs, with CAS, TAS and Groundspeed. Lastly, in figure (d) the aircraft weight comparison can be seen.

Experimental Scenarios

Let us briefly consider the design of the test case scenarios. As discussed, research has indicated persistent contrails typically form in ice-saturated atmospheric environments, with temperatures below 228 Kelvin and pressures below 300 hPa (ISA altitude $\geq 9.2km$)[29]. These characteristics are most likely satisfied at moderate latitude regions, in winter or early spring, in the months of February and March[9]. In agreement with this, the meteorologic data selected to be used during testing, which will be presented in the results, dates to (12-Febr-2014) and was published on the 12:00 UTC measurement.

Even though the horizontal spread of these regions with a high persistent contrail probability might be vast (in the order 150 km), the vertical extent is often only about 500 m[31], making it an interesting optimisation case. In order to be able to make full use of the before mentioned characteristics of contrails, the constraints on the flight and trajectory profile have been loosened as much as possible. This enables a flexible, yet technically feasible optimal flight trajectory, not constrained by standard air traffic control procedures. Air traffic control procedures have deliberately been discarded in order to investigate optimal contrail mitigation strategies.

This study focuses on the contrail mitigation during the cruise phase of the flight. The departure and arrival have therefore not been considered during this study. In the cases presented, the flight will start and end at an altitude of five kilometres.

For this study, a route flying through the Atlantic corridor was selected, because this represents a section of airspace with one of the worlds highest air traffic densities[19]. Aircraft travelling this route generally have a high probability of encountering regions prone to contrail formation[43]. Next to this, the jet stream, a manifestation of a high altitude wind field, is known to gravely affect the performance of flights traversing the Atlantic corridor. The intention of this study has been to investigate contrail mitigation under realistic circumstances. Testing the optimisation routine along a route affected by the jet stream enables the investigation of how wind affects the flight performance during contrail mitigation strategies.

The route connecting Amsterdam to Washington [AMS-KIAD] is investigated in this study, because it met all three criteria: (i) representing a route with significant amounts of air travel, (ii) encountering contrail prone regions and, (iii) considers the Atlantic jet stream.

Results

In this section the results for the scenario presented in section 6 will be discussed. As mentioned, multiple optimisation runs have been conducted for the criteria, Time, Fuel and their respective Contrail counterparts. These optimisation runs have been performed under varying conditions namely, with and without wind included. The behaviour of time and fuel optimisation is well understood, making it useful to look at the effect of contrail mitigation for these cases. From the differences in the cases the resulting contrail mitigation strategies and associated costs can be clearly identified. The Time and Fuel optimal cases can be considered, benchmark cases on the outer limits of commercial objectives and flight envelopes. These results will be discussed first in section 7.1. Next, test cases with a Direct Operating Cost objective will be presented, in section 7.2. First, a short haul flight will be considered, after which the results of a sensitivity analysis will be discussed in section 7.2.3. A sensitivity analysis in which multiple optimisation runs have been gathered to increase our understanding of the costs involved per % decrease in contrail-time. In this section, a case more representative for commercial flights will be discussed in which both time and fuel are weighed in the objective function. For all optimisation runs the meteorological data, dates to $(2014-02-12)$ obtained from the 12:00 UTC measurement.

In this thesis, a distinction is made between the *normal* and *mitigated* cases. In the "normal" cases the optimal trajectory is obtained whilst not considering contrail formation in any form. In the "mitigated" or "reduction" cases, the optimal trajectory is obtained while considering contrail avoidance. In Appendix E, the obtained feasibility and optimality criteria, together with the corresponding objective can be seen for all results presented in this study.

7.1 Time and Fuel optimisation cases

In this section the Time and Fuel optimal results and their contrail mitigated counterparts will be presented. Even though commercial flights will rarely be scheduled according to either a purely Time or Fuel optimal trajectory, (effectively) these criteria will, however, be factored in using Cost Indices representing the DOC which may vary from operator to operator. The Time and Fuel optimal results will be presented as a benchmark to get an understanding of the envelope within which results can realistically be obtained and at which cost. The optimisation runs have been performed without and with the wind components included, in order to gain more realistic cases.

7.1.1 *Flight-Time optimal results (No-Wind)*

In this first case, the time optimisation is run using the live atmospheric conditions without wind. The results are summarized in table 7.1. Significant reductions in contrail production can be achieved against marginal additional flight time and negligible changes in fuel consumption. The negligible change in fuel consumption can be explained by the rather low optimal (crossover) altitude at around 8km. At this altitude the maximum allowable operational airspeed can be obtained, but at a relatively high specific fuel consumption. The contrail mitigating manoeuvres, however, invoke an increase in flight altitude, flying at a

more efficient altitude, thereby offsetting for the fuel consumption induced by additional manoeuvring. In some cases this has even lead to a favourable or decreased fuel consumption. In table 7.1(a) the overall effect on the radiative forcing can be seen, resulting from the sharp decrease in contrail time. As a result, contrails in the initial case were responsible for 39% of total RF and in the contrail evading case for only 3%, whilst the absolute magnitude of fuel burn induced RF has remained constant. In this case, it is safe to state that a vast decrease in contrail can be achieved at a marginal increase in flight time.

In figure 7.1, both the Time and Contrail-Time optimal flight trajectories can be seen on the top (a and b) and bottom (c and d) respectively. Looking at the time optimal results, one might expect the horizontal trajectory to precisely follow the great circle route, this is, however, not the case. This can be explained by deviations in the local live atmospheric data used during this optimisation. The maximum velocity is constrained by the maximum operating speed in knots and the maximum Mach number. From this the optimal altitude is found at the crossover altitude. Due to this correlation with the Mach number (hence the speed of sound), the crossover altitude as well as the True Air Speed limit are subjective to the local temperature condition (See equation 4.10). Whereas in ISA, where temperatures are uniform, the temperature and so the maximum Mach number obtained from live atmospheric data will show local deviations. The effect of local temperatures on the maximum Mach number can be seen in figure 7.2.

As a result the optimal trajectory is relocated South of the great circle arc, because overall lower temperatures opt for re-routing south due to the slightly higher local temperatures enabling higher maximum velocities for the fixed Mach constraint whilst not compromising other performance parameters. The effect of the temperature on the velocity constraints can also be seen in the velocity flight envelope figure B.1(a) seen in Appendix B.
Comparing the Time optimal case in a live atmosphere to its ISA equivalent case, presented in validation section 5.2.2, results in an increase in flight time and fuel burn of 3.34% and 2.90% respectively.

One last note before the trajectories themselves will be compared. Looking at figure 7.1(d), one might observe the seemingly large deviations, whereas smaller deviations would also keep the aircraft from entering a "contrail area". As mentioned in section 4.5, this can be explained by a combination of the interpolation method used in the "*liveatmosphere*" function and the limited resolution of the vertical data available. With the vertical resolution of the data of about 1km, a "simulated" completely contrail free trajectory will always have to be separated from a contrail region by a 0.5km vertical distance.

Now comparing the trajectories of the Time and Contrail-Time optimised cases, one can observe the contrail case to follow a trajectory further South in order to avoid the outskirts of the "contrail area's" in the North Atlantic. Taking a horizontal detour at maximum velocity, is favoured over vertical detours through which time is lost due to both the additional trip length as well as flying at a sub-optimal flight speed.

Table 7.1: Time and Contrail-Time optimisation results excluding wind. Table (a) shows the final results, with the final time t_f, consumed fuel weight W_{fuel}, the contrail-time $t_{Contrail}$ and the radiative forcing RF from CO_2 resulting from fuel burn, from contrails and the combination. Table (b) presents the percentage and the absolute change for each of the parameters, required for the contrail evading trajectory.

(a)	Time opt	Con-Time	units
t_f	23170	23380	s
W_{fuel}	814	814	kN
$t_{Contrail}$	2670	120	s
$RF_{combined}$	1.58E-08	9.98E-09	W/m^2
RF_{fuel}	9.70E-09	9.70E-09	W/m^2
RF_{con}	6.10E-09	2.73E-10	W/m^2
$\%RF_{fuel}$	61%	97%	
$\%RF_{con}$	39%	3%	

(b)	(perc %)	(abs)	units
dt	0.91%	+210	s
dW	0.0%	0	kN
$dt_{Contrail}$	-95.5%	-2550	s
dRF	-36.9%	-5.82E-09	W/m^2

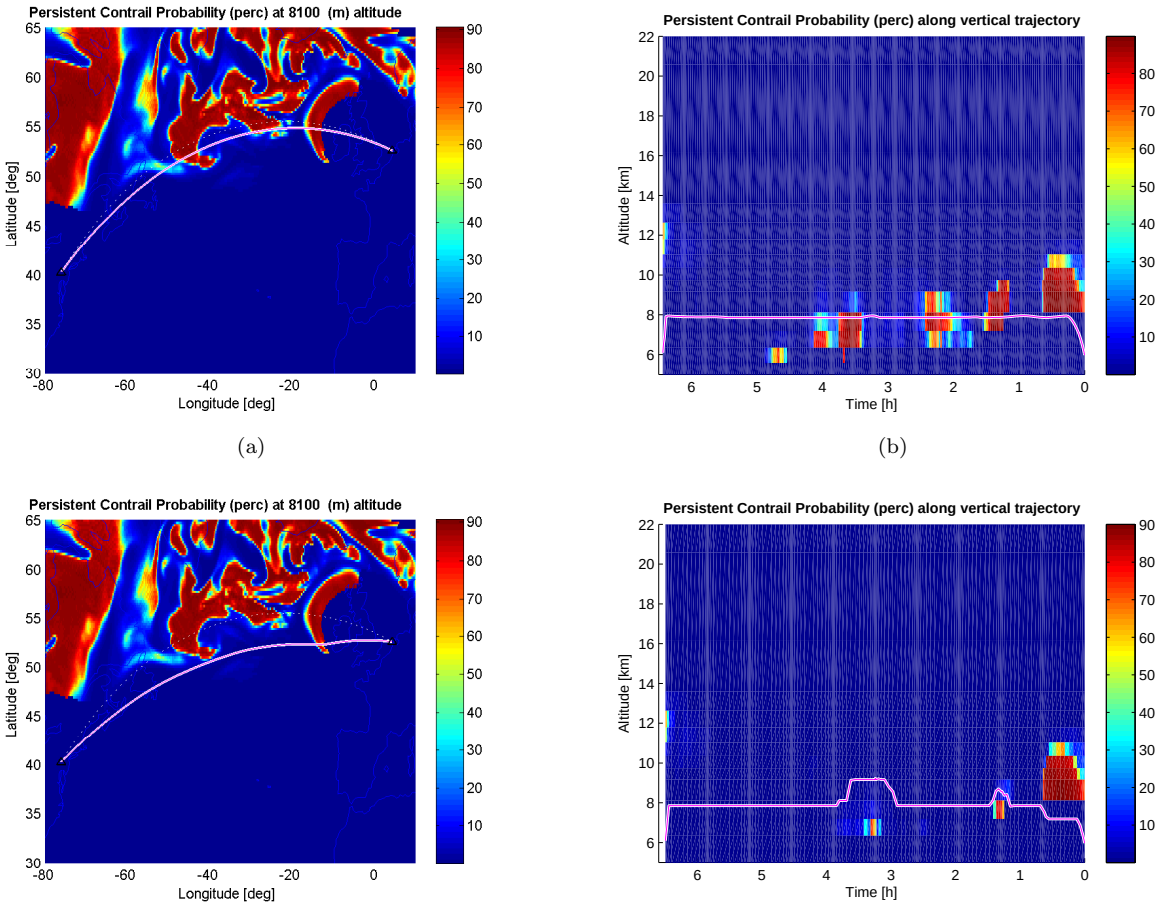

Figure 7.1: Time and Contrail-Time optimal results. The ground and vertical trajectory for the optimal result (a&b), and the contrail mitigated result (c&d) (trajectories are displayed as white and orange lines), set against the persistent contrail probability areas [%]. The great circle route (white dotted line) is shown as a reference in the horizontal overviews.

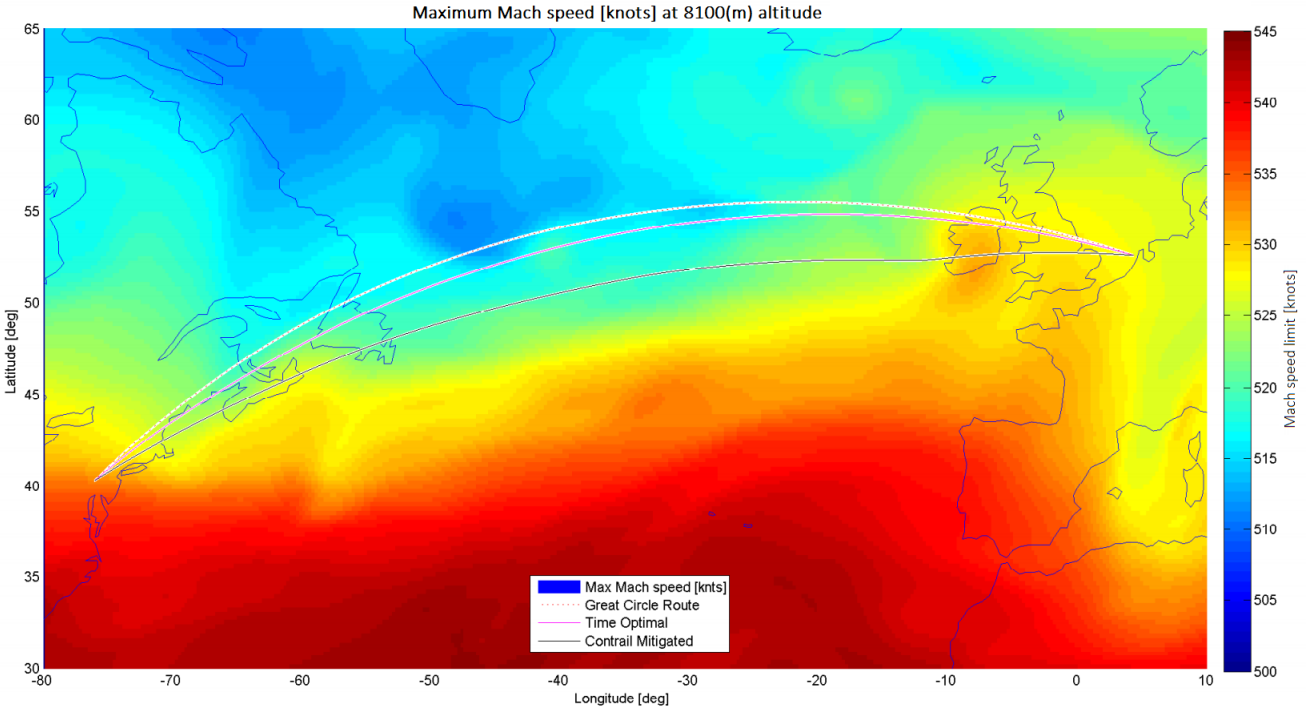

Figure 7.2: Time (pink) and Contrail-Time (black) optimal horizontal flight trajectories over the maximum Mach speed. The colours indicate the absolute Mach speed limit [knots]. The great circle route (white dotted line) is shown as a reference.

7.1.2 *Fuel optimal flight (No-Wind)*

The fuel optimal trajectories excluding wind can be seen in figures 7.3(a-d). Just as for the flight time optimal result without wind, the horizontal trajectory is located somewhat South of the great circle route. Just as with the Time optimal result, the Mach number, affected by the temperature, is the likely cause for this trajectory displacement, see figure 7.4. The effect of the temperature on the velocity constraints can also be seen in the velocity flight envelope figure B.1(a) seen in Appendix B. The most likely explanation for this lies in the aircraft model, in which a higher Mach numbers increases the maximum thrust limit, enlarging the allowable Thrust range and thereby enabling a lower throttle setting and resulting lower fuel consumption. These results, as well as the results presented in the previous section, show the significant impact the local atmospheric temperature can have on trajectory optimisation.

Regarding contrail mitigation, alterations in the ground track are minimal whereas in the vertical plane most of the contrail mitigation occurs (The ground track is relocated a fraction further South in order to avoid flying through the last tip of the contrail area near North Western Ireland). In order to mitigate for contrails, the aircraft deviates from the fuel optimal vertical trajectory in order to remain below the contrail area and ascends rapidly as soon as the chance occurs. In table 7.2, the tangible results are summarised.

The fuel optimal solution without wind takes place at higher altitudes than the time optimal result, but when comparing these solutions to their respective contrail mitigating counterpart, the overall results are similar. The largest difference is the fact that no negative correlation between fuel or time, and contrail optimisation is present. Contrary to the time (no-wind) optimal result, an additional fuel penalty is sustained as well. As the original trajectory was already fuel optimal, any alteration from it will induce a penalty in fuel consumption, in this case a penalty of 0.27% or 2kN. The percentage decrease in contrail time is lower than in the time optimisation. This is due to the original contrail time accumulated being somewhat lower and the resulting “mitigated” contrail time somewhat higher. The same can be observed from the radiative forcing composition.

Generally speaking, the effects of the contrail mitigating procedure are similar in scale as manifested in

the time optimal solution.

Table 7.2: Fuel and Contrail-Fuel optimisation results excl wind. Table (a) shows the final results, the final time t_f, burned fuel weight W_{fuel}, contrail-time $t_{Contrail}$ and the radiative forcing RF from CO_2 resulting from fuel burn, from contrails and the combination. In the bottom two rows the share of total radiative forcing from fuel burn and contrail production can be seen, respectively. Table (b) presents the percentage and the absolute change for each of the parameters, required for the contrail evading trajectory.

(a)	Fuel opt	Con-Fuel	units
t_f	25240	25410	s
W_{fuel}	739	741	kN
$t_{Contrail}$	1859	243	s
$RF_{combined}$	1.31E-08	9.39E-09	W/m^2
RF_{fuel}	8.81E-09	8.83E-09	W/m^2
RF_{con}	4.24E-09	5.56E-10	W/m^2
$\%RF_{fuel}$	67%	94%	
$\%RF_{con}$	33%	6%	

(b)	(perc %)	(abs)	units
dt	0.67%	+170	s
dW	0.27%	+2	kN
$dt_{Contrail}$	-86.9%	-1616	s
dRF	-28.1%	-3.67E-09	W/m^2

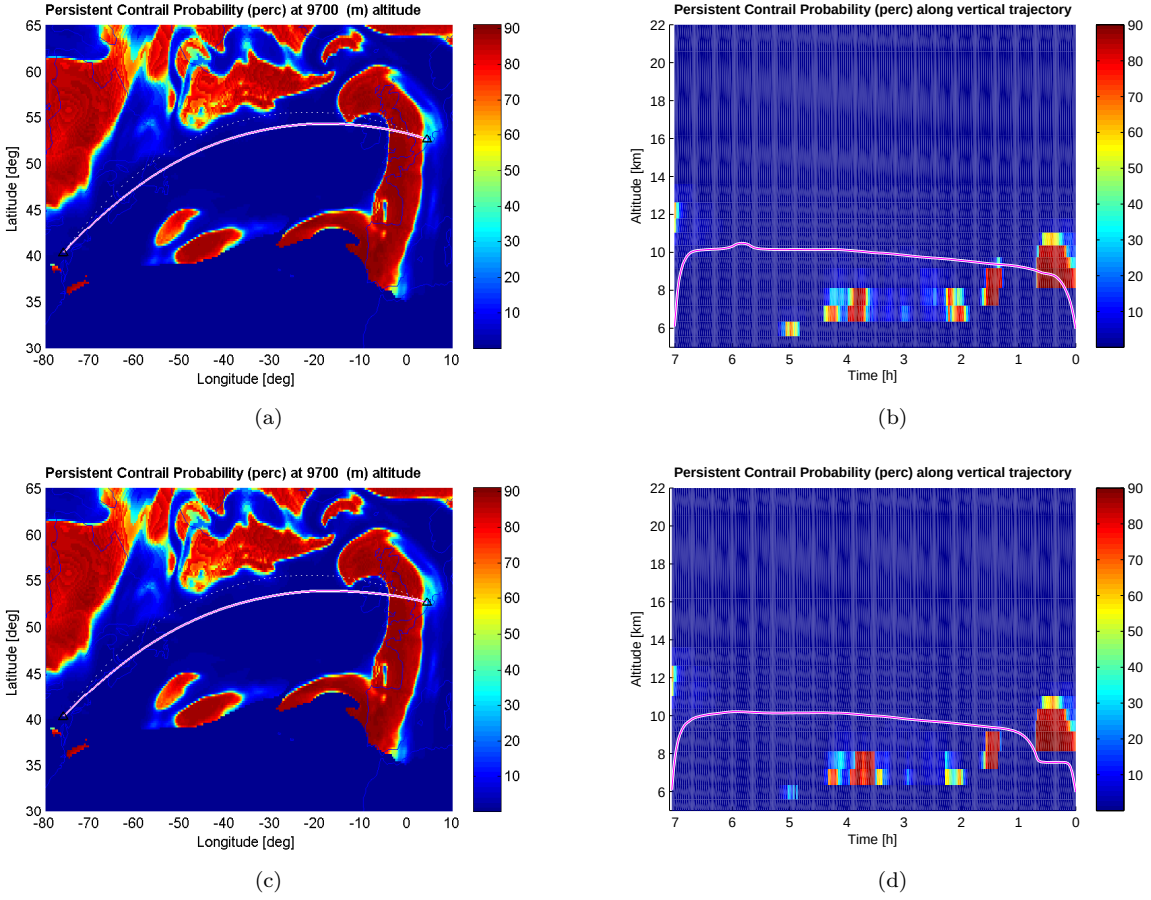

Figure 7.3: Fuel and Contrail-Fuel optimal results. The ground and vertical trajectory for the optimal result (a&b), and the contrail mitigated result (c&d) (trajectories are displayed as white and orange lines), set against the persistent contrail probability areas [%]. The great circle route (white dotted line) is shown as a reference in the horizontal overviews.

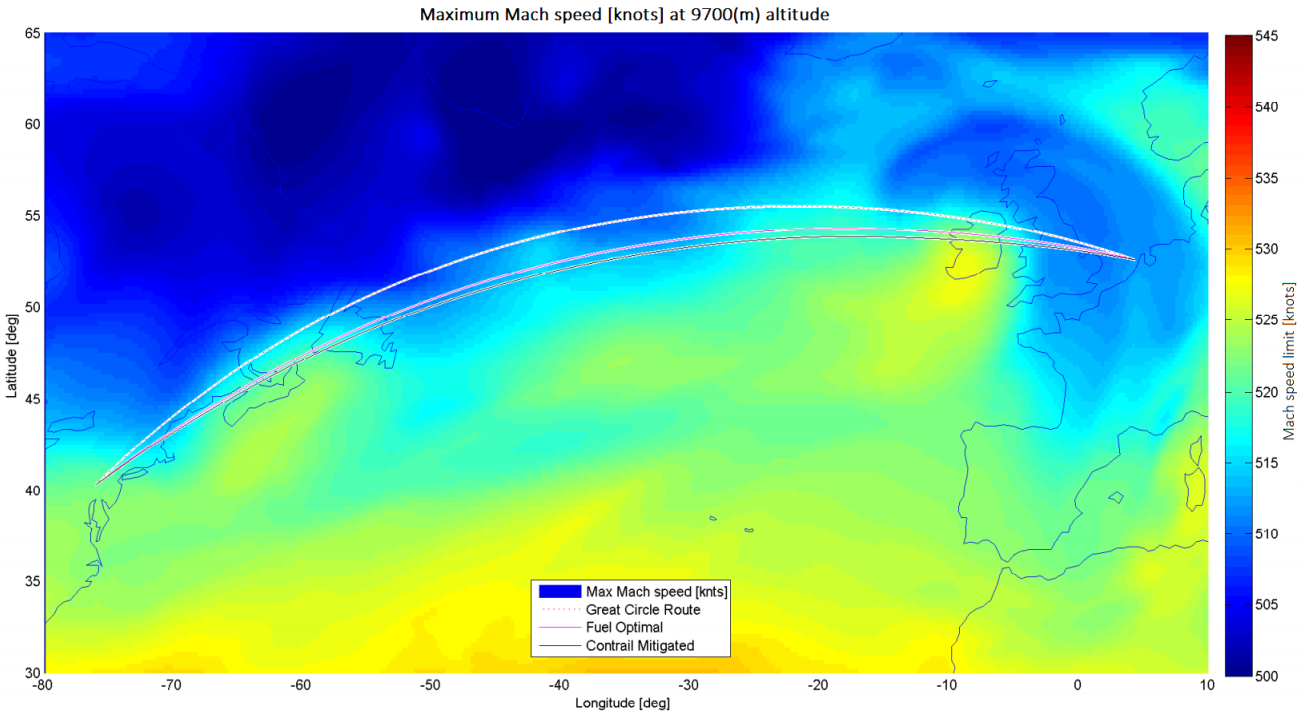

Figure 7.4: Fuel (pink) and Contrail-Fuel (black) optimal horizontal flight trajectories over the maximum Mach speed. The colours indicate the absolute Mach speed limit [knots]. The great circle route (white dotted line) is shown as a reference.

7.1.3 *Flight-Time optimal result (Wind)*

One issue that becomes apparent when comparing the time and contrail mitigated results, is the large increase in additional flight time required, namely 4.29%, seen in table 7.3. With the wind included the original great circle route becomes sub-optimal due to high head winds (Trans-Atlantic jet stream) and the route is therefore rescheduled further North, where winds are more favourable. As a result the trajectory is displaced into a huge area prone to persistent contrail formation, thereby resulting in a conflicting trade-off between wind and contrails, see figure 7.5(a,c).

As the aircraft is flying through contrail persistent areas for a larger part of the flight, when compared to the no-wind-trajectory, the resulting share in contrail induced radiative forcing is far larger. In fact the RF resulting from contrails, outweighs the fuel burn induced RF share of the total, as can be seen in table 7.3. So even though the percentage decrease of contrail time is similar, the decrease in radiative forcing is far larger. However, it requires a larger amount of both fuel burn and flight time.

From figure 7.5(a and b), it becomes apparent that small deviations will not suffice for large scale contrail mitigation. With the contrail regions accumulating around the crossover altitude small "jumps" over or under the regions will lead to long periods of flying on sub-optimal altitudes; horizontal manoeuvring will have to be applied as well. In figure 7.5(c) the resulting horizontal trajectory can be seen to have found a way South, out of the large contrail prone regions, flying through their outskirts. In figure 7.5(d) these outskirts can be seen as small patches of contrail area, avoided by small vertical corrections in the flight trajectory.

In figure 7.6 the ground track of both the reference and the contrail mitigated case are shown in combination with the wind vector field at the average flight altitude of 8100m. This figure clearly shows the deviation south resulting from the contrail mitigation strategy. For the contrail mitigated case an interesting feature can be seen East of Ireland. Due to a locally weak wind field, the optimisation sees an opportunity to briefly relocate the trajectory a fraction further south due to which the flight time through the contrail region is shortened.

As a result, 93.8% of the contrail time has been avoided at a cost of 1.7% additional fuel burn and 4.3% additional flight time, resulting in a 60% reduction of Radiative Forcing.

Table 7.3: Time and Contrail-Time optimisation incl wind. Table (a) shows the final results, with the final time t_f, consumed fuel weight W_{fuel}, the time for which contrails have been produced or contrail-time $t_{Contrail}$ and the radiative forcing RF from CO_2 resulting from fuel burn, from contrails and the combination. In the bottom two rows the share of total radiative forcing from fuel burn and contrail production can be seen, respectively. Table (b) presents the percentage and the absolute change for each of the parameters, required for the contrail evading trajectory.

(a)	Time opt	Con-Time	units
t_f	22830	23810	s
W_{fuel}	804	818	kN
$t_{Contrail}$	7610	474	s
$RF_{combined}$	2.70E-08	1.08E-08	W/m^2
RF_{fuel}	9.58E-09	9.75E-09	W/m^2
RF_{con}	1.74E-08	1.08E-09	W/m^2
$\%RF_{fuel}$	36%	90%	
$\%RF_{con}$	64%	10%	

(b)	(perc %)	(abs)	units
dt	4.29%	+980	s
dW	1.74%	+14	kN
$dt_{Contrail}$	-93.8%	-7137	s
dRF	-59.8%	-1.61E-08	W/m^2

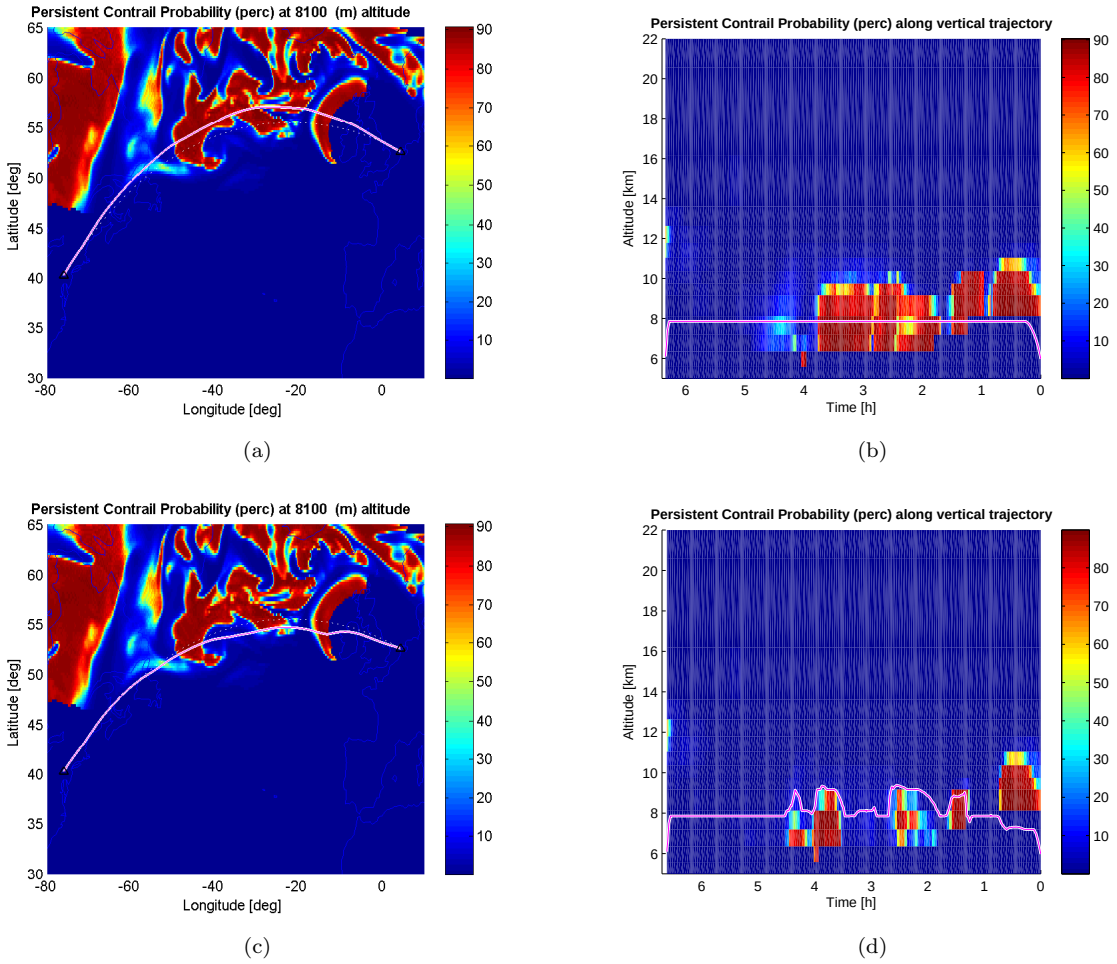

Figure 7.5: Time and Contrail-Time optimal results, incorporating the wind effects. The ground and vertical trajectory for the optimal result (a&b), and the contrail mitigated result (c&d) (trajectories are displayed as white and orange lines), set against the persistent contrail probability areas [%]. The great circle route (white dotted line) is shown as a reference in the horizontal overviews.

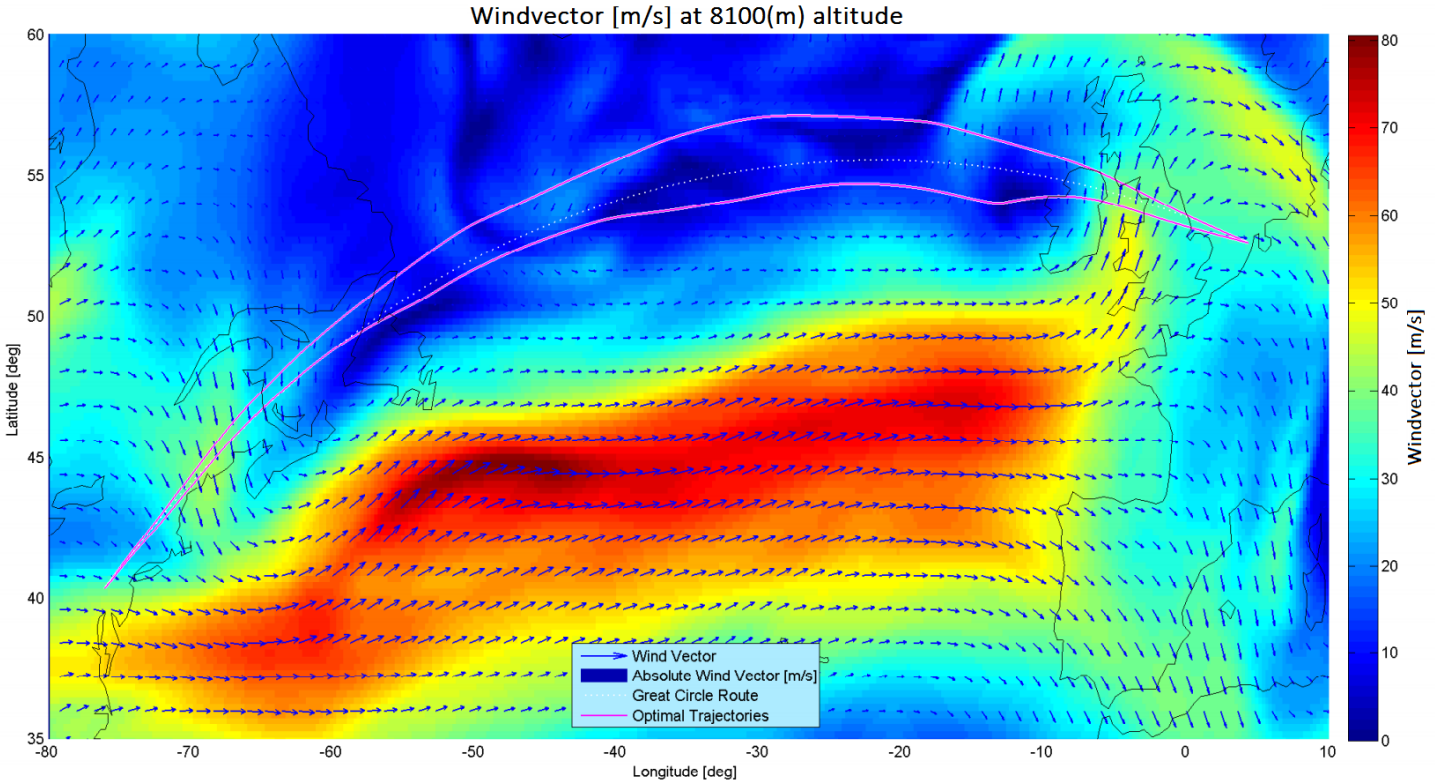

Figure 7.6: Time and Contrail-Time optimal horizontal flight trajectories (upper and lower pink and white outlined graph) over the wind vector field. The colours indicate the absolute windspeed [m/s]. The great circle route (white dotted line) is shown as a reference.

7.1.4 *Fuel optimal flight (Wind)*

Just as with the Time-optimal case, the presence of head wind has resulted in a trajectory flying through contrail prone regions further North, see figure 7.8. A similar ground trajectory is flown in combination with a vertical trajectory flying at a somewhat higher altitude, as can be seen in figure 7.7(a and b).

Comparing the vertical trajectory with the no-wind-case, it is clear to see a larger number of small deviations are present, which are most likely caused by a combination of perturbations in the local atmospheric conditions and differences in the favourable local wind vector. Looking at the last stretch of the contrail mitigated case, figure 7.7(c and d), both the horizontal and vertical trajectory are mostly similar to the purely fuel optimal result as seen in figure 7.7(a and b), encountering the same perturbations in local atmosphere. Now, comparing the alterations to the flight trajectory flying through contrail prone areas, some interesting results can be seen. Contrary to the Time optimal result in the previous section, the deviations in the horizontal trajectory are marginal in comparison. In the vertical trajectory figure 7.7(d) basically the same response as in the no-wind-case can be seen. The aircraft finds itself below a contrail prone region and remains there until a suitable opening presents itself, after which it will climb above the area. An earlier opportunity is neglected presumably because the contrail region reaches higher. After this the aircraft remains above the region incurring higher fuel burn at sub-optimal altitudes over an increase in contrail time.

In figure 7.8 the fuel optimal and contrail mitigated ground trajectories can be seen in combination with the wind vector field. The wind vector field at a pressure altitude of 9200m is displayed as this is the average flight altitude. Both trajectories are positioned North of the great circle route, due to more favourable winds.

The results in table 7.4 show that these deviations come at a marginal time increase of 0.64% or about 3 minutes and at a somewhat larger fuel burn increase of 1.9%, resulting in a contrail-time decrease of 91% and a RF decrease of 65%.

Table 7.4: The Fuel and Contrail-Fuel optimisation results including wind. Table (a) shows the direct results, the final time t_f, burned fuel weight W_{fuel}, contrail-time $t_{Contrail}$ and the radiative forcing RF from CO_2 resulting from fuel burn, from contrails and the combination. In the bottom two rows the share of total radiative forcing from fuel burn and contrail production can be seen, respectively. Table (b) presents the percentage and the absolute change for each of the parameters, required for the contrail evading trajectory.

(a)	Fuel opt	Con-Fuel	units
t_f	26380	26550	s
W_{fuel}	743	757	kN
$t_{Contrail}$	10210	935	s
$RF_{combined}$	3.22E-08	1.12E-08	W/m^2
RF_{fuel}	8.86E-09	9.02E-09	W/m^2
RF_{con}	2.33E-08	2.13E-09	W/m^2
$\%RF_{fuel}$	28%	81%	
$\%RF_{con}$	72%	19%	

(b)	(perc %)	(abs)	units
dt	0.64%	+170	s
dW	1.88%	+14	kN
$dt_{Contrail}$	-90.9%	-9275	s
dRF	-65.3%	-2.1E-08	W/m^2

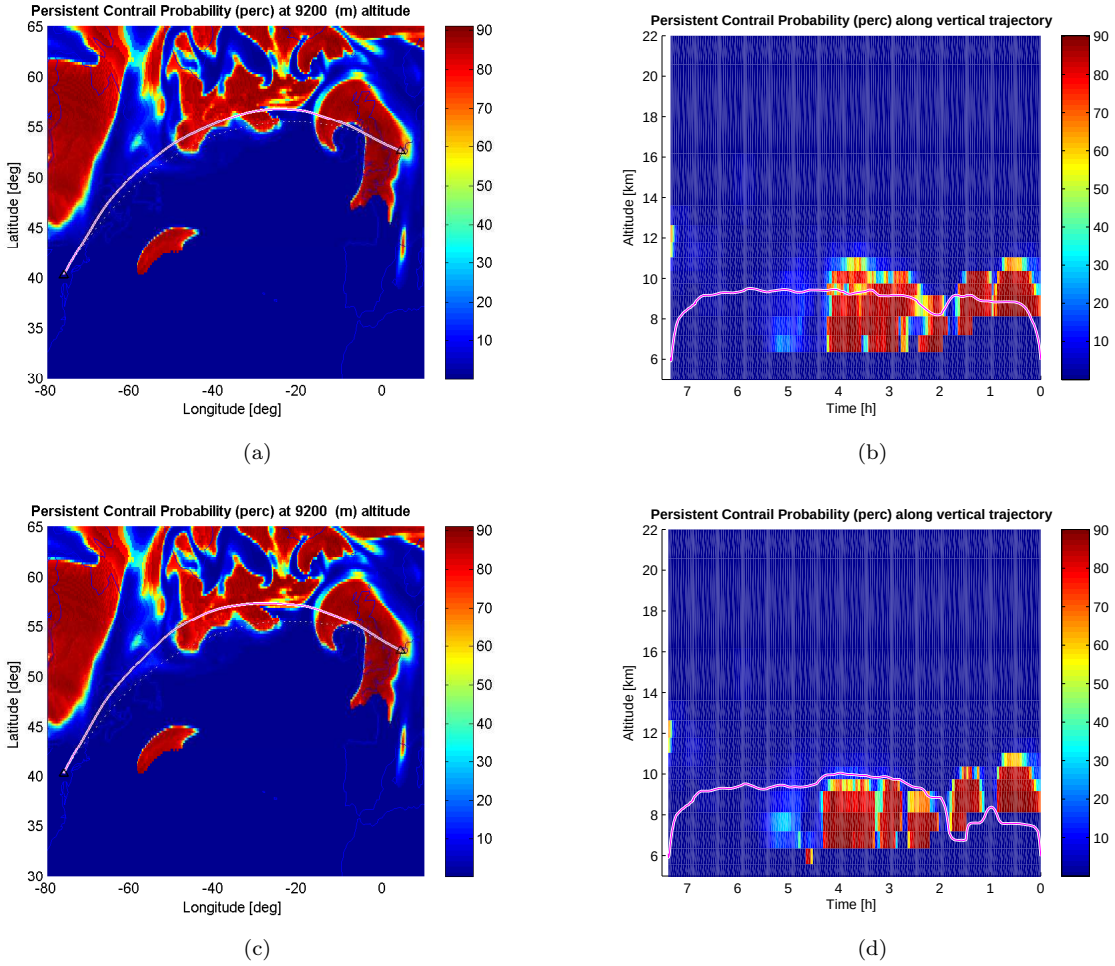

Figure 7.7: Fuel and Contrail-Fuel optimal results. The ground and vertical trajectory for the optimal result (a&b), and the contrail mitigated result (c&d) (trajectories are displayed as white and orange lines), set against the persistent contrail probability areas [%]. The great circle route (white dotted line) is shown as a reference in the horizontal overviews.

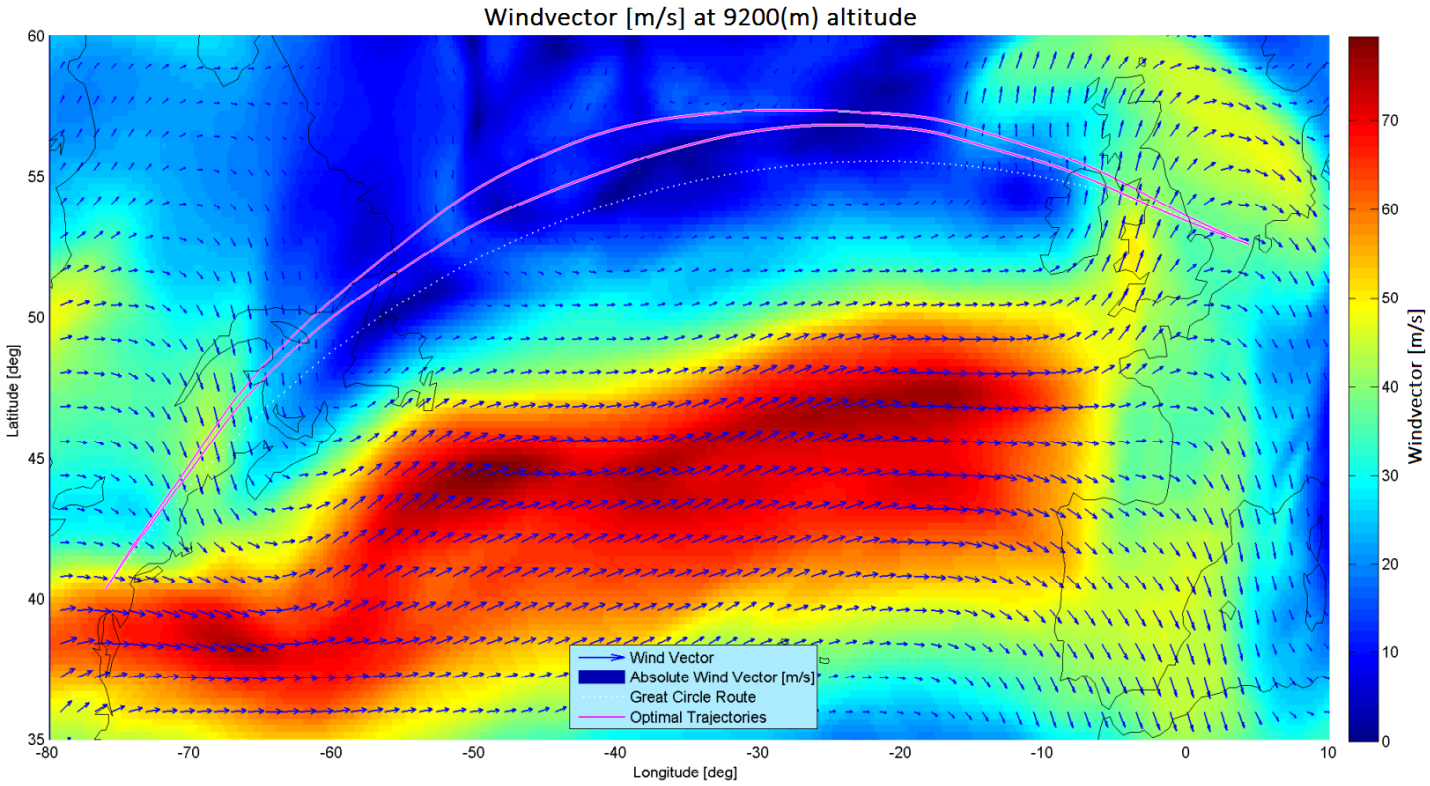

Figure 7.8: Time and Contrail-Time optimal horizontal flight trajectories (upper and lower pink and white outlined graph) over the wind vector field. The colours indicate the absolute wind speed [m/s]. The great circle route (white dotted line) is shown as a reference.

7.2 Direct Operating Cost optimised cases

In the previous section, purely time and fuel-optimal results have been compared to their contrail mitigated cases. It is useful to look at these cases, because the behaviour of time and fuel optimisation is well known and from it the effect of contrail mitigation can be derived clearly. The cases can be considered as benchmark cases on the outer limits of commercial objectives and the flight envelope. As discussed in section 4.6, airlines will in reality, however, use Cost Indices (CI) and specify an objective in which both time and fuel are considered. The scaling of the time and fuel parameter is chosen such that they are representative for their contributions to the Direct Operating Cost (DOC). This has been simulated in the cases presented .

7.2.1 *DOC optimised flight on a short-haul route (Wind)*

In the validation, presented in section 5.3, multiple runs were performed optimising the trajectory of a short-haul flight between [AMS-BFS]. For this optimisation the optimal trajectory was obtained using the cost equation 4.23, with a 15% weight for time and 85% weight on fuel burn. This cost funtion has been used because it serves as a representative case for the DOC of a commercial airliner. For the contrail mitigated case the contrail-time reduction was fixed at 90%. The results presented here represent the highest resolution trajectory optimisation of the cases presented in section 5.3, namely the one with 501 nodes and intervals.

The optimisation works rather well for this short haul flight. In table 7.5 and figure 7.9, the converged results can be seen to be rather similar to the long haul flights seen before. The costs for contrail mitigation in this case is a 1% increase in flight time and a 2.3% increase in fuel consumption, thereby decreasing the total RF component by 71%.

In figure 7.9(d), the accumulation of contrail-time can be seen for both cases. As expected the accumulation of contrail-time in the mitigation case is far slower and ends at a magnitude of 10% the contrail-time induced in the reference case. Looking at figure 7.9(b), the trajectory of the contrail mitigated case can

be seen to fall completely outside the region with a contrail probability. Between the 350hPa and 300hPa altitude grid points (*8.1-9.2km pressure altitude*) the persistent contrail probability is high, but for the gridpoints between the 350hPa and 400hPa pressure level (*7.2-8.1km*) the contrail probability is zero. This deviation has been explained in section 4.5, and is due to the interpolation in the vertical direction (altitude). As the contrail mitigated trajectory is set at an altitude of about 7.8km, falling right between the grid points the contrail probability is calculated from interpolation of both points, thereby explaining the accumulation of contrail-time.

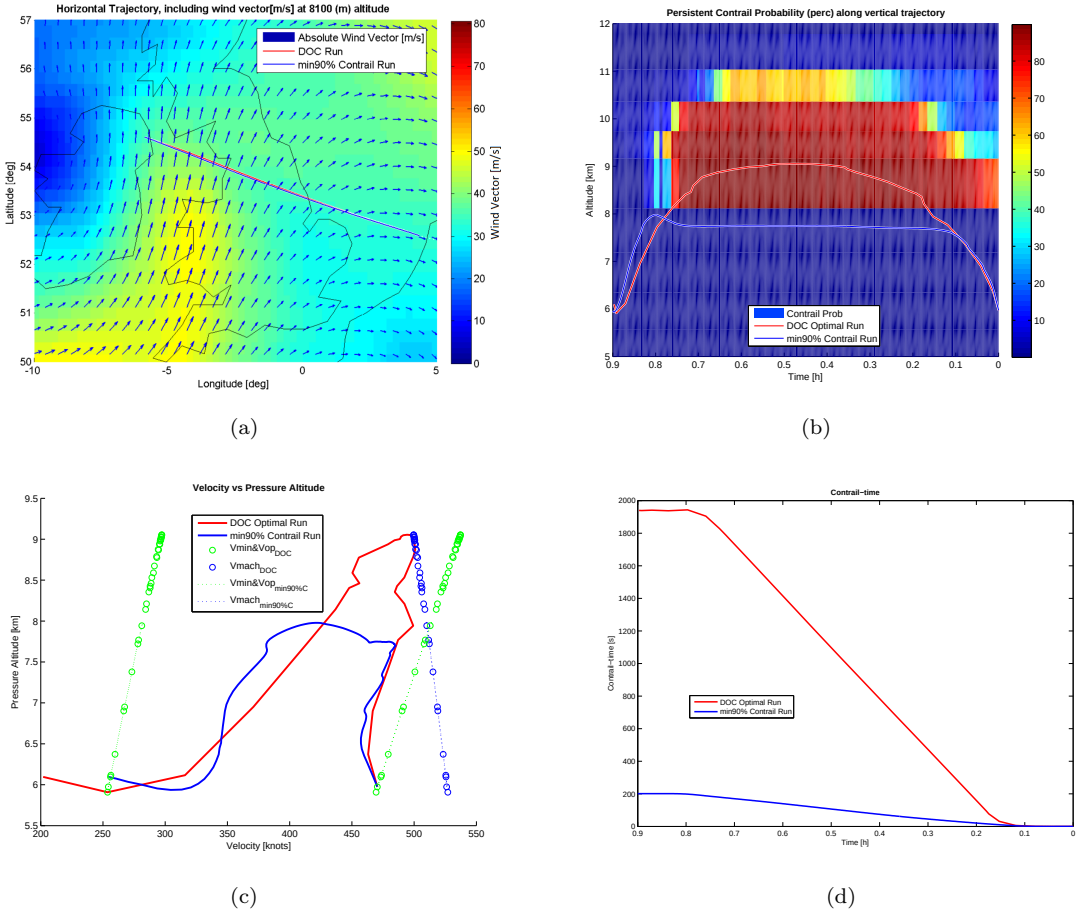

(a) (b)

(c) (d)

Figure 7.9: Short-haul flight results [AMS-BFS]. The ground track and wind vector field (a). The vertical flight trajectory with underlying the contrail probability shown (b). The velocity flight envelope (c). The contrail-time accumulation over flight time (d).

7.2.2 *Comparison of the DOC and Fuel Burn optimisation*

For this analysis, the optimal trajectory was derived using the Direct Operating Cost equation 4.23, with a 15% weight for time and 85% weight on fuel burn, and one using a purely fuel burn related optimisation. From this some interesting details can be seen.

First of all, let us compare the ground tracks and the vertical trajectories in figure 7.11(a & b). Only marginal deviations are present in the ground trajectory, whereas the deviations in the vertical trajectory are more significant.

Table 7.5: Results for the DOC and 90% contrail reduction optimisation between [AMS-BFS] including wind.

(a)	DOC opt	min90%C	units
t_f	3223	3258	s
W_{fuel}	98	101	kN
$t_{Contrail}$	2013	201	s
$RF_{combined}$	5.77E-09	1.66E-09	W/m^2
RF_{fuel}	1.17E-09	1.20E-09	W/m^2
RF_{con}	4.60E-09	4.60E-10	W/m^2
$\%RF_{fuel}$	20%	72%	
$\%RF_{con}$	80%	28%	

(b)	(perc %)	(abs)	units
dt	1.07%	34	s
dW	2.29%	2	kN
$dt_{Contrail}$	-90.0%	-1812	s
dRF	-71.2%	-7.43E-09	W/m^2

As the horizontal trajectories resemble each other so closely, the (live atmospheric) velocity constraints deviate little (see difference between o and : lines). The overall altitude vs velocity behaviour is similar, again indicating similar local atmospheric conditions. As a result the actual "live" flight envelopes of the DOC and Fuel Burn optimised runs can be compared directly in one graph, as seen in figure 7.10.

In figure 7.10, the flight envelopes of the, before mentioned standard DOC and Fuel burn optimised runs, are shown. This graph clearly shows the significance of the implementation of the "live" atmospheric data. Let us first consider the effects on the velocity constraints. Local temperatures are known to deviate from ISA-atmosphere and as a result the temperature related velocity constraints deviate as well. This phenomena has already been presented in the Time and Fuel optimisation cases were wind was not included, in figure 7.2 and 7.4. It causes a more erratically distributed velocity constraints, when compared to the neat, straight velocity constraints seen in ISA atmospheric conditions as presented in validation section 5.2.2 and the results seen here show their effect can be significant.

Comparing the DOC and Fuel optimised runs, one can instantly see how the 15% Time component in the DOC case affects the optimisation result. With similar overall altitude vs velocity behaviour, the True Airspeed is significantly higher for the DOC optimised case, indicating that for this case the additional velocity margin in the flight envelope is sacrificed at the cost of an increased fuel burn.

Another difference is the increased flight altitude in the DOC optimised case, this can also be seen in the vertical trajectory (figure 7.11(b)). This flight maintains this increased flight altitude in order gain a more favourable tail wind.

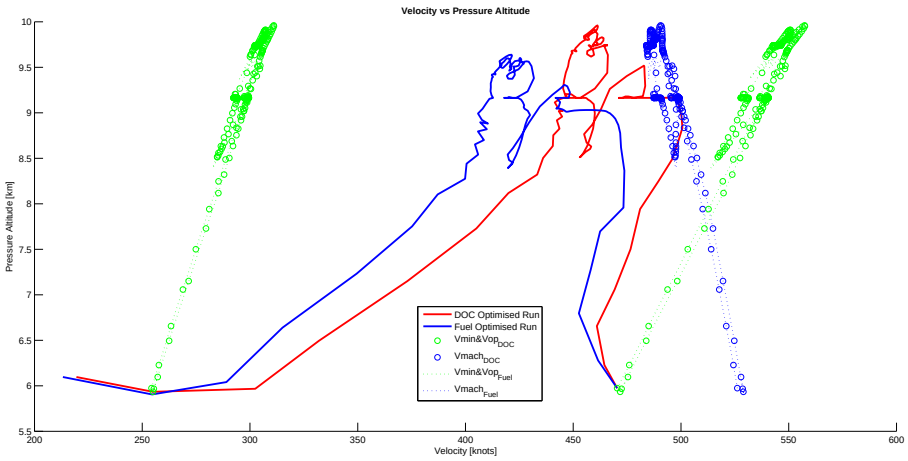

Figure 7.10: The flight envelope of the DOC (Red) and Fuel Burn (Blue) optimised runs on the AMS-KIAD route. The maximum and minimum velocity path constraints are also shown for both cases.

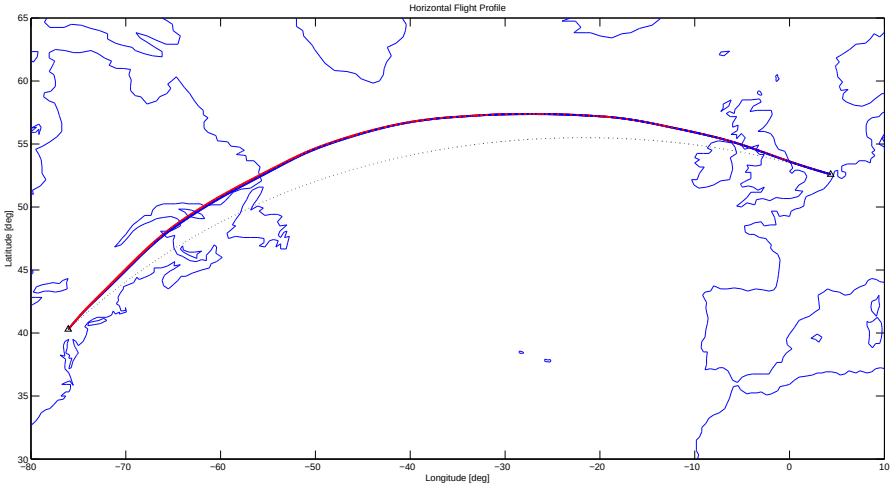

(a)

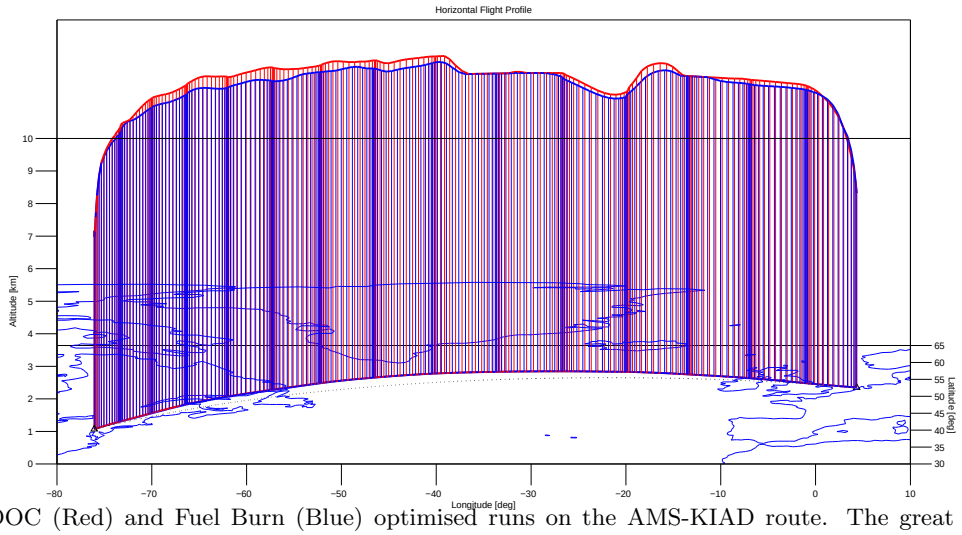

(b)

Figure 7.11: DOC (Red) and Fuel Burn (Blue) optimised runs on the AMS-KIAD route. The great circle route (dotted black) is shown as a reference.

7.2.3 *Sensitivity Study on Contrail Mitigation Cost*

In this section a sensitivity study will be performed to gain a better insight into the costs of contrail mitigation. In the previous section, the optimal trajectory was derived for a DOC with a 15% weight for time and 85% weight on fuel burn, respectively. Next to this, the previous section also presented an optimal trajectory for a fuel consumption objective optimisation. These two optimal trajectories will, in this section, be used as a reference.

For the two optimal reference solutions a certain amount of contrail-time was incurred. To gain a better insight into the costs for contrail mitigation, consecutive optimisations will be performed where the to be incurred contrail-time limit is decreased. These optimisations are performed by specifying a value of contrail-time, relative to the reference case. For this optimisation run this specific amount of contrail-time has to be incurred. An example contrail value is for instance: 1% below the amount of contrail-time incurred in the reference optimal result. This process is repeated while increasing the amount of contrail-time to be mitigated (e.g. 2,5,10,20,30,50,70,80,90,95,97,98%). Together, the final solutions from these runs are used for the sensitivity analysis.

One must understand that the combination between DOC or Fuel burn and contrail mitigation does not behave according to fixed patterns. Flight time and fuel burn are continuous functions, even though they may vary according to atmospheric conditions. However, due to the significant variability of the local atmosphere, the location and extent of contrail regions will shift on a daily basis. Due to this the interaction between flight time, fuel consumption and the mitigation of Contrail-time will also vary. Therefore, the contrail mitigation cost will depend on the atmospheric conditions along the optimal trajectory. For a more elaborate explanation of the case dependency of contrail mitigation costs, please consider the presentation in appendix C.

The results of the sensitivity study can be seen in table 7.7(A). In this table, the relative and absolute deviation with respect to the "Normal" trajectory is presented, for a number of parameters.

With every deviation from the reference trajectory, additional costs are incurred. The interesting question is: How large are the additional costs and how are the objective parameters (time/fuel) influenced by contrail mitigation?

In order to answer the question, let us look at the visualisations of the results. In figure 7.12(a) the Contrail Mitigation Potential is plotted against the DOC. The Contrail Mitigation Potential is the respective amount of contrail incurred, relative to the amount of contrail incurred in the DOC optimal reference case. From this graph it is clear that large gains in contrail mitigation can be made at the expense of an increasing DOC. A reduction of 90% contrail-time can be obtained for a (mere) 1% increase in cost (Direct Operating Cost, e.g. 15% Time and 85% Fuel weight). The costs incurred mitigating the remaining 10% of contrail-time will increase rapidly, however. To decrease the next 7% of contrail-time, an additional cost of 1.5% is incurred.

For the figure showing the change in RF against the change in DOC, seen in graph 7.12(b), the results are very similar. From this figure, it seems that the maximum to be mitigated RF is about 70% of the amount of RF induced in the reference case. The remaining 30% is attributed to the fuel burn related emission of CO_2. The magnitude of an RF "floor" may be case and atmosphere dependent, but it will be present under any circumstance. In fact, the RF in the last point is increasing again, be it only marginally (see the last RF values in table 7.7(A) and 7.7 (B). The increase in RF can be explained by the ever increasing fuel costs associated with the mitigation of the last bits of accumulated contrail-time. The mitigation costs of this remaining contrail-time is such that it negatively impacts the RF. The change in RF caused by the increase in fuel consumption is larger than the decrease in contrail induced RF.

In figure 7.13(a&c), similar graphs can be seen for the RF and Contrail index. This time, however, the results of the before mentioned DOC optimisation, as well as a fuel burn optimisation, are presented (both results are normalized for the reference DOC optimal result). In order to present them in one graph the x-axis has

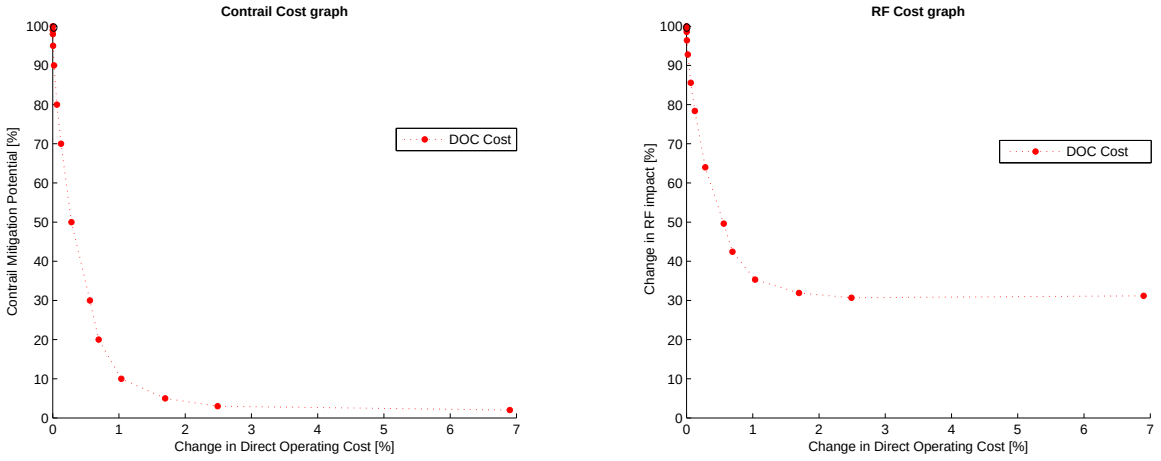

(a) (b)

Figure 7.12: Contrail and RF mitigation w.r.t. Direct Operating Cost. The reference optimal solutions are marked by a black circle.

been selected to only represent the change in Fuel consumption. From this graph, the effect of the 15% time weight in the direct operating cost optimisations can be seen, as the purely weight optimised results have a consequently lower fuel burn of about 0.9%. In graph 7.13(b), the time effects of this difference in strategy is seen [1]. The lower fuel burn of the fuel optimal case, consequently results in an, on average, 6.5% higher increased flight time.

When looking at the sensitivity of the weight and time cost response with respect to contrail mitigation, the general behaviour is seen to be similar for both the Fuel and the DOC optimisation results. Higher fuel burns are incurred to limit contrail-time and even the flight time is somewhat reduced.

This is most likely the result of the fact contrail-time has been chosen as a representative for contrails. One way to minimise contrail-time (i.e. the time it takes an aircraft to fly through a contrail prone area), is to increase the airspeed and spend less time flying through the area. This off course is not a valid mitigation strategy, but in our method forms a possibility none the less. Fortunately, this loophole in the method only represents a small portion of the contrail mitigation result. The extent of this effect is relatively small in scale, but might reach up to 2.5% of the total contrail mitigation (estimated using table 7.7 (A)). By far the largest reductions in contrail production are due to deviations in the 3D flight trajectory. Uncertainty margins like this might, however, affect the accuracy of the results in which allowable contrail quantities are extremely limited. This explains why the results as derived in the 98% reduction case do not give a realistically representation of the problem.

In the last columns of table 7.7 (A&B), the average fuel cost per mitigated contrail-second is seen, as well as the marginal mitigation fuel costs per contrail-second reduction. The average contrail mitigation costs are calculated by dividing the additional fuel consumption by the reduction in contrail-time. The marginal contrail mitigation cost represent the increase in fuel consumption, as a result of reducing one unit of contrail-time. It is the gradient of the contrail-time to Fuel consumption and is thereby estimated by dividing the increase in fuel consumption, incurred since the previous contrail mitigation point, by the amount of extra mitigated contrail-time.

On average the costs for contrail mitigation increase with every additional avoided contrail-time. The average fuel costs remain below or around $1N/s$ up to the 90% contrail mitigation cases, after which the

[1] (note, the original reference DOC optimal result is used to normalize the other results and is therefore fixed at 100% Contrail and 0% Time cost)

costs increase more rapidly. These results are comparable to the results obtained for the cases presented in the previous sections. For comparison purposes the average fuel cost results from the previous sections are presented here in table 7.6.

The last two columns of table 7.7 (A&B) show a large degree of variability amongst the marginal mitigation costs. The increase of contrail avoidance cost, seen before in the average mitigation cost, can in the marginal cost column be discerned even more clearly. This variability indicates that the costs for contrail reduction are dependent on the atmospheric conditions with respect to the optimal trajectory.

Information on the trajectories of the cases presented in this section are available in Appendix D. In the figures presented in Appendix D, the vertical trajectories, and the ground trajectories set against the PCP and windvector can be seen for all cost optimal cases.

Table 7.6: Average contrail mitigation fuel cost for the earlier presented cases.

			Average Fuel Cost	
			$dW/dCon$	$dW/dCon$
Case		**Section**	[N/s]	[%]
Time Optimal	No wind	7.1.1	0.00	0.0%
Fuel Optimal	No wind	7.1.2	1.24	0.3%
Time Optimal	Wind	7.1.3	1.96	1.9%
Fuel Optimal	Wind	7.1.4	1.51	2.1%
AMS-BFS	Wind	7.2.1	1.10	2.5%

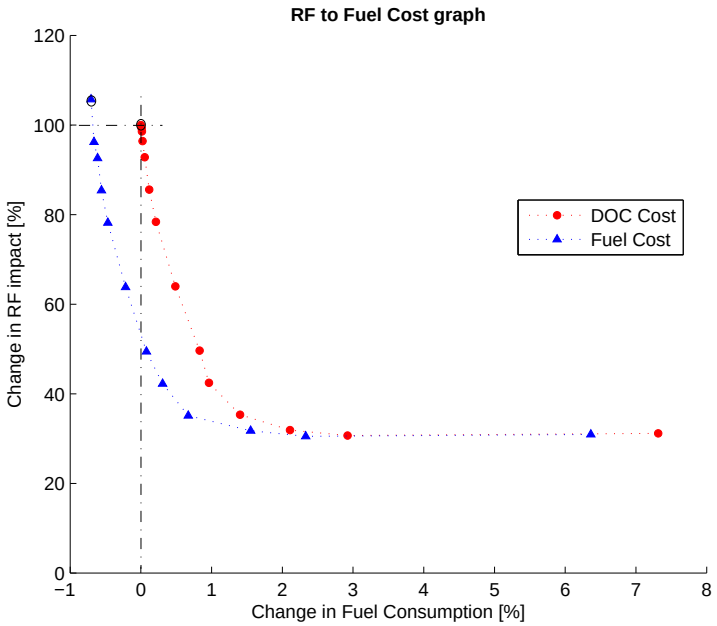

(a)

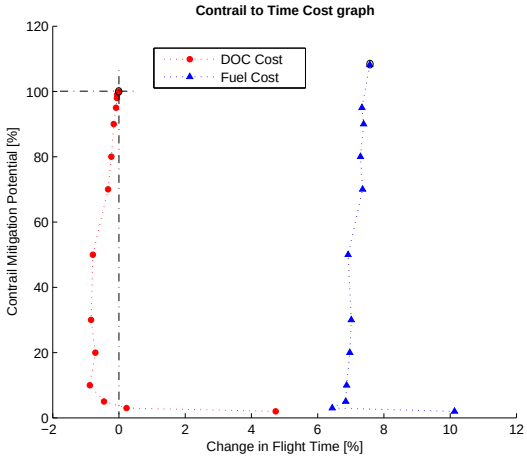

(b)

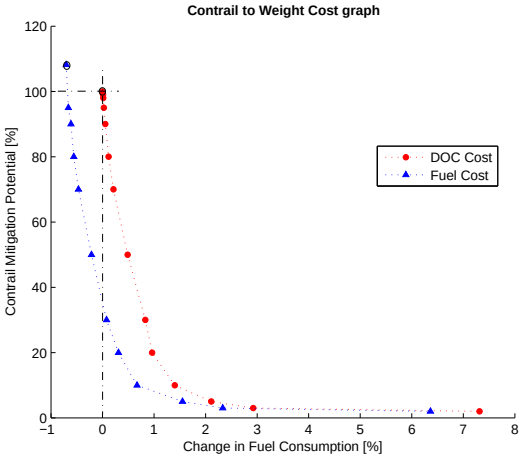

(c)

Figure 7.13: Sensitivity of the RF, Time and Fuel cost for both DOC and Fuel optimal results. The reference optimal solutions are marked by a black circle. The optimal DOC solution, according to which the other solutions are normalized, is indicated by the intersecting dashed lines.

Table 7.7: Sensitivity Results of the DOC (A) and the Weight optimisation (B).

A: Contrail DOC	**Relative Change**					**Absolute Change**			***Average Fuel Cost***		***Marginal Fuel Cost***	
	%Con	*%dt*	*%dW*	*%DOC*	*%RF*	*dCon [s]*	*dt [s]*	*dW [N]*	*dW/dCon*	*dW/dCon*	*dW/dCon*	*dW/dCon*
Normal	*100%*	*0.00%*	*0.00%*	*0.00%*	*100%*	*0*	*0*	*0*	[N/s]	[%]	[N/s]	[%]
min1C	99%	-0.05%	0.01%	0.00%	99%	95	-14	80	0.84	1.1%	0.84	1.1%
min2C	98%	-0.06%	0.01%	0.00%	99%	191	-15	99	0.52	0.7%	0.20	0.3%
min5C	95%	-0.09%	0.02%	0.01%	96%	477	-22	172	0.36	0.5%	0.26	0.4%
min10C	90%	-0.16%	0.05%	0.02%	93%	953	-40	379	0.40	0.5%	0.43	0.6%
min20C	80%	-0.23%	0.12%	0.06%	86%	1906	-58	831	0.44	0.6%	0.47	0.6%
min30C	70%	-0.33%	0.21%	0.13%	78%	2860	-83	1488	0.52	0.7%	0.69	0.9%
min50C	50%	-0.79%	0.49%	0.28%	64%	4766	-199	3406	0.71	1.0%	1.01	1.4%
min70C	30%	-0.84%	0.83%	0.56%	50%	6672	-213	5801	0.87	1.2%	1.26	1.7%
min80C	20%	-0.71%	0.96%	0.69%	42%	7625	-180	6722	0.88	1.2%	0.97	1.3%
min90C	10%	-0.88%	1.40%	1.04%	35%	8579	-222	9786	1.14	1.6%	3.22	4.4%
min95C	5%	-0.45%	2.11%	1.70%	31.8%	9055	-114	14719	1.63	2.2%	10.4	14%
min97C	3%	0.23%	2.92%	2.49%	30.6%	9246	58	20395	2.21	3.0%	29.8	41%
min98C	2%	4.73%	7.31%	6.90%	31.1%	9341	1195	51032	5.46	7.5%	321	439%

B: Contrail Weight Index	**Relative Change**					**Absolute Change**			***Average Fuel Cost***		***Marginal Fuel Cost***	
	%Con	*%dt*	*%dW*	*%DOC*	*%RF*	*dCon [s]*	*dt [s]*	*dW [N]*	*dW/dCon*	*dW/dCon*	*dW/dCon*	*dW/dCon*
Normal	*100%*	*0.00%*	*0.00%*	*0.00%*	*100%*	*0*	*0*	*0*	[N/s]	[%]	[N/s]	[%]
Case 1	88%	-0.22%	0.04%	0.00%	91%	1255	-61	295	0.23	0.3%	0.23	0.3%
Case 2	83%	-0.18%	0.09%	0.05%	88%	1731	-48	638	0.37	0.5%	0.72	1.1%
Case 3	74%	-0.26%	0.15%	0.08%	81%	2685	-72	1020	0.38	0.6%	0.40	0.6%
Case 4	65%	-0.20%	0.24%	0.16%	74%	3638	-55	1658	0.46	0.7%	0.67	1.0%
Case 5	46%	-0.61%	0.49%	0.30%	60%	5544	-166	3410	0.62	0.9%	0.92	1.4%
Case 6	28%	-0.52%	0.79%	0.56%	47%	7451	-142	5455	0.73	1.1%	1.07	1.6%
Case 7	18%	-0.56%	1.02%	0.75%	40%	8404	-153	7062	0.84	1.3%	1.69	2.5%
Case 8	9%	-0.65%	1.38%	1.03%	33%	9357	-177	9588	1.02	1.5%	2.65	3.9%
Case 9	5%	-0.68%	2.27%	1.76%	30.0%	9833	-184	15736	1.60	2.4%	12.9	19%
Case 10	3%	-1.06%	3.06%	2.35%	28.8%	10024	-287	21177	2.11	3.1%	28.5	42%
Case 11	2%	2.38%	7.12%	6.30%	29.2%	10119	646	49296	4.87	7.3%	295	439%

Discussion

In section 3.4 several previous contrail studies, making use of flexible free flight mitigation strategies, have been described. A short overview of the key differences between these studies can be seen in table 8.1, at the end of this section. The specifics concerning the herein presented research are shown in the second column of table 8.1. The column can be considered a summary of the key decisions and as such, can be used in comparing the methodology to the methodologies presented in literature. In this discussion the results as obtained in this study will be compared to previous Contrail Mitigation literature, namely Noppel 2007[39], Sridhar 2011[38] and Kaiser 2012[33].

In Sridhar et al.[38] a trajectory contrail mitigation was performed for 12 city-pairs in the United States in the presence of wind, optimising for minimum fuel consumption. The additional travel times required for completely avoiding persistent contrail formation at various flight altitudes ranged from approximately 0% to 4.3%, being similar to the time costs as found in our investigated transatlantic flights (noting the difference in contrail modelling methodology does not allow us to realistically compare completely contrail mitigated optimisation results). Furthermore, Sridhar et al.[38] conclude, that in case the altitude is optimised a two percent increase in total fuel consumption can lead to a reduction in contrail-time by more than 83%, after which the gains level out. Comparing this to the results of our sensitivity analysis, we can state that in the case the altitude is optimised throughout the flight this same result can in our case be obtained at a mere one percent increase in fuel burn.

In Kaiser[33] a flight profile optimisation was presented maximising specific range while minimizing contrail production, implementing a flight altitude ceiling, but allowing for en-route changes to the flight altitude. For the short-haul continental flight [AMS-LOWS] a contrail formation was avoided for an increased fuel burn of 2.5% in the case of fixing the en-route altitude and 1.5% in case of en-route altitude optimisation, quite similar to the results obtained herein. Unlike the study by Kaiser, where optimisation was limited to the vertical plane, this study has shown that in some cases, additional trajectory adjustments in the horizontal plane can be complimentary and is preferred over altitude adjustments alone.

In a study by Noppel[39], transatlantic flights between London and New York recorded over a full year, was studied in order to analyse possible contrail reduction. The study as performed by Noppel, however, makes use of parametrized contrail probabilities and does not take wind effects into consideration. In Noppel, a mean of 78% contrail-length reduction was achieved against an 0.8% increase in fuel burn. This result is in close agreement with the results as obtained in the sensitivity cases, where wind was included, as explored in this research. In our study large deviations have, however, become apparent between cases where wind effects are ex- and included. In order to make a fair comparison, the results from Noppel should ideally be compared to results in which wind effects have not been taken into account. Judging from the few results, excluding wind effects, obtained in our study, the exclusion of wind would most likely result in lower contrail mitigation costs, thereby providing an optimistic but simplistic picture of the problem.

Independent from this, Noppel also investigated the effect of a contrail mitigation strategy on the (aviation) induced temperature change. Noppel concluded that, despite a rather large additional fuel burn penalty of 10%, the share of CO_2 induced global warming was insignificant[39]. The study presented herein focusses

on individual flights, thereby making specific statements concerning the impacts on the global temperature unrealistic. The claim made by Noppel can, however, be made plausible. In our study, RF is seen to be far more sensitive to changes in contrail formation than it is to changes in CO_2 emission, next to this additional fuel burn required for contrail mitigation is far lower than assumed in Noppels scenario. The difference in sensitivity can also be seen by the difference in magnitude between the contrail and CO_2 RF-components[1], as presented in section 4.7.

The results, as obtained by Sridhar et al.[38], have been enhanced, showing the costs for contrail mitigation, under realistic conditions, could well be lower than observed by Sridhar et al. It must be noted however, that Sridhar et al.'s conclusions are based on multiple routes, whereas the study presented herein has focused on a single route. Sridhar et al.'s conclusions may therefore show a more generalised result of the implementation of flexible free flight contrail mitigation strategies in commercial aviation, whereas this study has deliberately focussed on mitigation strategies tailored to individual flights. Similar results, as published by Kaiser[33], have been obtained for not only short, but also long haul flights, for multiple different objective functions. In contrast to Kaiser's study, our study has shown the additional complementary benefit horizontal trajectory optimisation can have on contrail mitigation strategies. This means the results, as gained from this study are in line with, and sometimes exceed, the results as obtained in previous literature. The generalised and inaccurate estimates, as established in Noppel[39], have been independently verified, using a more accurate case-by-case based methodology. The feasibility of contrail mitigation, by means of trajectory optimisation of individual flights, using high resolution meteorologic data, has been independently verified in this study. The benefits of "free" flight regarding contrail mitigation, have been presented and indicate the case for contrail mitigation might well be more favourable, than previously assumed.

[1] $RF_{CO_2} = 1.19e^{-11}[W/(m^2 \cdot kN_{Fuel})]$
$RF_{Contrail} = 4.85e^{-9}[W/(m^2 \cdot hr_{Contrail})]$

Table 8.1: Comparison of Free Flight Contrail Mitigation studies

Literature comparison	**This Study**	**Sridhar [38]**	**Kaiser [33]**	**Noppel [39]**
Meteorologic data				
Source(type)	NWP(global):	RUC(global):	Radiosonde(local):	MetOffice(global):
Resolution (points)	750x1500x15 (lat,lon,vert)	37(vert)	5 points along route	432x325x19 (lat,lon,vert)
Resolution (km x km)	25kmx25km (hor)	40x40km (hor)		
Including wind	Yes	Yes	Yes	No
Contrail model				
Contrail parameter	Schmidt Appleman and RHI	RHI	Schmidt Appleman and RHI	Schmidt Appleman
Contrail model	Probability per grid cell	Radial penalty functions	Probability per point	Parameterized *monthly average probability per grid cell*
Method				
Route	Single long [AMS-KIAD]	Multiple [12 US City pairs]	Single short [AMS-LOWS]	Single long [LND-JFK]
Traffic data from	Individual flights	1 day (May 24, 2007)	Individual flight	1 year (2005)
Altitude	Free flight	En-Route fixed	Ceiling limit	Free flight
Ground trajectory	Free flight	Free flight	ATS route (Fixed)	Free flight
Contrail factor	Contrail-time	Contrail-time	Contrail-length	Contrail-length
Objective	Min Fuelburn, Time or DOC	Min Fuelburn	Max Specific Range	Min Fuelburn
Performance model	Enhanced Performance Model	Parametrization SFC(z)	Enhanced Performance Model	[Unknown]
Optimisation				
Optimisation method	Dynamic Optimisation *Gauss Pseudospectral Method*	Non-linear Optimal Control	Finite Element Method [a]	Simplex Optimisation algorithm
Results				
Sensitivity Analysis	Yes	Yes	No	No
Tradeoff level	RF/Con vs Time, Fuel, DOC	Con vs Time, Fuel	RF/Env. Cost vs Fuel	Con vs Fuel
Conclusion				
In numbers	See Report	-100% Con = +[0-4.3%]Time +2.5% Fuel = -83% Con	-100% Con = +2.5% Fuel[fixed z] -100% Con = +1.5% Fuel[en-route dz]	+0.8% Fuel = -78% Con

[a]Below the tropopause: 2D non-linear optimisation. Above tropopause: the optimum is directly at the minimum drag speed and the respective altitude at its intersection with selected high speed buffed boundary

Conclusions & Recommendations

The purpose of this study has been to explore to what extent the effects of contrail formation can be mitigated, within an allowable additional fuel burn or flight time cost margin. The main objective of this study was to develop a methodology optimising the socio-economic costs of a 4D aircraft trajectory while mitigating the effects of contrails formation. This methodology was verified and implemented in the existing GPOPS optimisation framework. Relevant case studies have been performed in which flight trajectories, subjected to realistic atmospheric conditions, have been optimised for a combination of fuel usage, flight time and contrail mitigation. In this section, the final objective will be considered, namely assessing whether it is both economically and technically feasible to mitigate contrail formation by alterations in the flight trajectory.

In this thesis a distinction is made between the *normal* and *mitigated* cases. In the "Normal" cases the optimal trajectory is obtained whilst not considering contrail formation in any form. In the "mitigated" or "reduction" cases, the optimal trajectory is obtained while considering contrail avoidance.

9.1 Conclusions

Aviation has a significant impact on the global atmosphere. Next to particle and gas emissions, the increase of cloud cover might increasingly contribute to aviation induced climate change. Water contained in the exhaust of jet engines locally raises the relative humidity levels sufficiently for contrail formation to occur. These contrails can persist and evolve into anthropogenic clouding, often indiscernible from natural clouding, in case the ambient atmosphere is saturated. With the projected continued growth of air traffic, increasing propulsive efficiencies and possible introduction of fuels with higher hydrogen to carbon ratios, the importance of contrail mitigation is likely to increase. In this study, contrail mitigation by means of flexible free flight was studied, as this is likely the most efficient (short term) mitigation strategy. Contrail avoidance strategies by means of flexible free flight have been in use with airforces around the globe for some decades[6]. For commercial aviation however, the implementation of any such strategies, requires a thorough assessment of cost-effectiveness.

In order to assess the socio-economic cost of contrail mitigation by means of aircraft trajectory optimisation, a methodology was developed and implemented in the existing GPOPS[14] optimisation framework. A methodology was developed enabling the incorporation of up-to-date meteorologic data as atmospheric input for the flight performance model. The methodology pre-processes the data to incorporate a Persistent Contrail Probability factor (PCP). This PCP factor is derived using the Schmidt-Appleman criterion, applied according the methodology created by Schumann[46], in combination with an analysis of the relative humidity levels with respect to ice formation. The pre-processed meteorologic input is accessed by the Live Atmospheric function and thereby enables the implementation of realistic contrail, wind, and temperature data in the optimisation routine. The tool presented here enables the quantification of the costs and benefits of contrail mitigation for individual flights. It has been tested successfully for multiple objectives under varying conditions.

In the Time and Fuel optimisation results section, quantifiable proof was given for the costs of large scale contrail mitigation for the two most extreme commercial cases, in which the flight is optimised for minimum time and minimum fuel consumption, respectively. In this section results were generated both with and without wind effects included. These optimisations showed that at the expense of less than 2% additional fuel burn, significant contrail reductions (around 90%) were possible. The contrail reductions are more than sufficient to offset the additional CO_2 emission, induced by the increases in fuel burn, and lead to an overall reduction in the flights effective Radiative Forcing. In the cases in which wind effects are neglected, the reduction in RF is about 30%, whereas in the cases where wind is included it could be as high as 65%. These differences are not so much related to the implementation of the wind effects in itself, as they are on how the inclusion of wind affects the optimal flight trajectory. In this case, the addition of the wind vector field causes a deviation of the optimal trajectory, away from a strong disadvantageous wind field into a sector prone to persistent contrail production. The results show the susceptibility of the required additional mitigation costs to ambient atmospheric conditions. This susceptibility is primarily caused by the following two factors: the contrail prone regions and the wind vector field. The location and extent of local contrail prone regions determines the magnitude of the deviations from the optimal flight trajectory required for contrail mitigation. In some cases small deviations suffice for large scale contrail mitigation, in other cases large deviations have to be made. The wind vector field can have a similar effects, depending on its direction and magnitude relative to the optimal flight trajectory.

In order to assess the costs for specific contrail mitigation targets, a sensitivity study was performed. This sensitivity study clearly shows a classic cost index graph where the largest contrail mitigating gains can be incurred with small increments of Direct Operating Cost. These costs will, however, increase rapidly for additional gains in contrail mitigation. In this study it was found that a 90% reduction in contrail cost could be achieved for a mere 1% increase in Direct Operating Cost (i.e. a combination of the Time and Fuel cost). With this the results as found in literature are sometimes even surpassed. Translating the results of the DOC optimisation in an RF index it is found that 65% of RF can be prevented for a 1% increase in DOC.

The implementation of realistic, high resolution atmospheric data, significantly impact the optimal solution in the following ways:

1 *Contrail data*: The high resolution and realistic nature of the data allows for interesting contrail evading manoeuvres. While analysing the results, let us make a distinction between manoeuvres performed in the vertical plane and manoeuvres performed in the horizontal plane.

   a In pursuit of contrail mitigation, this study has seen the following manoeuvres performed in the vertical plane:

      1. Cases in which the aircraft remains flying below and above contrail regions for extended periods of time, see figure 7.3(b) and 7.9(b).

      2. Cases where brief "windows of opportunity" are utilized to rapidly climb, and thereby evading contrail regions, see figure 7.7(b) and lastly,

      3. Cases where "hopping" manoeuvres, small and short term alterations in the altitude, over small patches of contrail region are performed, see figure 7.1(b) and 7.5(b).

   b In addition to these manoeuvres in the vertical plane, trajectory deviations in the horizontal plane are utilized when vertical manoeuvres alone do not suffice. In some cases these deviations are minor, in other cases they have a major influence as seen in the time optimal cases. In figure 7.1(a&c) and 7.5(a&c) horizontal deviations are required to enable the "hopping" strategy. In figure 7.7(a&c) the horizontal deviation enables the evasion of a high altitude contrail region halfway through the flight. In this case the optimal contrail mitigated trajectory flies over a contrail region manifesting at a high altitude. The trajectory is redirected over an area where this contrail region reaches less high, so that a marginally elevated trajectory deviation (500m) suffices for large scale contrail mitigation.

2 *Temperature data*: Deviations in the optimal horizontal trajectory indicate that the realistic non-uniform temperature distribution significantly affect the path constraints. In the "Normal" optimisation cases, where both contrail mitigation and wind effects are excluded, perturbations in the trajectory are present. The maximum True Airspeed changes depending on temperature, even at constant altitudes this can lead to a deviations in the range of 30knots, as seen in figure 7.2 and 7.4. In the absence of wind effects, these deviations can only be attributed to the non-uniformity of the temperature data.

   a In the horizontal trajectory, these effects are most significant, evidenced by the deviations from the great circle route as seen in figure 7.2 and 7.4.
   b In the vertical trajectory, these effects are less significant as evidenced by the smaller scale and lower occurrence rate of the deviations, see figure 7.1(b) and 7.3(b).

3 *Wind vector field*: The realistic wind data greatly enhances the accurate representation of commercial flight. Whereas "windless" optimisations follow the great circle route more closely, the addition of wind in the cases presented herein show large scale deviations in the trajectory, notably in figures 7.8 and 7.6. The addition of a realistic wind field enhances the dynamics of the optimisation. The optimal trajectory evades high magnitude disadvantageous wind, but thereby places the aircraft directly in a large region prone to contrail formation. As a result, the wind and contrail data affect the objective function in a conflicting fashion.

   a In the horizontal trajectory, these effects are most significant, indicated by the deviations from the "Normal" optimal trajectory between the case were wind is in- and excluded. This can be seen when comparing the figures 7.1(a) and 7.3(a) to their wind-optimal counterparts in respectively figure 7.5 (a) and 7.7 (a) .
   b In the vertical trajectory, the differences amongst the trajectory smoothness of the cases were wind is in- and excluded, seems to indicate the significance of the wind field. This is manifested most clearly in the fuel optimal cases. Whereas in the case were wind is excluded a very smooth vertical trajectory is seen, see figure 7.3(b&d), in the case were wind is included the trajectory is more erratic, see figure 7.7(b&d). These effects have so far not been traced to be specifically caused by deviations in the wind vector field (deviations in the temperature distribution could also be responsible for this).

The results have confirmed the hypothesis that trajectory adjustments in the vertical plane are preferred over adjustments in the horizontal plane. This is due to the large horizontal extent and limited vertical thickness of contrail regions. In most cases, contrail evading adjustments in the vertical plane require smaller sacrifices when compared to deviations in the horizontal plane, as can be seen the short-haul flight and fuel optimal flight excluding wind effects. Only when the atmospheric conditions are such that contrail prone regions leave no option for cost effective altitude alteration, large-scale horizontal rescheduling will be attempted. These horizontal deviations are required to search for conditions where altitude alterations can again be performed cost-effectively. This behaviour was seen in the Fuel and Time optimal flight cases in which wind effects were included. Only the results derived in the Time optimal case, excluding wind effects, appear to conflict with this statement. For this case, however, the atmospheric impact on the maximum velocity constraint, might have contributed to this southern deviation of the trajectory. As a result, the time penalty of vertical plane deviations would in this case be higher than the present horizontal deviations, where the model is adventitiously subjected to less stringent velocity constraints.

Whereas it has not yet been possible to create a tool which can perform contrail mitigating optimisations in real time, this study has been successful at creating a tool which can assess these operations for academic purposes. This tool allows to evaluate the cost and benefit of contrail mitigating operations for specific individual flights. Exact margins for allowable additional costs can be specified during these optimisations.

The result of this study gives an indication for feasible and cost-effective implementation of this contrail mitigation strategy for general and commercial aviation. Indeed, it is technically feasible for general and commercial aviation to evade contrail regions, thereby greatly reducing the effective anthropogenic cloud cover. However, it comes at a cost.

In commercially representative cases the additional time required for large scale contrail mitigation is negligible in the order of seconds to minutes. In the case the DOC are selected as objective, additional flight time incurred can be compensated by increasing the flight velocity, as demonstrated in the flight envelope diagrams 7.9(c) and 7.11(c). The sensitivity study in fact even indicates a reduction in flight time in the contrail mitigated cases, see figure 7.13(b). However, this reduction in flight time might be due to the set up of the contrail mitigation problem, more than it is an inherent benefit of contrail mitigation itself, as has been discussed in section 7.2.3.

The sensitivity analysis has indicated that for this case, 90% of the induced contrail can be mitigated at an increase in consumed fuel weight of less than 1.5%. In tables 7.7 (a&b) this is seen to compare to a Radiative Forcing reduction of 65%. Tables 7.7 (a&b) also show the non-uniformity of the contrail mitigation costs. The more contrail is avoided, the higher the average fuel burn penalty becomes. This non-uniformity in contrail mitigation costs is seen even more clearly in the presentation of the marginal cost. Up to 80% contrail mitigation the marginal costs are non-uniform, but remain relatively low at 3%. This means that for every 1% contrail-time avoided an 0.03% increase in fuel burn is required. However, beyond an 80% contrail reduction, the costs for every additional reduction increase rapidly. According to these results it might therefore be more cost-effective for commercial aviation to implement a partial contrail-reduction plan rather than a zero-tolerance contrail strategy. A form of effective contrail mitigation might therefore be to reduce contrails for as long as the average and marginal costs remain below pre-specified limiting values. For instance, allowing contrail mitigation as long as the average fuel costs for mitigation remain below 1N per contrail-second and the marginal cost remain below 4%.

This study has shown the case dependency of contrail mitigation costs. Whereas for some cases large contrail mitigation can be achieved at relatively low cost, for other cases large costs are incurred. This shows the potential benefit of using up-to-date atmospheric data over parametrized and more generic atmospheric models often used in climate studies. Future research is required to analyse these variations in mitigation cost and to optimise a more holistic aviation wide contrail mitigation strategy. The research presented herein however, clearly shows the feasibility and benefits of individual flight optimisation with respect to contrail mitigation using realistic short term meteorologic forecasts. Next to this, additional benefits for the allowance of a less restrictive control of airspace and air traffic, required for the implementation of more flexible flight optimisation, are presented.

Finally, this study has shown the great merit of implementing flexible free flight contrail mitigation in commercial aviation. It has presented an academic methodology potentially forming the basis of a commercial tool to be used for scheduling of environmental optimal trajectories throughout the aviation sector. This would enable airliners to optimise their fleet movements while accounting for both economic and ecological impact factors.

9.2 Recommendations

The work as presented herein shows the first attempt to incorporate a contrail avoidance strategy in the GPOPS optimisation routine; as such, multiple improvements can be made in future work. Therefore, recommendations on further research and working methods are presented in the following.

With respect to the pre-processing of the meteorologic data, primarily the analysis of contrail formation is time consuming. Due to the large amount of grid points, much of this time is spend on the iteration determining the temperature for which the mixing line slope equals the ratio G, see equation 2.2. A look-up table, of the critical mixing line slope dependency on temperature and relative humidity, can be constructed which might possibly reduce computation times.

In the sensitivity analysis results, reductions in flight time could be seen in the cases where contrail formation is mitigated. These gains in flight time are most likely a result of the way the contrail parameter is defined. Increasing the aircraft's velocity reduces the time during which it is flying through a contrail region, thereby effectively reducing the incurred contrail-time. A better objective contrail parameter in future research,

might for instance be: contrail-length ($\int_{t_0}^{t_f} t_{contrail} \cdot V_{TAS} dt_{contrail}$). Implementing this alternative objective parameter would eliminate this phenomenon.

The "live" atmosphere routine is one of the most critical additions this project has made. It enables the interpretation of up-to-date meteorologic data, by means of which "live" velocity path constraints, wind vector fields and contrail data can enhance the accuracy of the optimisation routine. To solve the issue with problem convergence discussed in section 5.3, it might be required to replace the linear interpolation with an interpolation technique that is more compatible with the gradient-based routines of Intlab (e.g. B-splines). The interpolation with respect to the altitude seems to be causing most of these issues. Altering the interpolation technique used in the vertical direction, might therefore suffice in solving the issue. The gains from a faster convergence, requiring fewer iterations, might offset the additional computation time required by more demanding interpolation schemes. It might even require fewer data points or an extended flight range to convergence.

With the inclusion of several parameters possibly conflictingly affecting the objective (e.g. wind vector field and contrail data), the presence of local minima might negatively impact the solution's optimality. In order to solve this it might be useful to investigate ways to pre-process the data, including a crude global optimiser, after which the local optimisation routine employed herein could be started.

The work as presented here shows how "live" or forecast atmospheric data can be implemented in aviation related optimisation routines. The live atmospheric routine can be adapted to incorporate time dependent atmospheric changes, for long haul flights. As a result, persistent contrail formation could possibly be forecast at a higher accuracy. Before doing so, the possible significance of this alteration should be assessed in order to determine whether it is worth the additional investment in computation power.

The contrail model used to pre-process the atmospheric data for areas prone to contrail formation could, with little effort, be modified to calculate (mean) persistent contrail probabilities for specific regions or even globally. These probabilities could henceforth be used in parametrized models. In section 5.1 a similar process was presented for one latitude.

Another recommendation is to integrate a tool assessing the evolution of contrails into the program. At this stage the academic understanding of aviation induced cirrus clouding are yet to be improved, in order to assess the true magnitude of its impact on climate change. Assessing the life time, the spreading and evolution process of contrails could significantly enhance the accuracy of the tool.

Next to this the contrail cost function could be expanded facilitating the assessment of RF contribution of most notably O_3, CH_4, H_2O and $Sulfate$ emissions. Whereas the study presented herein considers the effect of CO_2 and contrails on RF, including the RF contributions of additional emissions would help to generate a more holistic optimisation routine in which "genuine" green flight trajectories can be assessed.

Furthermore, the routine could be enhanced such that the radiative forcing metric is transformed into a more holistic parameter measuring the effect of mitigation strategies on the climate. As radiative forcing is a fairly short term metric, considering the long periodic scope required for climate change, a better approach could be to estimate the effect in terms of a long term metric like global temperature change.

As seen in this study the costs for contrail mitigation vary greatly with changing atmospheric conditions. First the case dependency of mitigation costs needs to be better understood. After which it might be interesting to investigate contrail mitigation strategies from an airliners perspective seeking to reduce yearly radiative forcing. It could prove valuable to understand how and to what degree the mitigation costs can be lowered by changing the mitigation strategy from a case by case strategy, to a company wide mitigation strategy. Rather than opting for a 90% contrail reduction for all cases, an alternative approach aiming at a company wide 90% contrail reduction could possibly prove more cost efficient.

A. Constraint limits & Aircraft Parameters

Figure A.1: Boeing 747-400, the modelled aircraft used in this study[11].

Table A.1: Aircraft parameters [57]

Parameter	*Value*	*Unit*
V_{mo}	365	Knots
M_{mo}	0.9	-
V_{min}	192	Knots

Table A.2: Path Constraints

Parameter	*Min*	*Max*	*Unit*
$\dot{z}$	-10	10	m/s
$\dot{V}_{TAS}$	-20	20	m/s^2
$V_{TAS} - V_{mo}$		≤ 0	m/s
$V_{TAS} - V_{Mach}$		≤ 0	m/s
$V_{Min} - V_{TAS}$		≤ 0	m/s

Table A.3: Flight destination constraints[57]

Parameter	*Value*	*Unit*
ϕ_{AMS}	52.588	deg
λ_{AMS}	4.333	deg
z_{AMS}	5974	m
ϕ_{KIAD}	40.299	deg
λ_{KIAD}	-76.064	deg
z_{KIAD}	6096	m
ϕ_{BFS}	54.601	deg
λ_{BFS}	-5.909	deg
z_{BFS}	6096	m

B. Time and Fuel Optimal Flight Envelopes

The flight envelopes for the Time and Fuel optimal trajectories, both excluding and including wind, presented in section 7.1, can be seen in figure B.1.

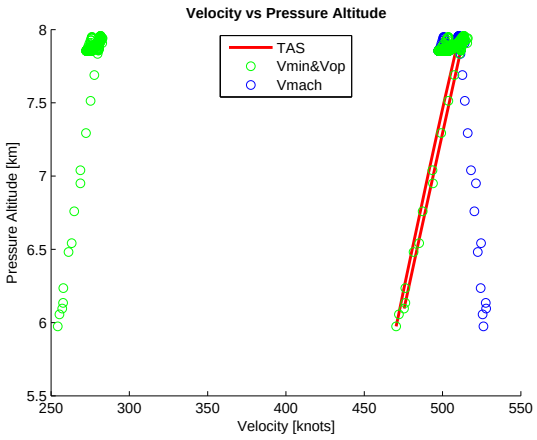

(a) Time optimal (excl. wind)

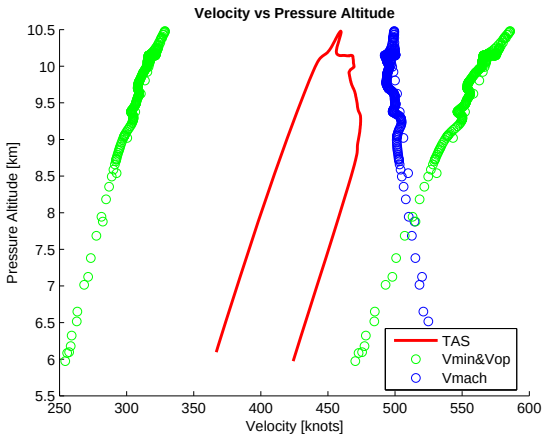

(b) Fuel optimal (excl. wind)

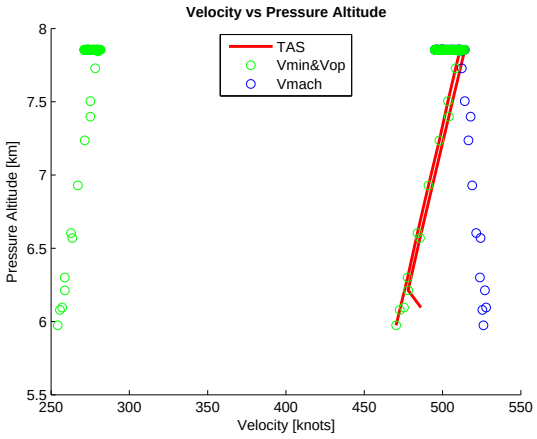

(c) Time Optimal (incl. wind)

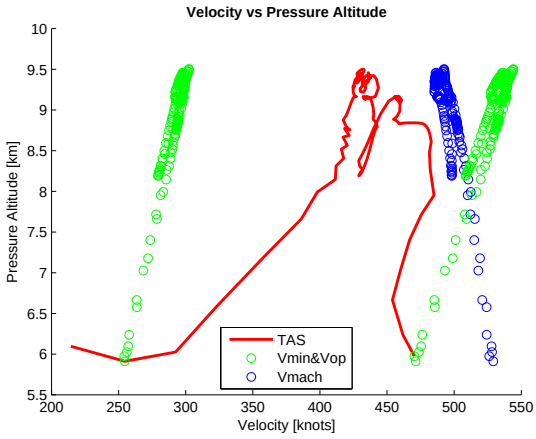

(d) Fuel Optimal (incl. wind)

Figure B.1: Time and Fuel optimal flight envelopes. The in flight True Airspeed is plotted against the pressure altitude (red). The minimum and maximum operating velocity (green o) and the maximum Mach limit (blue o) are marked for each node and interval.

C. Contrail Cost Index

In this appendix a brief explanation on the case dependency of contrail mitigation cost will be given. As this thesis has shown, contrail mitigation can be performed in 4D, this section will however consider 2 dimensional contrail mitigation only in the horizontal plane for the sake of clarity.

Figure C.1 shows an imaginary persistent contrail probability map in combination with the ground track of six different flights. The left image shows the DOC optimised trajectories, while the right image depicts the contrail-time optimised trajectories.

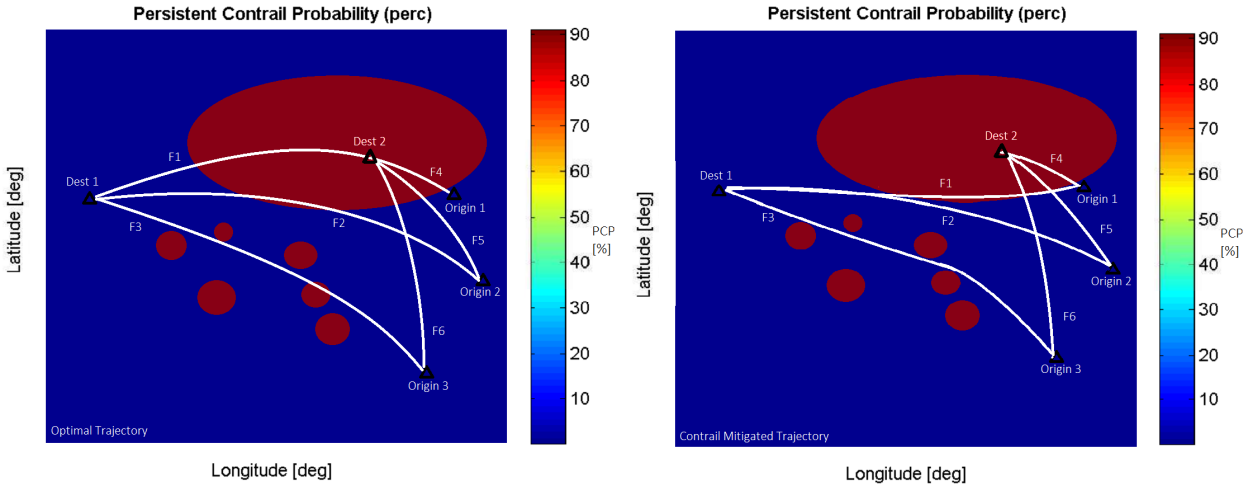

Figure C.1: Case dependency of Contrail Mitigation Cost. Schematic representation of optimal trajectories (left) and contrail mitigated cases (right).

In table C.1 the DOC, normalised for the DOC of Flight 1, and the inquired Contrail-time (as a ratio of the total flight time) are given for each of these six cases, for the Optimal and the Contrail Mitigated trajectories respectively. The figures are fictional, but represent realistic behaviour.

The great circle distance for the first three flights are the same, and hence the cost of each of these flights are equal. However, Flight 1 flies through some big contrail prone regions, whereas Flight 2 barely touches it, Flight 3 on the hand, flies through small patches of contrail prone area. As a result the time these flights are flying through the contrail regions deviate. Now, these flights are optimised for a 90% reduction of contrail-time and as a result additional costs are incurred, in table C.1 the % deviations in cost and contrail-time are shown.

In the last column of table C.1, the Cost over Contrail-time reduction is presented. For flight 1, where large deviations are required to evade the big contrail region, the costs to contrail mitigation ratio are rather high, 5.6%. For flight 2, where only a small southward correction is required to evade 90% of the contrail-time incurred, the required cost are lowest. The case of Flight 3, finds itself in between the previous two cases with a contrail mitigation cost of 2.2%.

The flights 4,5 and 6 all have the same destination, lying in the centre of a contrail prone region. The absolute contrail-time incurred on these flights is roughly the same, the stage length of these routes however vary and as a result the incurred contrail-time ratio varies. Obtaining a 90% contrail reduction for these three flights will be unlikely, as the destination lies in the centre of a contrail region. For the contrail mitigated cases of flights 4 to 6, a 1% decrease in contrail-time will be considered. The induced extra cost, required to obtain this contrail-time reduction, is assumed to be 0.1667% to the proportion of contrail-time.

In the case of Flight 4,5 and 6 no large scale contrail mitigation is realistically possible. Small scale contrail mitigation is possible at a relatively high cost. The larger the share of contrail-time, with respect to the total flight time, the higher the contrail mitigation cost will be, as can be seen the last column of table C.1. Where for flight 4, for every 1% of contrail reduction, 16.7% additional flight cost are incurred. The contrail mitigation cost for flight 5 and 6 vary relative to the percentage the flight has been flying through contrail prone regions.

These examples are meant to illustrate the large degree of variance of contrail mitigation cost. The costs are case dependent and vary enormously on the presence of atmospheric contrail prone regions and their respective magnitude and location with respect to the optimal flight trajectory. As a result a Contrail Cost Index will only be valid for the case around which it was obtained. This however does not mean that CCI behaviour for one case can not be the same as for another case. More research is required to see how similarities between cases can be used to predict CCI curves.

Table C.1: Case dependency of Contrail Mitigation Cost

Basic Info			Optimal Trajectory		Contrail Mitigated		Deviations		Reduction
Flight	Origin	Dest.	DOC	Contrail-Time	DOC	Contrail-Time	DOC %	Contrail %	Cost
F1	O1	D1	100%	80%	105.0%	8%	5%	-90%	5.6%
F2	O2	D1	100%	10%	100.8%	1%	1%	-90%	0.9%
F3	O3	D1	100%	10%	102.0%	1%	2%	-90%	2.2%
F4	O1	D2	20%	100%	20.03%	99.0%	0.17%	-1.0%	16.7%
F5	O2	D2	40%	30%	40.02%	29.7%	0.05%	-1.0%	5.0%
F6	O3	D2	60%	10%	60.01%	9.9%	0.02%	-1.0%	1.7%

D. The Sensitivity study Trajectories

Information on the trajectories of the cases presented in the sensitivity study of section 7.2.3.

In figure D.1, multiple vertical flight trajectories are shown as obtained from the sensitivity study. In figure D.2(a), the ground trajectories can be seen for the same cases. In figure (b& c), the same ground track profiles are plotted in combination with the persistent contrail probability and the wind vector, respectively. The higher the contrail reductions, the higher the deviations from the original trajectory. However, looking at the 90% reduction trajectories, the alterations in the horizontal profile seem to be relatively small still.

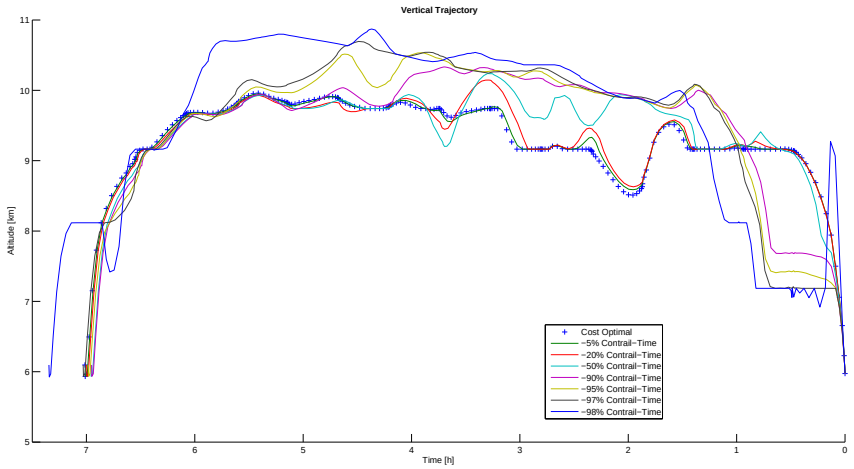

Figure D.1: Vertical trajectories of selected sensitivity results

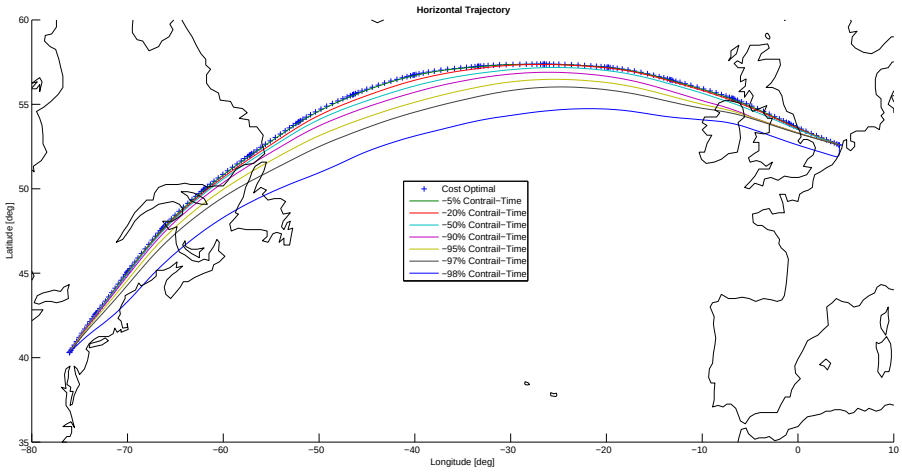

(a)

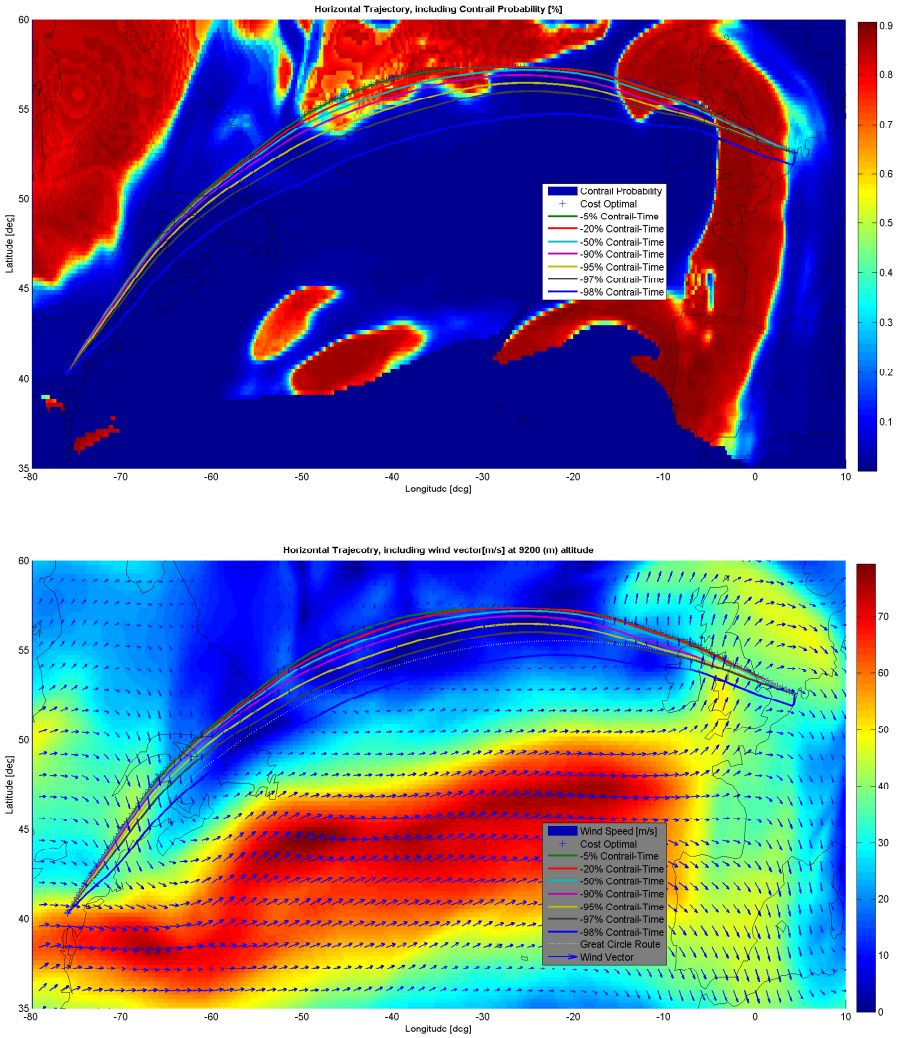

Figure D.2: Horizontal trajectories of selected sensitivity results, including contrail probability and wind (c)

E. Optimisation Results: Objective, Feasibility & Optimality Criteria

Table E.1: Conditions and results for the optimisations between AMS-BFS.
For the fields with a [-], the criterion was no longer available.

Route	**Objective**	**Atmospheric Conditions**	**Nodes & Intervals**	**Final Result**		
				Feasability	*Optimality*	*Objective value*
Verification: Convergence Behaviour						*(Section 5.3.1 & 7.2.1)*
AMS-BFS	DOC	Wind	501	6,90E-10	9,70E-07	9,820E+04
	DOC	Wind	401	6,20E-10	9,50E-07	9,822E+04
	DOC	Wind	301	2,00E-09	7,00E-07	9,824E+04
	DOC	Wind	201	2,00E-09	5,80E-07	9,829E+04
	DOC	Wind	101	-	-	9,840E+04
	DOC	Wind	51	1,40E-08	5,40E-07	9,854E+04
	DOC	Wind	43	4,90E-08	9,40E-07	9,860E+04
	DOC	Wind	36	7,70E-07	2,90E-06	9,888E+04
	DOC	Wind	26	1,30E-08	3,20E-06	9,869E+04
Verification: Convergence Behaviour						*(Section 5.3.1 & 7.2.1)*
AMS-BFS	min90C	Wind	501	6,40E-12	9,60E-07	1,003E+05
	min90C	Wind	401	2,40E-10	1,00E-06	1,003E+05
	min90C	Wind	301	1,20E-10	6,80E-07	1,003E+05
	min90C	Wind	201	7,20E-10	9,70E-07	1,004E+05
	min90C	Wind	101	8,40E-09	9,90E-07	1,004E+05
	min90C	Wind	51	6,10E-07	8,70E-06	1,005E+05
	min90C	Wind	43	2,90E-07	8,50E-06	1,005E+05
	min90C	Wind	36	4,30E-09	9,30E-06	1,006E+05
	min90C	Wind	26	2,90E-07	8,50E-06	1,005E+05

Table E.2: Conditions and results for the optimisations between AMS-KIAD.
For the fields with a [-], the criterion was no longer available.

Route	**Objective**	**Atmospheric Conditions**	**Nodes & Intervals**	**Final Result**		
				Feasability	*Optimality*	*Objective value*
Verification: Optimisation routine in ISA						*(Section5.2.2)*
AMS-KIAD	Time	ISA no wind	226	-	-	-
	Fuel	ISA no wind	226	1,90E-09	9,50E-07	6,73E+05
	DOC	ISA no wind	226	2,00E-10	7,90E-07	7,21E+05
Results: Excluding Wind						*(Section 7.1.1 & 7.1.2)*
AMS-KIAD	Time Optimal	No wind	226	-	-	-
	Fuel Optimal	No wind	226	-	-	-
	Contrail-time	No wind	226	-	-	-
	Contrail-fuel	No wind	226	-	-	-
Results: Including Wind						*(Section 7.1.3 & 7.1.4)*
AMS-KIAD	Time Optimal	Wind	226	-	-	-
	Fuel Optimal	Wind	226	6,10E-08	4,70E-04	7,43E+05
	Contrail-time	Wind	226	6,80E-13	8,70E-04	2,42E+04
	Contrail-fuel	Wind	226	1,20E-09	5,10E-04	7,65E+05
Sensitivity Study DOC						*(Section 7.2.2 & 7.2.3)*
AMS-KIAD	DOC	Wind	226	9,90E-11	8,80E-04	7,07E+05
	min1C	Wind	226	1,40E-13	6,10E-04	7,07E+05
	min2C	Wind	226	1,50E-08	7,50E-04	7,07E+05
	min5C	Wind	226	4,10E-12	5,70E-04	7,07E+05
	min10C	Wind	226	3,80E-11	1,00E-03	7,07E+05
	min20C	Wind	226	8,40E-11	1,30E-03	7,08E+05
	min30C	Wind	226	8,80E-11	8,10E-04	7,08E+05
	min50C	Wind	226	7,50E-12	2,50E-03	7,09E+05
	min70C	Wind	226	1,90E-09	3,90E-04	7,11E+05
	min80C	Wind	226	2,80E-13	3,50E-04	7,12E+05
	min90C	Wind	226	5,00E-12	3,70E-04	7,14E+05
	min95C	Wind	226	3,20E-14	1,40E-04	7,19E+05
	min97C	Wind	226	2,20E-11	3,90E-03	7,25E+05
	min98C	Wind	226	1,10E-07	2,80E-03	7,59E+05
Sensitivity Study Fuel						*(Section 7.2.2 & 7.2.3)*
AMS-KIAD	Fuel	Wind	226	5,90E-12	3,40E-03	6,93E+05
	min5C	Wind	226	4,80E-09	1,90E-03	6,94E+05
	min10C	Wind	226	1,00E-12	1,40E-03	6,94E+05
	min20C	Wind	226	4,70E-09	4,80E-04	6,94E+05
	min30C	Wind	226	4,10E-12	1,10E-03	6,95E+05
	min50C	Wind	226	6,40E-13	4,60E-04	6,97E+05
	min70C	Wind	226	6,00E-11	5,70E-04	6,99E+05
	min80C	Wind	226	2,50E-08	2,10E-04	7,00E+05
	min90C	Wind	226	3,80E-07	4,10E-03	7,03E+05
	min95C	Wind	226	1,10E-13	6,80E-04	7,09E+05
	min97C	Wind	226	4,10E-11	9,70E-03	7,15E+05
Verification: Convergence Behaviour						*(Section 5.3.2)*
AMS-KIAD	DOC	Wind	226	9,90E-11	8,80E-04	7,07E+05
Unconverged Section			24	Section	Section	9,26E+04
Converged Section	DOC	Wind	801	4,30E-14	6,80E-07	9,26E+04

Bibliography

[1] International standard atmosphere model. http://www.mathworks.nl/help/aerotbx/ug/atmosisa.html.

[2] Picture: Airplane condensation trails (contrails) across the englisch channel, 2003. http://eoimages.gsfc.nasa.gov/images/imagerecords/69000/69546/France.A2003343.1045.250m.jpg.

[3] Contrail cirrus prediction tool (cocip), 2013. http://www.dlr.de/pa/en/desktopdefault.aspx/tabid-8859/15306_read-19960/.

[4] United States Energy Information Administration. World jet fuel consumption by year, 14-10-2014. http://www.indexmundi.com/energy.aspx?product=jet-fuel.

[5] National Geospatial-Intelligence Agency. World geodetic system 1984 (wgs 84), 6 February 2015. http://web.archive.org/web/20120402143802/https://www1.nga.mil/ProductsServices/GeodesyandGeophysics/WorldGeodeticSystem/Pages/default.aspx.

[6] Air Weather Service. *Forecasting Aircraft Condensation Trails*, September 1981. ADA111876.

[7] O. Alduchov and R. Eskridge. Improved magnus form approximation of saturation vapor pressure. Vol. 35:601–609, 1996.

[8] H. Appleman. The formation of exhaust condensation trails by jet aircraft. *Bulletin of American Meteorological Society*, pages 14–20, 1953.

[9] P. Minnis J. Ayers and S. Weaver. Surface-based observations of contrail occurrence frequency over the u.s., april 1993 - april 1994, 1997.

[10] Staff Sgt. K. L. Bishop. Picture: Two soviet mig-29 aircraft intercepted by f-15 eagle aircraft of the 21st tactical fighter wing, 22:47, 1 August 1989. http://media.nara.gov/stillpix/330-cfd/1990/DF-ST-90-05759.jpeg.

[11] BriYYZ. Picture: Klm asia boeing 747-400(m) ph-bfh, 15:57, 27 January 2013.

[12] U. Burkhardt and B. Kärcher. Global radiative forcing from contrail cirrus. VOL 1:54–58, 2011.

[13] K.J. Mach M.D. Mastrandrea M. van Aalst W.N. Adger D.J. Arent J. Barnett R. Betts T.E. Bilir J. Birkmann J. Carmin D.D. Chadee A.J. Challinor M. Chatterjee W. Cramer D.J. Davidson Y.O. Estrada J.-P. Gattuso Y. Hijioka O. Hoegh-Guldberg H.Q. Huang G.E. Insarov R.N. Jones R.S. Kovats P. Romero-Lankao J.N. Larsen I.J. Losada J.A. Marengo R.F. McLean L.O. Mearns R. Mechler J.F. Morton I. Niang T. Oki J.M. Olwoch M. Opondo E.S. Poloczanska H.-O. Prtner M.H. Redsteer A. Reisinger A. Revi D.N. Schmidt M.R. Shaw W. Solecki D.A. Stone J.M.R. Stone K.M. Strzepek A.G. Suarez P. Tschakert R. Valentini S. Vicua A. Villamizar K.E. Vincent R.Warren L.L.White T.J.Wilbanks P.P.Wong C.B., V.R. Barros and G.W. Yohe. In: Climate change 2014: Impacts, adaptation, and vulnerability. part a: Global and sectoral aspects. contribution of working group ii to the fifth assessment report of the intergovernmental panel on climate change, 2014.

[14] A.V. Rao D. Benson C.L. Darby and G.T. Huntington. *User's Manual for GPOPS Version 3.3*, 2010.

[15] R. F. de Oliveira and Prof. Dr. C. Büskens. Benefits of optimal flight planning on noise and emissions abatement at the frankfurt airport. In editor, editor, *booktitle*. American Institute of Aeronautics and Astronautics, August 2012.

[16] (Eds. R. Sausen et al.), editor. *Climate sensitivity of radiative impacts from transport systems*. European Communities, 2010.

[17] M. Ponater et al. Contrails in a comprehensive global climate model: Parameterization and radiative forcing results. *Journal of Geophysical research*, 107(D13), July 2002.

[18] F. Fahroo and I. M. Ross, editors. *Advances in Pseudospectral Methods for Optimal Control*, number 7309. American Institute of Aeronautics and Astronautics, August 2008. http://www.elissarglobal.com/wp-content/uploads/2012/04/Advances-in-Pseudospectral-Methods-for-Optimal-Control.pdf.

[19] Airbus forecasting team. Delevering the future. AIRBUS S.A.S., September 2011.

[20] K. Gierens and E. Jensen. A numerical study of the contrail-to-cirrus transition. 25:43414344, 1998.

[21] P. Spichtinger H. Mannstein and K. Gierens. A note on how to avoid contrail cirrus. *Transportation Research*, Part D(10):421426, 2005.

[22] S. Hartjes and H. Visser. Optimization of rnav noise and emission abatement departure procedures. *American Institute of Aeronautics and Astronautics*, September 2009.

[23] E. Jensen O. Toon S. Kinne G. Sachse B. Anderson K. Chan C. Twohy B. Gandrud A. Heymsfield and R. Miake-Lye. Environmental conditions required for contrail formation and persistence. Vol. 103(D4):3929–3936, 1998.

[24] H. Hirabayashi and Y. Fukuda. Air traffic management and systems, 2014.

[25] J. K. Hochwarth. Aviation calculations & conversions, 14-7-2014. www.hochwarth.com/misc/AviationCalculator.html.

[26] ICAO. Aviation and climate change, 2010. http://www.icao.int/environmental-protection/Documents/Publications/ENV_Report_2010.pdf.

[27] D.H. Lister et al. J.E. Penner. Aviation and the global atmosphere. a special report of ipcc. Technical report, IPCC, Cambridge Univ. Press, 1999.

[28] D.H. Lister et al. J.E. Penner. Aviation and the global atmosphere. a special report of ipcc. Technical report, IPCC, Cambridge Univ. Press, 1999. http://www.grida.no/publications/other/ipcc_sr/?src=/climate/ipcc/aviation/.

[29] B. Kärcher and F. Yu. Role of aircraft soot emissions in contrail formation. 36, 2009.

[30] B. L. Koff. Gas turbine technology evolution: A designers perspective. Vol. 20(No. 4), JulyAugust 2004.

[31] P. Spichtinger K. Gierens U. Leiterer and H. Dier. Ice supersaturation in the tropopause region over lindenberg, germany. (12):143156, 2003.

[32] D.C. Lewellen and W.S. Lewellen. The effects of aircraft wake dynamics on contrail formation. 58:390406, 2001.

[33] H. Fricke M. Kaiser, J. Rosenow and M. Schultz. Tradeoff between optimum altitude and contrail layer to ensure maximum ecological en-route performance using the enhanced trajectory prediction model (etpm). 2012.

[34] Page Curator: J. Madigan. The contrail education project, 12:52, 21 November 2014. `http://science-edu.larc.nasa.gov/contrail-edu/contrails.php`.

[35] H. Mannstein and U. Schumann. Aircraft induced contrail cirrus over europe. 2005. in press.

[36] G. Rädel N. Stuber, O. Forster and K. Shine. The importance of the diurnal and annual cycle of air traffic for contrail radiative forcing. page 864867, 2006.

[37] NASA. The importance of understanding clouds, 2005. `http://www.nasa.gov/pdf/135641main_clouds_trifold21.pdf`.

[38] B. Sridhar H. Ng and N. Chen. Aircraft trajectory optimization and contrails avoidance in the presence of winds. *JOURNAL OF GUIDANCE, CONTROL, AND DYNAMICS*, 34(5):1577–1583, September 2011.

[39] F. Noppel and R. Singh. Overview on contrail and cirrus cloud avoidance technology. *JOURNAL OF AIRCRAFT*, 44(5):1721–1726, September-October 2007.

[40] Government of Canada. 25km resolution numerical data of the global deterministic prediction system (gdps) model - grib2 format, 14-10-2014. `http://weather.gc.ca/grib/grib2_glb_25km_e.html`.

[41] Papafrezzo. Picture: A river runs through it, 2009.

[42] W.Murray P.E. Gill and M.A. Saunders. *Users Guide for SNOPT Version 7*. University of California and Stanford University, 2008.

[43] M. Ponater R. Sausen, K. Gierens and U. Schumann. A diagnostic study of the global distribution of contrails. (61):pages: 127141, 1998.

[44] S. M. Rump. INTLAB - INTerval LABoratory. In Tibor Csendes, editor, *Developments in Reliable Computing*, pages 77–104. Kluwer Academic Publishers, Dordrecht, 1999. `http://www.ti3.tuhh.de/rump/`.

[45] M. Schrader. Calculations of aircraft contrail formation critical temperatures, December 1997.

[46] U. Schumann. On conditions for contrail formation from aircraft exhaust. *Meteorological Zeitschrift*, pages 4–23, 1996.

[47] U. Schumann. Influence of propulsion efficiency on contrail formation. *Aerosp. Sci. Technol.*, 4:391401, May 2000. S1270-9638(00)01062-2/FLA.

[48] U. Schumann. Formation, properties and climatic effects of contrails. *Physique*, 6:549–565, July 2005. 5.

[49] U. Schumann. A contrail cirrus prediction model. 5:543580, 2012.

[50] O. Möhler S. Büttner C. Linke M. Schnaiter H. Saathoff O. Stetzer R. Wagner M. Krämer A. Mangold U. Ebert U. Schurath. Effect of sulfuric acid coating on heterogeneous ice nucleation by soot aerosol particles. 2005. in press.

[51] J. Shull. A validation study of the air force weather agency (afwa) jetrax contrail forecast algorithm, 1998.

[52] K. Gierens U. Schumann M. Helten H. Smit and A. Marenco. A distribution law for relative humidity in the upper troposphere and lower stratosphere derived from three years of mozaic measurements. pages 1218–1226, 1999.

[53] T. Soler and L. Hothem. Coordinate systems used in geodesy: Basic definitions and concepts. Volume 114:8497, 1988.

[54] D. Sonntag. Advancements in the field of hygrometry. *METEOROL. Z.*, 3:5166, 1994.

[55] M.J.G. Spierings. Optimizing tailored arrival trajectories for noise abatement, October 2012.

[56] A. Levermann V. Huber K. Frieler D. M. Lawrence T. Schneider von Deimling, M. Meinshausen and V. Brovkin. Estimating the near-surface permafrost-carbon feedback on global warming. 2011. `http://www.biogeosciences.net/9/649/2012/bg-9-649-2012.pdf`.

[57] M. Teengs. *Model of the boeing 747-400 with CF6-80C2B1F engines.* TU-Delft, 2006.

[58] T. Koop B. Luo A. Tsias and T. Peter. Water activity as the determinant for homogeneous ice nucleation in aqueous solutions. (406):611614, 2000.

[59] S. Unterstrasser and K. Gierens. A numerical study of the contrail-to-cirrus transition. 10:20172036, 2010.

[60] S. Unterstrasser and K. Gierens. A numerical study of the contrail-to-cirrus transition. 10:20372051, 2010.

[61] H. Visser and S. Hartjes. Economic and environmental optimization of flight trajectories conneting a city-pair. *Journal of Aerospace Engineering*, March 2013.

[62] Wegmann. Picture: Effect of the ashcloud, 12:47, 29 May 2010. `http://en.wikipedia.org/wiki/File:Ashcloud.png`.

[63] R. Whitford. *Design for Air Combat.* Number 978-0710604262. Jane's Publishing Company Ltd., april 1987.

[64] T. Phillips G. Potter D. Williamson R. Cederwall J. Boyle M. Fiorino J. Hnilo J. Olson S. Xie and J. Johnyio. Evalutating parameterization in general circulation models. *Bulletin of the American Meteorological Society*, 85(12):1903–1915, December 2004. `http://journals.ametsoc.org/doi/abs/10.1175/BAMS-85-12-1903`.

[65] K. Xu and S. Krueger. Evaluation of cloudiness parameterizations using a cumulus ensemble model. *American Meteorological Society*, Vol 119:342–367, 1991.